THREE-DIMENSIONAL DLM/FD METHODS FOR SIMULATING THE MOTION OF SPHERES IN BOUNDED SHEAR FLOWS OF OLDROYD-B FLUIDS

A Dissertation Presented to

the Faculty of the Department of Mathematics

University of Houston

In Partial Fulfillment

of the Requirements for the Degree

Doctor of Philosophy

By

Shang-Huan Chiu

August 2017

THREE-DIMENSIONAL DLM/FD METHODS FOR SIMULATING THE MOTION OF SPHERES IN BOUNDED SHEAR FLOWS OF OLDROYD-B FLUIDS

Shang-Huan Chiu

APPROVED:

Dr. Tsorng-Whay Pan, Chairman
Department of Mathematics, University of Houston

Dr. Roland Glowinski,
Department of Mathematics, University of Houston

Dr. Jiwen He,
Department of Mathematics, University of Houston

Dr. Dong Liu,
Department of Mechanical Engineering,
University of Houston

Dean, College of Natural Sciences and Mathematics

Acknowledgements

I would like to thank the University of Houston and the faculty of Mathematics Department for giving me the chance to be here. It was the beginning of this extraordinary journey. It started five years ago but it was just like yesterday. They have built one of the best Mathematcis PhD programs for me to study further and support my life in the U.S. finanically.

I would like to thank Dr. Tsorng-Whay Pan for having me as his apprentice. Because of his talent and patience, I learned how to do research properly and carefully. Under his teaching and leading, we have this interesting dissertation today. I am glad I have the chance to study applied mathematics from him. He is not only an exact scholar and advisor but also a genial mentor.

I would like to thank Dr. Roland Glowinski for the beautiful works he has created over fifty years. All the things we have are base on his works. I would like to thank Dr. Shanyu Ji and Dr. Jiwen He. I always get strong support and valuable advice from them. I would like to thank Dr. Dong Liu for the useful and professional comments on this dissertation. He helped me to see some of my blind points and then I have the chance to improve the results in this dissertation.

Last but not least, I would like to thank my family and all my friends. With my parents unconditional support, I have been able to study abroad thousands of miles away. With their encouragement, I feel I am not alone and have the power to go forward. There were many moments they needed help but I wasn't there for them and my brother took my position to take care of them. I am glad I have this sibling and I thank him for all his sacrifices. In the past five years, I have gotten so much help from friends I met in the U.S. They include Dr. Pan's research group members: Lingling Shi, Yao Yu, Xingting Niu, Shihai Zhao, Aixia Guo. They include my classmates, students, and friends from UH. They make my life different and colorful. I would like to give special thanks to Robert Mendez. He is very kind to read this dissertation for me. et

THREE-DIMENSIONAL DLM/FD METHODS FOR SIMULATING THE MOTION OF SPHERES IN BOUNDED SHEAR FLOWS OF OLDROYD-B FLUIDS

An Abstract of a Dissertation

Presented to

the Faculty of the Department of Mathematics

University of Houston

In Partial Fulfillment

of the Requirements for the Degree

Doctor of Philosophy

By

Shang-Huan Chiu

August 2017

Abstract

In this dissertation, we present a novel distributed Lagrange multiplier/fictitious domain (DLM/FD) method for simulating fluid-particle interaction in Newtonian and Oldroyd-B fluids under creeping conditions. The categories go as follows: terminal speed of single ball in Newtonian fluid, rotaing speed of single ball for the Weissenberg number up to 5.5, trajactories migration and two ball encounters in a three dimensional (3D) bounded shear flow for the Weissenberg number up to 1. For rotating speed, two different methodolgies have been considered and the results are consistent with the exponential results for the Weissenberg number up to 1. For trajactories migration, the ball in Oldroyd-B fluid migrates toward the moving wall and it moves faster under higer value of the Weissenberg number. For two ball encounters, the pass and return trajectories of the two ball mass centers are similar to those in a Newtonian fluid, but they lose the symmetry due to the effect of elastic force arising from viscoelastic fluids. A chain of two balls can be formed in a bounded shear flow driven by the upper wall, depending on the value of the Weissenberg number and the initial vertical displacement of the ball mass center to the middle plane between two walls, and then such chain tumbles and migrates.

Contents

List of Figures

List of Tables

CHAPTER 1

Introduction

Suspensions of particles in fluids appear in many applications of chemical, biological, petroleum, and environmental areas. For the dynamics of rigid non-Brownian particles suspended in viscoelastic fluids, peculiar phenomena of the particle motion and pattern induced by fluid elasticity have been reviewed on theoretical predictions, experimental observations, and numerical simulations in [9]

For particle suspensions in Newtonian fluids, many numerical and experimental results have been published. Several topics are considered by researchers, such as random displacements resulting from particle encounters under creeping-flow conditions and the rotation of a neutrally buoyant particle in simple shear flow. The displacements from particle encounters lead to hydrodynamically induced particle migration, which constitutes an important mechanism for particle redistribution in the suspending fluid (see, e.g., [42] and the references therein). Binary encounters of particles is a phenomenon seen when two balls either pass each other or swap their streamline position.

Particle suspensions in viscoelastic fluids have different behaviors, e.g., strings of spherical particles aligned in the flow direction (e.g., see [25, 36, 40, 33]) and 2D crystalline patches of particles along the flow direction [32] in shear flow. As mentioned in [38], these flow-induced self-assembly phenomena have great potency for creating ordered macroscopic structures by exploiting the complex rheological properties of the suspending fluid as driving forces, such as shear-thinning and elasticity. To better understand particle interaction in viscoelastic fluids, Snijkers *et al.*, (2013) [38] have studied experimentally the two ball interaction in Couette flow of viscoelastic fluids in order to understand flow-induced assembly behavior associated with the string formation. In a high elasticity Boger fluid, the pass trajectories have a zero radial shift, but are not completely symmetric. In a wormlike micellar surfactant with a single dominant relaxation time and a broad spectrum shear-thinning elastic polymer solution, interactions are highly asymmetric and both pass and return trajectories have been obtained. Furthermore, shear-thinning of the viscosity seems to be the key rheological parameter that determines the overall nature of the hydrodynamical interactions, rather than the relative magnitude of the normal stress differences. The Same conclusion about the role of shear-thinning on the aggregation of many particles has been reported [36, 40]. There are numerical studies of the two particle interaction and aggregation in viscoelastic fluids (e.g., see [6, 20, 41]). Several non-Newtonian fluid models in bounded shear flow have been considered, such as Oldroyd-B fluid and Giesekus fluid.

Hwang *et al.*, (2004) [20] applied a finite element scheme to perform two-dimensional (2D) computational study and obtained the existence of complex kissing-tumbling-tumbling interactions for two inertialess cylinders in an Oldroyd-B fluid in sliding bi-periodic frames. The two circular disks keep rotating around each other while their midpoints come closer and closer to each other.

Choi *et al.*, (2010) [6] used an extended finite element method to simulate two circular particles in a 2D bounded shear flow between two moving walls for a Giesekus fluid. Besides that the two disks either passed each other, have reversing trajectories (return) or rotate as a pair (tumble), they also had another interaction, the two disks rotated at a constant speed with their mass centers remaining at fixed positions, respectively.

To simulate the interaction of two spherical particles interacting in an Oldroyd-B fluid, Yoon *et al.*, (2012) [41] applied a finite element method to discretize fluid flow with a discontinuous Galerkin approximation for polymer stress. In their numerical approach, the rigid property of the particles is imposed by treating them as a fluid having a much higher viscosity than the surrounding fluid. For the two balls initially located in the same vorticity plane, the balls either pass, return, or tumble in a bounded shear flow with two moving walls for Weissenberg numbers up to 0.3.

To study numerically the alignment of two and three balls in a viscoelastic fluid, Jaensson *et al.*, (2016) [21] developed a computational method which mainly combines the finite element method, the arbitrary Lagrange-Euler method [18], the log-conformation representation for the conformation tensor [13, 19], SUPG stabilization [3], and second-order time integration schemes. Using this computational method, they simulated the motion of two and three balls in bounded shear flows of a viscoelastic fluid of Giesekus type with the effect of the shear-thinning. They concluded that the presence of normal stress differences is essential for particle alignment to occur, although it is strongly promoted by shear-thinning.

In this dissertation, the phenomena in the fluid-particle system have been investigated numerically via several different mathematics models. To simulate the interaction of neutrally buoyant balls in a 3D bounded shear flow of Newtonian and Oldroyd-B fluids, we have generalized a distributed Lagrange multiplier/fictitious domain method (DLM/FD) developed in [31] for simulating the motion of neutrally buoyant particles in Stokes flows of Newtonian fluids from 2D to 3D and then combined this method with the operator splitting scheme and matrix-factorization approach for treating numerically the constitutive equations of the conformation tensor of Oldroyd-B fluids. In this matrix-factorization approach, the technique close to the one developed by Lozinski and Owens in [24], we solve the equivalent equations for the conformation tensor so that the positive definiteness of the conformation tensor at the discrete time level can be preserved. In order to capture the exponential behavior and preserve the positive definiteness of the conformation tensor, another approach for solving conformation tensor of Oldroyd-B fluids, called log-conformation tensor, has been developed by Fattal and Kupferman [13]. We derive the formula of a three dimensional log-conformation tensor and solve the constitutive equation by using this methodology with operator splitting Lie's scheme and a finite element method. Beside the Oldroyd-B model, we have introduced the Carreau model to simulate the flow of Oldroyd-B fluids with shear-thinning property.

For numerical simulations, we have obtained the following numerical results: the terminal speed of single ball in a Newtonian fluid, the rotating speed of single ball in an Oldroyd-B fluid, the migration of the balls in an Oldroyd-B fluid and the binary encounter of two balls in Newtonian and Oldroyd-B fluids. For the rotating speed of a single ball in a bounded shear flow, the wall effect and the viscoelasticity of fluids are two major factors that cause the varying of the rotation speed. We have simulated the rotating speed under four different ratios of the height between two wall over the diameter of balls to study the wall effect and using ten different Weissenberg numbers to investigate the effect of viscoelasticity of fluids. For the encounter of two balls in a bounded shear flow, the trajectories of the two ball mass centers presented in this dissertation are consistent with those obtained in [41]. We have further tested the cases of two balls for Weissenberg numbers up to 1 and obtained they either pass, return, or tumble in a bounded shear flow with two moving walls. The trajectories of the two ball mass centers lose symmetry due to the elastic force arising from Oldroyd-B fluids. For the interaction of the two balls in one-wall driven shear flow, two balls form a loosely connected chain if the initial gap between two balls is small and the two balls keep rotating with respect to the midpoint between their mass centers and migrate toward the moving wall.

CHAPTER 2

Three-dimensional DLM/FD methods for simulating the motion of spheres in bounded shear flows of Newtonian fluids

2.1 DLM/FD method for simulating fluid-particle interaction in Stokes flow

2.1.1 The governing equations

Let Ω be a bounded domain in $\mathbb{R}^3$ and let Γ be the boundary of Ω. We suppose that Ω is filled with a viscous fluid with density, ρ_f, and contains N moving balls of density ρ_s. Let $B(t) = \bigcup_{i=1}^{N} B_i(t)$ where $B_i(t)$ is the i-th solid ball in the fluid for $i = 1, 2, \cdots, N$. We denote by $\gamma_i(t)$ the boundary $\partial B_i(t)$ of $B_i(t)$ for $i = 1, 2, \cdots, N$ and let $\gamma(t) = \bigcup_{i=1}^{N} \gamma_i(t)$.

For some $T > 0$, the governing equations for the fluid-particles system is as follows:

For the fluid flow, we consider the following Stokes equations for Newtonian fluid

$$-\nabla \cdot \sigma = \rho_f \mathbf{g} \quad in \ \Omega \setminus \overline{B(t)}, t \in (0, T), \tag{2.1}$$

$$\nabla \cdot \mathbf{u} = 0 \quad in \ \Omega \setminus \overline{B(t)}, t \in (0, T), \tag{2.2}$$

$$\mathbf{u} = \mathbf{g_0} \quad on \ \Gamma \times (0, T), with \ \int_\Gamma \mathbf{g_0} \cdot \mathbf{n} d\Gamma = 0, \tag{2.3}$$

$$\mathbf{u}(\mathbf{x}, t) = \mathbf{V}_i(t) + \omega_i(t) \times \overrightarrow{\mathbf{G}_i(t)\mathbf{x}}, \quad \forall \mathbf{x} \in \gamma_i(t), \ i = 1, 2, \cdots, N, \tag{2.4}$$

where $\mathbf{u}$ is the flow velocity, p is the pressure, $\mathbf{g}$ denotes the gravity, ρ_f is the density of fluid, $\sigma = -p\mathbf{I} + 2\mu_f \mathbf{D}(\mathbf{u})$, $\mathbf{D}(\mathbf{u}) = (\nabla \mathbf{u} + (\nabla \mathbf{u})^\mathbf{t})/\mathbf{2}$ is the rate of deformation tensor, and μ_f is the dynamic viscosity of the fluid.

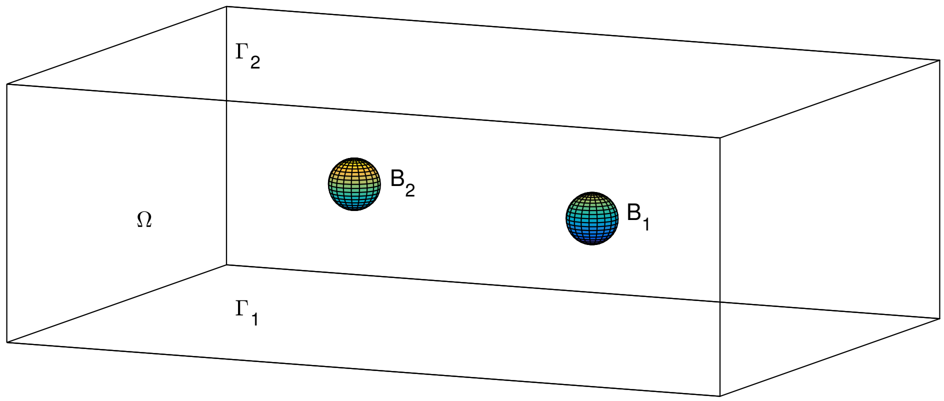

Figure 2.1: An example of a region Ω with two spheres.

In (2.3), Γ is the union of the bottom boundary Γ_1 and top boundary Γ_2 as in Figure 2.1 and $\mathbf{n}$ is the unit normal vector pointing outward to the flow region. The boundary conditions given in (3.17) are $\mathbf{g}_0 = \{-U, 0, 0\}^t$ on Γ_1 and $\mathbf{g}_0 = \{U, 0, 0\}^t$ on Γ_2 for a bounded shear flow. We assume also that the flow is periodic in the x_1 and x_2 directions with the periods L_1 and L_2, respectively, and in (2.4), a no-slip condition takes place on the boundary of particles on $\gamma(t)$, namely

$$\mathbf{u}(\mathbf{x}, t) = \mathbf{V}_i(t) + \omega_i(t) \times \overrightarrow{\mathbf{G}_i(t)\mathbf{x}}, \quad \forall \mathbf{x} \in \gamma_i(t),\ i = 1, 2, \cdots, N, \tag{2.5}$$

where $\mathbf{V}_i$ is the translation velocity, ω_i is the angular velocity, $\mathbf{G_i}$ is the center of mass and $\mathbf{x}$ is a point on the surface of the particle with $\overrightarrow{\mathbf{G}_i(t)\mathbf{x}} = \{x_1 - G_{i,1}(t), x_2 - G_{i,2}(t), x_3 - G_{i,3}(t)\}^t$.

The motion of particle satisfies the following Euler-Newton's equations:

$$\mathbf{v}_i(\mathbf{x}, t) = \mathbf{V}_i(t) + \boldsymbol{\omega}_i(t) \times \overrightarrow{\mathbf{G}_i(t)\mathbf{x}}, \quad \forall \{\mathbf{x}, t\} \in \overline{B_i(t)} \times (0, T),\ i = 1, 2, \cdots, N, \tag{2.6}$$

$$\frac{d\mathbf{G}_i}{dt} = \mathbf{V}_i, \tag{2.7}$$

$$M_{p,i}\frac{d\mathbf{V_i}}{dt} = M_i\mathbf{g} + \mathbf{F}_i, \tag{2.8}$$

$$\frac{d(\mathbf{I_{p,i}}\boldsymbol{\omega}_\mathbf{i})}{dt} = \mathbf{T}_i, \tag{2.9}$$

$$\mathbf{G}_i(0) = \mathbf{G}_i^0,\ \mathbf{V}_i(0) = \mathbf{V}_i^0,\ \omega_i(0) = \omega_i^0, \tag{2.10}$$

for $i = 1, 2, \cdots, N$, where $M_{p,i}$ and $\mathbf{I}_{p,i}$ are the mass and the moment of inertia of the i-th particle, respectively; $\mathbf{F}_i$ and $\mathbf{T}_i$ are the hydrodynamic force and torque imposed on the i-th particle by the fluid.

In (2.8) and (2.9), the hydrodynamic force $\mathbf{F}_i$ and torque $\mathbf{T}_i$ imposed on the i-th particle by the fluid are given by

$$\mathbf{F}_i = -\int_{\gamma_i} \sigma\mathbf{n}\,d\gamma, \quad \mathbf{T}_i = -\int_{\gamma_i} \overrightarrow{\mathbf{G}_i\mathbf{x}} \times \sigma\mathbf{n}\,d\gamma. \tag{2.11}$$

2.2 Variational formulation

To obtain a distributed Lagrange multiplier/fictitious domain formulation for the above problem (2.1)-(2.11), we proceed as in [15, 16], namely: (i) we derive a global variational formulation of the virtual power type of problem (2.1)-(2.11), (ii) we then fill the region occupied by the rigid body by the surrounding fluid (i.e. embed $\Omega \setminus \overline{B(t)}$ in Ω) with the constraint that the fluid inside the rigid body region has a rigid body motion, and then (iii) we relax the rigid body motion constraint by using a distributed Lagrange multiplier, obtaining the following fictitious domain formulation over the entire region Ω.

For convenience of derivation, we assume there is only one ball in the fluid, that is, we set $B(t)$ as a solid ball in the fluid, $\gamma(t)$ the boundary of $B(t)$, $\mathbf{G}(t)$ the center of mass of this particle. In the equations of the motion of particle, we set $\mathbf{V}$ the translation velocity of the ball $B(t)$, $\boldsymbol{\omega}$ the angular velocity of the ball $B(t)$, M_p and $\mathbf{I_p}$ the mass and the moment of inertia of the ball $B(t)$, respectively; $\mathbf{F}$ and $\mathbf{T}$ the hydrodynamic force and torque imposed on the ball $B(t)$ by the fluid, respectively.

To obtain a variational formulation for above problem (2.1)-(2.4), we first define the following function spaces

$$\begin{aligned}\mathbf{W}_{\mathbf{g}_0}(t) = \{\mathbf{v}|\mathbf{v} \in (H^1(\Omega \setminus \overline{B(t)}))^3,\ \mathbf{v} = \mathbf{V}(t) + \boldsymbol{\omega}(t) \times \overrightarrow{\mathbf{G}(t)\mathbf{x}} \quad &\textit{on } \partial B(t), \\ \mathbf{v} = \mathbf{g}_0(t) \ \ \textit{on}\, \Gamma, \mathbf{v} \textit{ is periodic in the } x_1 \textit{ and } x_2 \textit{ directions with}& \\ \textit{periods } L_1 \textit{ and } L_2, \textit{ respectively}\},&\end{aligned}$$

$$\begin{aligned}\mathbf{W}_0(t) = \{(\mathbf{v}, \mathbf{Y}, \boldsymbol{\theta})|(\mathbf{v}, \mathbf{Y}, \boldsymbol{\theta}) \in (H^1(\Omega \setminus \overline{B(t)}))^3 \times \mathbb{R}^3 \times \mathbb{R}^3, \mathbf{v} = 0 \ \textit{on}\, \Gamma,& \\ \mathbf{v} = \mathbf{Y} + \boldsymbol{\theta} \times \overrightarrow{\mathbf{G}(t)\mathbf{x}} \quad \textit{on } \partial B(t), \mathbf{v} \textit{ is periodic in the } x_1 \textit{ and } x_2& \\ \textit{directions with periods } L_1 \textit{ and } L_2, \textit{ respectively}\},&\end{aligned}$$

and

$$L_0^2(\Omega \setminus \overline{B(t)}) = \left\{ q \,\middle|\, q \in L^2(\Omega \setminus \overline{B(t)}), \int_{\Omega \setminus \overline{B(t)}} q \, d\mathbf{x} = 0 \right\}.$$

The variational formulation of the system (2.1)-(2.4) is as follows:

For a.e. $t > 0$, find $\mathbf{u}(t) \in \mathbf{W}_{\mathbf{g}_0}(t)$, $p(t) \in L^2_0(\Omega \setminus \overline{B(t)})$,$\mathbf{V}(t) \in \mathbb{R}^3$, $\mathbf{G}(t) \in \mathbb{R}^3$, $\omega(t) \in \mathbb{R}^3$, such that

$$\begin{cases} -\int_{\Omega\setminus\overline{B(t)}} p\nabla\cdot\mathbf{v}\,d\mathbf{x} + 2\mu_f\int_{\Omega\setminus\overline{B(t)}} \mathbf{D}(\mathbf{u}):\mathbf{D}(\mathbf{v})\,d\mathbf{x} + \mathbf{I_p}\dfrac{d\boldsymbol{\omega}}{dt}\cdot\boldsymbol{\theta} \\ \quad + \left(M_p\dfrac{d\mathbf{V}}{dt} - M_p\mathbf{g}\right)\cdot\mathbf{Y} = \rho_f\int_{\Omega\setminus\overline{B(t)}} \mathbf{g}\cdot\mathbf{v}\,d\mathbf{x}, \\ \quad \forall(\mathbf{v},\mathbf{Y},\boldsymbol{\theta}) \in \mathbf{W}_0(t), \end{cases} \tag{2.12}$$

$$\int_{\Omega\setminus\overline{B(t)}} q\nabla\cdot\mathbf{u}\,d\mathbf{x} = 0, \quad \forall q \in L^2(\Omega\setminus\overline{B(t)}), \tag{2.13}$$

$$\frac{d\mathbf{G}}{dt} = \mathbf{V}, \tag{2.14}$$

$$\mathbf{u}(\mathbf{x},0) = \widetilde{\mathbf{u}}_0(\mathbf{x}) = \begin{cases} \mathbf{u}_0(\mathbf{x}), \quad \forall\mathbf{x} \in \Omega\setminus\overline{B(0)}, \\ \mathbf{V}_0 + \boldsymbol{\omega}_0 \times \overrightarrow{\mathbf{G}_0\mathbf{x}}, \quad \forall\mathbf{x} \in \overline{B(0)}. \end{cases} \tag{2.15}$$

$$\mathbf{G}(0) = \mathbf{G}_0, \quad \mathbf{V}(0) = \mathbf{V}_0, \quad \boldsymbol{\omega}(0) = \boldsymbol{\omega}_0. \tag{2.16}$$

To obtain an equivalent fictitious domain formulation, first we fill the ball $B(t)$ with a fluid of density ρ_f and suppose that this fluid follows the same rigid body motion as $B(t)$ itself, which is

$$\mathbf{u}(\mathbf{x},t) = \mathbf{V}(t) + \boldsymbol{\omega}(t) \times \overrightarrow{\mathbf{G}(t)\mathbf{x}}, \quad \forall\mathbf{x} \in B(t). \tag{2.17}$$

Define a function space

$$\widetilde{\mathbf{W}}_0(t) = \left\{(\mathbf{v},\mathbf{Y},\boldsymbol{\theta}) \,\middle|\, (\mathbf{v}|_{\Omega\setminus\overline{B(t)}},\mathbf{Y},\boldsymbol{\theta}) \in \mathbf{W}_0(t), \mathbf{v}(\mathbf{x},t) = \mathbf{Y} + \boldsymbol{\theta} \times \overrightarrow{\mathbf{G}(t)\mathbf{x}} \quad \forall\mathbf{x} \in B(t)\right\}.$$

Suppose sphere B is made of an homogeneous material of density, ρ_f, which follows

$$\rho_f \int_{B(t)} \mathbf{g} \cdot \mathbf{v}\, d\mathbf{x} = \frac{\rho_f}{\rho_s} M_p \mathbf{g} \cdot \mathbf{Y}, \quad \forall(\mathbf{v}, \mathbf{Y}, \theta) \in \widetilde{\mathbf{W}}_0(t), \tag{2.18}$$

$$\nabla \cdot \mathbf{v} = 0 \;\; in\; B(t), \quad \forall(\mathbf{v}, \mathbf{Y}, \theta) \in \widetilde{\mathbf{W}}_0(t), \tag{2.19}$$

$$\nabla \cdot \mathbf{u} = 0 \;\; in\; B(t) \;\; and\; \mathbf{D}(\mathbf{u}) = 0 \;\; in\; B(t). \tag{2.20}$$

To obtain a fictitious domain formulation, we now define the following function spaces

$$\mathbf{V}_{\mathbf{g}_0}(t) = \left\{ \mathbf{v} \,\middle|\, \mathbf{v} \in (H^1(\Omega))^3, \mathbf{v} = \mathbf{g}_0(t) \; on\, \Gamma \right\},$$

$$L_0^2(\Omega) = \left\{ q \,\middle|\, q \in L^2(\Omega), \int_\Omega q\, d\mathbf{x} = 0 \right\}.$$

Combining (2.12)-(2.16) with (2.17)-(2.20), we obtain the fictitious domain formulation as follows:

For a.e. $t > 0$, find find $\mathbf{u}(t) \in \mathbf{V}_{\mathbf{g}_0}(t)$, $p(t) \in L_0^2(\Omega)$, $\mathbf{V}(t) \in \mathbb{R}^3$, $\mathbf{G}(t) \in \mathbb{R}^3$, $\boldsymbol{\omega}(t) \in \mathbb{R}^3$, such that

$$\begin{cases} -\displaystyle\int_\Omega p \nabla \cdot \mathbf{v}\, d\mathbf{x} + 2\mu_f \int_\Omega \mathbf{D}(\mathbf{u}) : \mathbf{D}(\mathbf{v})\, d\mathbf{x} + M_p \frac{d\mathbf{V}}{dt} \cdot \mathbf{Y} \\ +\mathbf{I}_p \dfrac{d\boldsymbol{\omega}}{dt} \cdot \boldsymbol{\theta} - \mathbf{F}^r \cdot \mathbf{Y} = \rho_f \displaystyle\int_\Omega \mathbf{g} \cdot \mathbf{v}\, d\mathbf{x} + \left(1 - \frac{\rho_f}{\rho_s}\right) M_p \mathbf{g} \cdot \mathbf{Y}, \\ \forall(\mathbf{v}, \mathbf{Y}, \boldsymbol{\theta}) \in \widetilde{\mathbf{W}}_0(t), \end{cases} \tag{2.21}$$

$$\int_\Omega q \nabla \cdot \mathbf{u}\, d\mathbf{x} = 0, \quad \forall q \in L^2(\Omega), \tag{2.22}$$

$$\frac{d\mathbf{G}}{dt} = \mathbf{V}, \tag{2.23}$$

$$\mathbf{u}(\mathbf{x}, t) = \mathbf{V}(t) + \boldsymbol{\omega}(t) \times \overrightarrow{\mathbf{G}(t)\mathbf{x}}, \quad \forall \mathbf{x} \in B(t). \tag{2.24}$$

$$\mathbf{u}(\mathbf{x}, 0) = \widetilde{\mathbf{u}}_0(\mathbf{x}), \quad \forall \mathbf{x} \in \Omega, \tag{2.25}$$

$$\mathbf{G}(0) = \mathbf{G}_0, \quad \mathbf{V}(0) = \mathbf{V}_0, \quad \boldsymbol{\omega}(0) = \boldsymbol{\omega}_0. \tag{2.26}$$

To relax the rigid body motion constraint (2.24), we introduce a Lagrange multiplier, $\boldsymbol{\lambda} \in \Lambda(t) = (H^1(B(t)))^3$, and a pairing for any $\mu \in (H^1(B(t)))^3$ and $\mathbf{v} \in (H^1(\Omega))^3$:

$$\langle \mu, \mathbf{v} \rangle_{\Lambda(t)} = \int_{B(t)} \left(\mu \cdot \mathbf{v} + d^2 \nabla \mu \cdot \nabla \mathbf{v} \right) \, d\mathbf{x},$$

where d is a scaling constant. Typically, we can use the diameter of the particles as the value for d.

Then we obtain a fictitious domain formulation with Lagrange multiplier as follows:

For a.e. $t > 0$, find $\mathbf{u}(t) \in \mathbf{V}_{\mathbf{g}_0}(t)$, $p(t) \in L_0^2(\Omega)$, $\mathbf{V}(t) \in \mathbb{R}^3$, $\mathbf{G}(t) \in \mathbb{R}^3$, $\boldsymbol{\omega}(t) \in \mathbb{R}^3$, $\boldsymbol{\lambda} \in \Lambda(t)$ such that

$$\begin{cases} -\int_\Omega p \nabla \cdot \mathbf{v} \, d\mathbf{x} + 2\mu_f \int_\Omega \mathbf{D}(\mathbf{u}) : \mathbf{D}(\mathbf{v}) \, d\mathbf{x} + M_p \dfrac{d\mathbf{V}}{dt} \cdot \mathbf{Y} + \mathbf{I}_p \dfrac{d\boldsymbol{\omega}}{dt} \cdot \boldsymbol{\theta} \\ -\left\langle \boldsymbol{\lambda}, \mathbf{v} - \mathbf{Y} - \boldsymbol{\theta} \times \overrightarrow{\mathbf{G}\mathbf{x}} \right\rangle_{\Lambda(t)} = \rho_f \int_\Omega \mathbf{g} \cdot \mathbf{v} \, d\mathbf{x} \\ +\left(1 - \dfrac{\rho_f}{\rho_s}\right) M_p \mathbf{g} \cdot \mathbf{Y}, \ \ \forall (\mathbf{v}, \mathbf{Y}, \boldsymbol{\theta}) \in (H_0^1(\Omega))^3 \times \mathbb{R}^3 \times \mathbb{R}^3, \end{cases} \tag{2.27}$$

$$\int_\Omega q \nabla \cdot \mathbf{u} \, d\mathbf{x} = 0, \quad \forall q \in L^2(\Omega), \tag{2.28}$$

$$\frac{d\mathbf{G}}{dt} = \mathbf{V}, \tag{2.29}$$

$$\mathbf{u}(\mathbf{x}, 0) = \widetilde{\mathbf{u}}_0(\mathbf{x}), \quad \forall \mathbf{x} \in \Omega, \tag{2.30}$$

$$\left\langle \boldsymbol{\mu}, \mathbf{u}(\mathbf{x}, t) - \mathbf{V}(t) - \boldsymbol{\omega}(t) \times \overrightarrow{\mathbf{G(t)x}} \right\rangle_{\Lambda(t)} = 0, \forall \boldsymbol{\mu} \in \Lambda(t), \tag{2.31}$$

$$\mathbf{G}(0) = \mathbf{G}_0, \quad \mathbf{V}(0) = \mathbf{V}_0, \quad \boldsymbol{\omega}(0) = \boldsymbol{\omega}_0. \tag{2.32}$$

Remark 2.1. Since $\mathbf{u}$ is divergence free and satisfies the Dirichlet boundary conditions on Γ, we can obtain

$$2 \int_\Omega \mathbf{D}(\mathbf{u}) : \mathbf{D}(\mathbf{v})\, d\mathbf{x} = \int_\Omega \nabla \mathbf{u} : \nabla \mathbf{v}\, d\mathbf{x}, \quad \forall \mathbf{v} \in (H_0^1(\Omega))^3,$$

which simplifies the numerical scheme from the computational point of view.

2.3 Finite element approximation and operator splitting scheme

2.3.1 Finite element approximation

For the purpose of finding an approximation solution to problem (2.27)-(2.26) by finite element methods, we need a partition of the flow region, $\Omega \in \mathbb{R}^3$. We have used an uniform finite element mesh (e.g., see in Figure 2.2) for Ω.

For the space discretization, we have chosen P_1-*iso*-P_2 finite element space for the velocity field and conformation tensor and P_1 finite element space for the pressure (like in Bristeau et al. [2] and Glowinski [14]). Then we define the following function spaces:

$$\begin{aligned}
\mathbf{V}_h = \{&\mathbf{v}_h \,\big|\mathbf{v}_h \in \left(C^0(\bar{\Omega})\right)^3, \mathbf{v}_h|_T \in (P_1)^3, \forall T \in \mathcal{T}_h,\ \mathbf{v}_h \textit{ is periodic in the } x_1 \\
&\textit{and } x_2 \textit{ directions with period } L_1 \textit{ and } L_2, \textit{ respectively } \}, \\
\mathbf{V}_{\mathbf{g}_{0h}(t)} &= \{\mathbf{v}_h|\mathbf{v}_h \in \mathbf{V}_h, \mathbf{v}_h|_\Gamma = \mathbf{g}_{0h}(t)\}, \\
\mathbf{V}_{0h} &= \{\mathbf{v}_h|\mathbf{v}_h \in \mathbf{V}_h, \mathbf{v}_h|_\Gamma = 0\}, \\
L^2_h = \{&q_h|q_h \in C^0(\bar{\Omega}), q_h|_T \in P_1, \forall T \in \mathcal{T}_{2h},\ q_h \textit{ is periodic in the } x_1 \\
&\textit{and } x_2 \textit{ directions with period } L_1 \textit{ and } L_2, \textit{ respectively } \}, \\
L^2_{0h} &= \{q_h|q_h \in L^2_h, \int_\Omega q_h \, d\mathbf{x} = 0\},
\end{aligned}$$

where h is the space mesh size, $\mathcal{T}_h$ is a regular tetrahedral mesh of Ω, $\mathcal{T}_{2h}$ is another tetrahedral mesh of Ω, twice coarser than $\mathcal{T}_h$, and P_1 is the space of the polynomials in three variables of degree ≤ 1 and $\mathbf{g}_{0h}(t)$ is an approximation of $\mathbf{g}_0(t)$ satisfying

$$\int_\Gamma \mathbf{g}_{0h}(t) \cdot \mathbf{n} \, d\Gamma = 0.$$

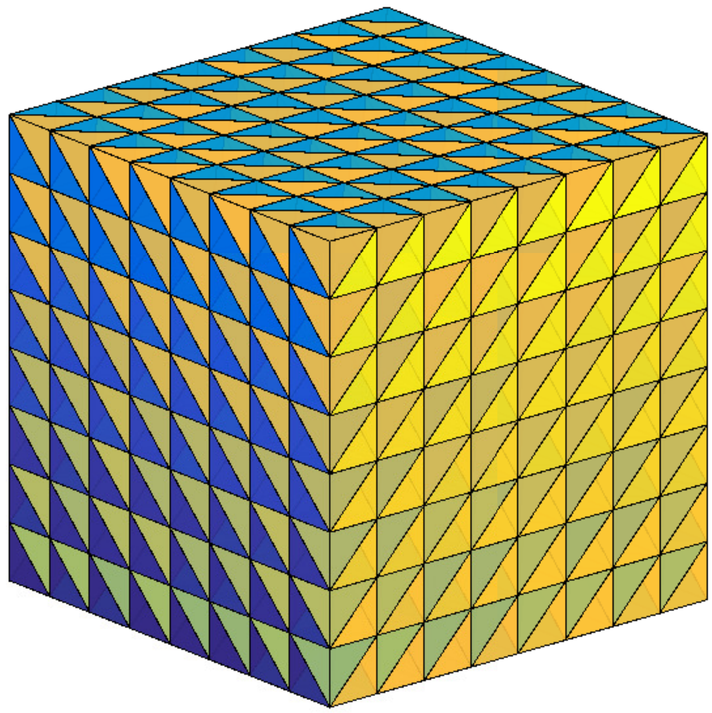

Figure 2.2: A tretrahedrization of a cube.

For simulating the particle motion in fluid flow, let us define the finite dimensional space to approach the space of Lagrange multiplier $\Lambda(t)$ (e.g., see [28], [30]). Let $\{\boldsymbol{\xi}_i\}_{i=1}^N$ be a set of points from $\overline{B(t)}$ which cover $\overline{B(t)}$ evenly. The discrete Lagrange multiplier space is defined by

$$\Lambda_h(t) = \left\{ \boldsymbol{\mu}_h \,\middle|\, \boldsymbol{\mu}_h = \sum_{i=1}^{N} \boldsymbol{\mu}_i \delta(\mathbf{x} - \xi_i), \boldsymbol{\mu}_i \in \mathbb{R}^3, \forall i = 1, \cdots, N \right\},$$

where $\mathbf{x} \to \delta(\mathbf{x} - \boldsymbol{\xi}_i)$ is the Dirac measure at $\mathbf{x} = \boldsymbol{\xi}_i$. There are two different definitions of discretize scalar pairing $< \cdot, \cdot >_{\Lambda_h(t)}$, which will be introduced in next section.

Using the finite dimensional spaces defined above, we obtain the following semi-discretization of the problem (2.27)-(2.32):

For $t > 0$, find find $\mathbf{u}_h(t) \in \mathbf{V}_{\mathbf{g}_{0h}}(t)$, $p(t) \in L^2_{0h}$, $\mathbf{V}(t) \in \mathbb{R}^3$, $\mathbf{G}(t) \in \mathbb{R}^3$, $\boldsymbol{\omega}(t) \in \mathbb{R}^3$, $\boldsymbol{\lambda}_h \in \Lambda_h(t)$ such that

$$\begin{cases} -\int_\Omega p\nabla\cdot\mathbf{v}\,d\mathbf{x} + 2\mu_f\int_\Omega \nabla\mathbf{u}_h : \nabla\mathbf{v}\,d\mathbf{x} + M_p\dfrac{d\mathbf{V}}{dt}\cdot\mathbf{Y} + \mathbf{I}_p\dfrac{d\boldsymbol{\omega}}{dt}\cdot\boldsymbol{\theta} \\ = \left(1-\dfrac{\rho_f}{\rho_s}\right)M_p\mathbf{g}\cdot\mathbf{Y} + \left\langle \boldsymbol{\lambda}_h, \mathbf{v}-\mathbf{Y}-\boldsymbol{\theta}\times\overrightarrow{\mathbf{G}\mathbf{x}}\right\rangle_{\Lambda_h(t)}, \\ \forall(\mathbf{v},\mathbf{Y},\boldsymbol{\theta}) \in \mathbf{V}_{0h}\times\mathbb{R}^3\times\mathbb{R}^3, \end{cases} \tag{2.33}$$

$$\int_\Omega q\nabla\cdot\mathbf{u}_h\,d\mathbf{x} = 0, \quad \forall q \in L^2_h, \tag{2.34}$$

$$\frac{d\mathbf{G}}{dt} = \mathbf{V}, \tag{2.35}$$

$$\mathbf{u}_h(\mathbf{x},0) = \widetilde{\mathbf{u}}_{0h}(\mathbf{x}), \quad \forall\mathbf{x}\in\Omega, \tag{2.36}$$

$$\left\langle \boldsymbol{\mu}_h, \mathbf{u}_h(t)-\mathbf{V}(t)-\boldsymbol{\omega}(t)\times\overrightarrow{\mathbf{G(t)x}}\right\rangle_{\Lambda_h(t)} = 0, \quad \forall\boldsymbol{\mu}_h\in\Lambda_h(t), \tag{2.37}$$

$$\mathbf{G}(0) = \mathbf{G}_0, \quad \mathbf{V}(0) = \mathbf{V}_0, \quad \boldsymbol{\omega}(0) = \boldsymbol{\omega}_0, \tag{2.38}$$

where $\widetilde{\mathbf{u}}_{0h}$ is an approximation of $\widetilde{\mathbf{u}}_0$ such that

$$\int_\Omega q\nabla\cdot\widetilde{\mathbf{u}}_{0h}\,d\mathbf{x} = 0, \quad \forall q\in L^2_h.$$

2.3.2 Collocation method and immersed boundary method

When dealing with a moving particle, $B(t)$, there are several methods have been considered for enforcing the rigid body motion inside $B(t)$(e.g., see [16], [18]). First we introduce the method developed in [16], which is a collocation method and then discuss a new method which combines the aforementioned collocation method with the other method which is like immersed boundary methods. (see Section 3.3.1)

For the collocation method, we define the following scalar pairing:

$$\langle \boldsymbol{\mu}_h, \mathbf{v}_h \rangle_{\Lambda_h(t)} = \sum_{i=1}^{N} \boldsymbol{\mu}_i \cdot \mathbf{v}_h(\boldsymbol{\xi}_i), \ \ \forall \boldsymbol{\mu}_h \in \Lambda_h(t), \mathbf{v}_h \in \mathbf{V}_{\mathbf{g}_{0h}(t)} \ \ or \ \mathbf{V}_{0h}.$$

For immersed boundary methods, we define the following scalar pairing:

$$\langle \boldsymbol{\mu}_h, \mathbf{v}_h \rangle_{\Lambda_h(t)} = \sum_{i=1}^{N} \sum_{j=1}^{M} \boldsymbol{\mu}_i \cdot \mathbf{v}_h(\boldsymbol{\xi}_j) D_h(\boldsymbol{\xi}_i - \mathbf{x}_j) h^3, \ \ \forall \boldsymbol{\mu}_h \in \Lambda_h(t), \mathbf{v}_h \in \mathbf{V}_{\mathbf{g}_{0h}(t)} \ \ or \ \mathbf{V}_{0h},$$

where $\{\mathbf{x}_j\}_{j=1}^{M}$ are the grid points of the finite elements for the velocity, and the function $D_h(\mathbf{X} - \mathbf{y})$ is defined as

$$D_h(\mathbf{X} - \mathbf{y}) = \delta_h(X_1 - y_1)\delta_h(X_2 - y_2)\delta_h(X_3 - y_3)$$

with $\mathbf{X} = (X_1, X_2, X_3)$ and $y = (y_1, y_2, y_3)$, and the one-dimensional discrete δ_h

defined by

$$\delta_h(z) = \begin{cases} \dfrac{1}{8h}\left(3 - \dfrac{2|z|}{h} + \sqrt{1 + \dfrac{4|z|}{h} - 4\left(\dfrac{|z|}{h}\right)^2}\right), & |z| \leq h, \\ \dfrac{1}{8h}\left(5 - \dfrac{2|z|}{h} - \sqrt{-7 + \dfrac{12|z|}{h} - 4\left(\dfrac{|z|}{h}\right)^2}\right), & h \leq |z| \leq 2h, \\ 0, & \textit{otherwise}. \end{cases}$$

2.3.3 Operator splitting scheme

To fully discretize the system (2.27)-(2.32), we first reduce it to a finite dimensional initial value problem using the above finite element spaces (after dropping most of the sub-scripts h's). Next, we use the Lie scheme [7] to decouple the above finite element analogue of system, (2.27)-(2.32), into a sequence of subproblems and apply the backward Euler schemes to time-discretize some of these subproblems.

First we consider the following initial value problem:

$$\begin{cases} \dfrac{d\phi}{dt} + A(\phi) = 0 on\ (0, T), \\ \phi(0) = \phi_0, \end{cases}$$

with $0 < T < +\infty$. We suppose that operator A has a decomposition such as $A = \sum_{j=1}^{J} A_j$ with $J \geq 2$.

Let $\tau > 0$ be a time-discretization step, we denote $n\tau$ by t^n. Let ϕ^n be an approximation of $\phi(t^n)$, we can write down the Lie's scheme as follows:

Given $\phi^0 = \phi_0$.

For $n \geq 0$, ϕ^n is known and we compute ϕ^{n+1} via

$$\begin{cases} \dfrac{d\phi}{dt} + A_j(\phi) = 0 on \ (t^n, t^{n+1}), \\ \phi(t^n) = \phi^{n+\frac{j-1}{J}}; \phi^{n+\frac{j}{J}} = \phi(t^{n+1}), \end{cases}$$

for $j = 1, \cdots, J$. Applying the Lie's scheme to the discrete analogue of the problem (2.27)-(2.32) and using backward Euler's method to some subproblems, we obtain the following algorithm:

Given $\mathbf{u}^0 = \mathbf{u}_{0h}, \mathbf{G}^0 = \mathbf{G}_0, \mathbf{V}^0 = \mathbf{V}_0, \boldsymbol{\omega}^0 = \boldsymbol{\omega}_0$.

For $n \geq 0$, $\mathbf{u}^n, \mathbf{G}^n, \mathbf{V}^n, \boldsymbol{\omega}^n$ are known, we compute $\mathbf{u}^{n+1}$, $\mathbf{G}^{n+1}$, $\mathbf{V}^{n+1}$, ω^{n+1} via the following steps.

1. We predict the position and the translation velocity of the center of mass at $t = t^{n+1}$as follows.

$$\frac{d\mathbf{G}}{dt} = \mathbf{V}(t), \tag{2.39}$$

$$M_p \frac{d\mathbf{V}}{dt} = \mathbf{0}, \tag{2.40}$$

$$\mathbf{I_p} \frac{d\boldsymbol{\omega}}{dt} = \mathbf{0}, \tag{2.41}$$

$$\mathbf{V}(t^n) = \mathbf{V}^n, \boldsymbol{\omega}(t^n) = \boldsymbol{\omega}^n, \mathbf{G}(t^n) = \mathbf{G}^n, \tag{2.42}$$

for $t^n < t < t^{n+1}$. Then set $\mathbf{V}^{n+\frac{1}{2}} = \mathbf{V}(t^{n+1})$, $\boldsymbol{\omega}^{n+\frac{1}{2}} = \boldsymbol{\omega}(t^{n+1})$, and $\mathbf{G}^{n+\frac{1}{2}} = \mathbf{G}(t^{n+1})$.

Now we get $B_h^{n+\frac{1}{2}}$ based on the center of particle $\mathbf{G}^{n+\frac{1}{2}}$.

2. We enforce the rigid body motion in $B_h^{n+\frac{1}{2}}$ and solve for $\mathbf{u}^{n+1}$ and p^{n+1} simultaneously as follows:

Find $\mathbf{u}^{n+1} \in \mathbf{V}_{\mathbf{g}_{0h}}^{n+1}$, $p^{n+1} \in L_{0h}^2$, $\boldsymbol{\lambda}^{n+1} \in \Lambda_h^{n+1}$, $\mathbf{V}^{n+} \in \mathbb{R}^3$, $\boldsymbol{\omega}^{n+1} \in \mathbb{R}^3$ such that

$$\begin{cases} -\displaystyle\int_\Omega p^{n+1}\nabla\cdot\mathbf{v}\,d\mathbf{x} + 2\mu_f\int_\Omega \nabla\mathbf{u}^{n+1} : \nabla\mathbf{v}\,d\mathbf{x} \\ +M_p\dfrac{\mathbf{V}^{n+1}-\mathbf{V}^{n+\frac{1}{2}}}{\Delta t}\cdot\mathbf{Y} + \mathbf{I}_p\dfrac{\boldsymbol{\omega}^{n+1}-\boldsymbol{\omega}^{n+\frac{1}{2}}}{\Delta t}\cdot\boldsymbol{\theta} \\ = \left(1-\dfrac{\rho_f}{\rho_s}\right)M_p\mathbf{g}\cdot\mathbf{Y} + \left\langle \boldsymbol{\lambda}^{n+1}, \mathbf{v}-\mathbf{Y}-\boldsymbol{\theta}\times\overrightarrow{\mathbf{G}^{n+\frac{1}{2}}\mathbf{x}}\right\rangle_{\Lambda_h^{n+\frac{1}{2}}}, \\ \forall\,(\mathbf{v},\mathbf{Y},\boldsymbol{\theta}) \in \mathbf{V}_{0h}\times\mathbb{R}^3\times\mathbb{R}^3, \end{cases} \tag{2.43}$$

$$\int_\Omega q\nabla\cdot\mathbf{u}^{n+1}\,d\mathbf{x} = 0, \quad \forall q \in L_h^2, \tag{2.44}$$

$$\left\langle \boldsymbol{\mu}, \mathbf{u}^{n+1} - \mathbf{V}^{n+1} - \boldsymbol{\omega}^{n+1}\times\overrightarrow{\mathbf{G}^{n+\frac{1}{2}}\mathbf{x}}\right\rangle_{\Lambda_h^{n+\frac{1}{2}}} = 0, \quad \forall\boldsymbol{\mu}\in\Lambda_h^{n+\frac{1}{2}}. \tag{2.45}$$

Finally, we set $\mathbf{G}^{n+1} = \mathbf{G}^{n+\frac{1}{2}}$.

In the above, $\mathbf{V}_{\mathbf{g}_{0h}}^{n+1} = \mathbf{V}_{\mathbf{g}_{0h}(t^{n+1})}$, $\Lambda_h^{n+\frac{1}{2}} = \Lambda_h(t^{n+\frac{1}{2}})$, and $B_h^{n+s} = B_h(t^{n+s})$.

2.4 On the solution of subproblems from operator splitting

2.4.1 Solution of the rigid body motion enforcement problems

In the system (2.43)-(2.45), there are two multipliers, p and $\boldsymbol{\lambda}$. We have solved this system via an Uzawa type conjugate gradient method [15] driven by both multipliers simultaneously. The general problem of system (2.43)-(2.45) is given as follows:

Find $\mathbf{u} \in \mathbf{V}_{\mathbf{g}_{0h}}$, $p \in L^2_{0h}$, $\boldsymbol{\lambda} \in \Lambda_h$, $\mathbf{V} \in \mathbb{R}^3$, $\boldsymbol{\omega} \in \mathbb{R}^3$ such that

$$\begin{cases} -\displaystyle\int_\Omega p\nabla \cdot \mathbf{v}\, d\mathbf{x} + \mu_f \int_\Omega \nabla \mathbf{u} : \nabla \mathbf{v}\, d\mathbf{x} + M_p \frac{\mathbf{V} - \mathbf{V}_0}{\triangle t} \cdot \mathbf{Y} \\ +\mathbf{I_p} \dfrac{\boldsymbol{\omega} - \boldsymbol{\omega}_0}{\triangle t} \cdot \boldsymbol{\theta} = \left(1 - \dfrac{\rho_f}{\rho_s}\right) M_p \mathbf{g} \cdot \mathbf{Y} + \left\langle \boldsymbol{\lambda}, \mathbf{v} - \mathbf{Y} - \boldsymbol{\theta} \times \overrightarrow{\mathbf{Gx}} \right\rangle_{\Lambda_h}, \\ \forall\ (\mathbf{v}, \mathbf{Y}, \boldsymbol{\theta}) \in \mathbf{V}_{0h} \times \mathbb{R}^3 \times \mathbb{R}^3, \end{cases} \tag{2.46}$$

$$\int_\Omega q\nabla \cdot \mathbf{u}\, d\mathbf{x} = 0, \quad \forall q \in L^2_h, \tag{2.47}$$

$$\left\langle \boldsymbol{\mu}, \mathbf{u} - \mathbf{V} - \boldsymbol{\omega} \times \overrightarrow{\mathbf{Gx}} \right\rangle_{\Lambda_h} = 0, \quad \forall \boldsymbol{\mu} \in \Lambda_h. \tag{2.48}$$

We solve the system, (2.46)-(2.48), by the following Uzawa type conjugate gradient algorithm operating in the space $L^2_{0h} \times \Lambda_h$:

Assume $p^0 \in L^2_{0h}$ and $\boldsymbol{\lambda}^0 \in \Lambda_h$ are given.

We solve the problem:

Find $\mathbf{u}^0 \in \mathbf{V}_{\mathbf{g}_{0h}}$, $\mathbf{V}^0 \in \mathbb{R}^3$, $\boldsymbol{\omega}^0 \in \mathbb{R}^3$ *satisfying*

$$\begin{cases} \mu_f \displaystyle\int_\Omega \nabla \mathbf{u}^0 : \nabla \mathbf{v}\, d\mathbf{x} = \int_\Omega p \nabla \cdot \mathbf{v}\, d\mathbf{x} + \left\langle \boldsymbol{\lambda}^0, \mathbf{v} \right\rangle_{\Lambda_h}, \\ \forall\ \mathbf{v} \in \mathbf{V}_{0h}; \mathbf{u}^0 \in \mathbf{V}_{\mathbf{g}_{0h}}, \end{cases} \tag{2.49}$$

$$M_p \frac{\mathbf{V}^0 - \mathbf{V}_0}{\triangle t} \cdot \mathbf{Y} = \left(1 - \frac{\rho_f}{\rho_s}\right) M_p \mathbf{g} \cdot \mathbf{Y} - \left\langle \boldsymbol{\lambda}^0, \mathbf{Y} \right\rangle_{\Lambda_h}, \quad \forall\ \mathbf{Y} \in \mathbb{R}^3, \tag{2.50}$$

$$\mathbf{I_p} \frac{\boldsymbol{\omega}^0 - \boldsymbol{\omega}_0}{\triangle t} \cdot \boldsymbol{\theta} = -\left\langle \boldsymbol{\lambda}^0, \boldsymbol{\theta} \times \overrightarrow{\mathbf{Gx}} \right\rangle_{\Lambda_h}, \quad \forall\ \boldsymbol{\theta} \in \mathbb{R}^3, \tag{2.51}$$

and then compute

$$\mathrm{g}_1^0 = \nabla \cdot \mathbf{u}^0; \tag{2.52}$$

next find $\mathbf{g}_2^0 \in \Lambda_h$ *satisfying*

$$\left\langle \boldsymbol{\mu}, \mathbf{g}_2^0 \right\rangle_{\Lambda_h} = \left\langle \boldsymbol{\mu}, \mathbf{u}^0 - \mathbf{V}^0 - \boldsymbol{\omega}^0 \times \overrightarrow{\mathbf{Gx}} \right\rangle_{\Lambda_h}, \quad \forall\ \boldsymbol{\mu} \in \Lambda_h, \tag{2.53}$$

and set

$$\mathrm{w}_1^0 = \mathrm{g}_1^0, \quad \mathbf{w}_2^0 = \mathbf{g}_2^0. \tag{2.54}$$

Then for $k \geq 0$, *assuming that* p^k, $\boldsymbol{\lambda}^k$, $\mathbf{u}^k$, $\mathbf{V}^k$, $\boldsymbol{\omega}^k$, $\mathrm{g}_1^{\mathrm{k}}$, $\mathbf{g}_2^k$, w_1^k *and* $\mathbf{w}_2^k$ *are known, compute* p^{k+1}, $\boldsymbol{\lambda}^{k+1}$, $\mathbf{u}^{k+1}$, $\mathbf{V}^{k+1}$, $\boldsymbol{\omega}^{k+1}$, $\mathrm{g}_1^{\mathrm{k+1}}$, $\mathbf{g}_2^{k+1}$, ${\mathrm{w}_1}^{k+1}$ *and* $\mathbf{w}_2^{k+1}$ *as follows:*

$$\begin{cases} \mu_f \displaystyle\int_\Omega \nabla \overline{\mathbf{u}}^k : \nabla \mathbf{v}\, d\mathbf{x} = \int_\Omega \mathrm{w}_1^k \nabla \cdot \mathbf{v}\, d\mathbf{x} + \left\langle \mathbf{w}_2^k, \mathbf{v} \right\rangle_{\Lambda_h}, \\ \forall\ \mathbf{v} \in \mathbf{V}_{0h}; \overline{\mathbf{u}}^k \in \mathbf{V}_{\mathbf{g}_{0h}}, \end{cases} \tag{2.55}$$

$$M_p \frac{\overline{\mathbf{V}}^k}{\triangle t} \cdot \mathbf{Y} = -\left\langle \mathbf{w}_2^k, \mathbf{Y} \right\rangle_{\Lambda_h}, \quad \forall\ \mathbf{Y} \in \mathbb{R}^3, \tag{2.56}$$

$$\mathbf{I_p} \frac{\overline{\boldsymbol{\omega}}^k}{\triangle t} \cdot \boldsymbol{\theta} = -\left\langle \mathbf{w}_2^k, \boldsymbol{\theta} \times \overrightarrow{\mathbf{Gx}} \right\rangle_{\Lambda_h}, \quad \forall\ \boldsymbol{\theta} \in \mathbb{R}^3, \tag{2.57}$$

and then compute

$$\overline{\mathrm{g}}_1^{\mathrm{k}} = \nabla \cdot \overline{\mathbf{u}}^{\mathrm{k}}; \tag{2.58}$$

next find $\overline{\mathbf{g}}_2^k \in \Lambda_h$ satisfying

$$\left\langle \boldsymbol{\mu}, \overline{\mathbf{g}}_2^k \right\rangle_{\Lambda_h} = \left\langle \boldsymbol{\mu}, \overline{\mathbf{u}}^k - \overline{\mathbf{V}}^k - \overline{\boldsymbol{\omega}}^k \times \overrightarrow{\mathbf{Gx}} \right\rangle_{\Lambda_h}, \quad \forall\ \boldsymbol{\mu} \in \Lambda_h, \tag{2.59}$$

and compute

$$\rho_k = \frac{\displaystyle\int_\Omega \left|\mathrm{g}_1^{\mathrm{k}}\right|^2 d\mathbf{x} + \left\langle \mathbf{g}_2^k, \mathbf{g}_2^k \right\rangle_{\Lambda_h}}{\displaystyle\int_\Omega \overline{\mathbf{g}}_1^k \mathrm{w}_1^k \, d\mathbf{x} + \left\langle \overline{\mathbf{g}}_2^k, \mathbf{w}_2^k \right\rangle_{\Lambda_h}}, \tag{2.60}$$

and

$$p^{k+1} = p^k - \rho_k {\mathrm{w}_1}^k, \tag{2.61}$$

$$\boldsymbol{\lambda}^{k+1} = \boldsymbol{\lambda}^k - \rho_k \mathbf{w}_2^k, \tag{2.62}$$

$$\mathbf{u}^{k+1} = \mathbf{u}^k - \rho_k \overline{\mathbf{u}}^k, \tag{2.63}$$

$$\mathbf{V}^{k+1} = \mathbf{V}^k - \rho_k \overline{\mathbf{V}}^k, \tag{2.64}$$

$$\boldsymbol{\omega}^{k+1} = \boldsymbol{\omega}^k - \rho_k \overline{\boldsymbol{\omega}}^k, \tag{2.65}$$

$$\mathrm{g}_1^{k+1} = \mathrm{g}_1^k - \rho_k \overline{\mathrm{g}}_1^k, \tag{2.66}$$

$$\mathbf{g}_2^{k+1} = \mathbf{g}_2^k - \rho_k \overline{\mathbf{g}}_2^k. \tag{2.67}$$

If

$$\frac{\displaystyle\int_{\Omega}\left|\mathrm{g}_1^{\mathrm{k+1}}\right|^2 d\mathbf{x}+\left\langle \mathbf{g}_2^{k+1},\mathbf{g}_2^{k+1}\right\rangle_{\Lambda_h}}{\displaystyle\int_{\Omega}\left|\mathrm{g}_1^{0}\right|^2 d\mathbf{x}+\left\langle \mathbf{g}_2^{0},\mathbf{g}_2^{0}\right\rangle_{\Lambda_h}}\leq\varepsilon, \tag{2.68}$$

then take $p = p^{k+1}$, $\boldsymbol{\lambda} = \boldsymbol{\lambda}^{k+1}$, $\mathbf{u} = \mathbf{u}^{k+1}$, $\mathbf{V} = \mathbf{V}^{k+1}$, *and* $\boldsymbol{\omega} = \boldsymbol{\omega}^{k+1}$. *Otherwise, compute*

$$\gamma_k=\frac{\displaystyle\int_{\Omega}\left|\mathrm{g}_1^{\mathrm{k+1}}\right|^2 d\mathbf{x}+\left\langle \mathbf{g}_2^{k+1},\mathbf{g}_2^{k+1}\right\rangle_{\Lambda_h}}{\displaystyle\int_{\Omega}\left|\mathrm{g}_1^{\mathrm{k}}\right|^2 d\mathbf{x}+\left\langle \mathbf{g}_2^{k},\mathbf{g}_2^{k}\right\rangle_{\Lambda_h}}, \tag{2.69}$$

and set

$$\mathrm{w}_1^{k+1}=\mathrm{g}_1^{k+1}+\gamma_k {\mathrm{w}_1}^{k}, \tag{2.70}$$

$$\mathbf{w}_2^{k+1}=\mathbf{g}_2^{k+1}+\gamma_k \mathbf{w}_2^{k}. \tag{2.71}$$

Then do $m = m + 1$ *and go back to* (2.55).

2.5 Numerical results

2.5.1 Rotation of a single particle

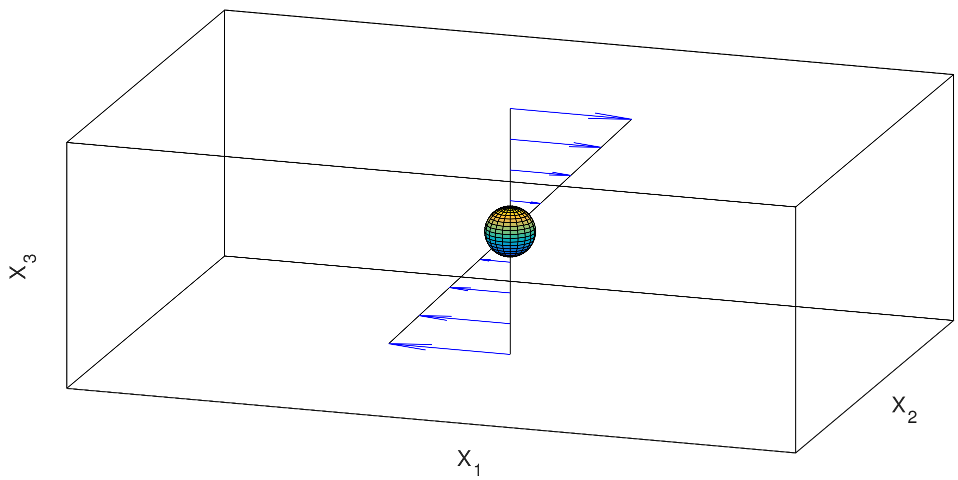

Figure 2.3: Single ball in a two-wall driven bounded shear flow.

We first have considered the cases of a single neutrally buoyant ball in a bounded shear flow of a Newtonian fluid. The ball is initially placed at the middle between two walls, and it remains there in simulation even though it can move freely in fluid. The computational domain is $\Omega = (-1, 1) \times (-1, 1) \times (-H/2, H/2)$ (i.e. $L_1 = 2$ and $L_2 = 2$) for different values of the height H. The ball radius is $a = 0.15$ and its mass center is initially located at (0,0,0). The blockage ratio is defined by $K = 2a/H$. The shear rate $\dot{\gamma} = 1$ so the velocity of the top wall is $U = H/2$ and that of the bottom wall is $-U = -H/2$. The fluid and particle densities are $\rho_f = \rho_s = 1$ and the fluid viscosity is $\mu = 1$. The mesh sizes for the velocity field is $h = 1/48$ or $1/64$ and the mesh size for the pressure is $2h$, the time step is $\Delta t = 0.001$. For all the numerical simulations considered in this section, we assume that all dimensional quantities are in the CGS (centimeter, gram, and second) units.

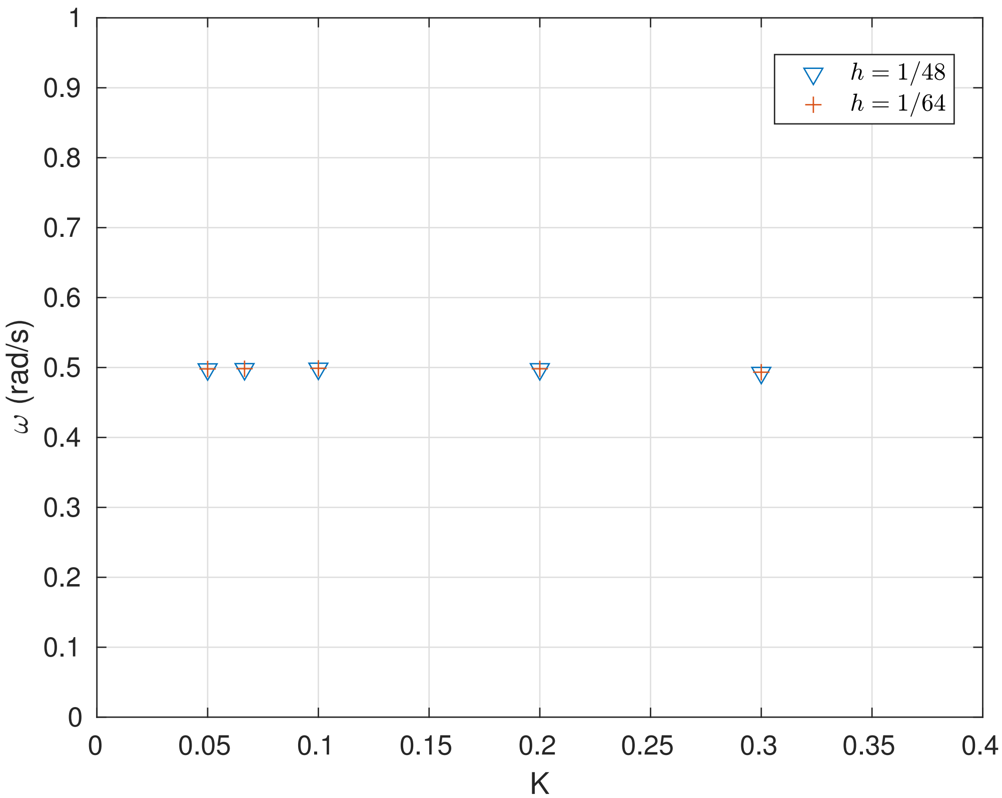

Figure 2.4: The rotating speed with respect to the blockage ratio K for two different mesh sizes. K is a dimensionless number.

Under creeping conditions, the rotating velocity of the ball with respect to the x_2-axis (see Figure 2.3) is $\dot{\gamma}/2 = 0.5$ in an unbounded shear flow in a Newtonian fluid, according to the associated Jeffery's solution [22]. In Figure2.4, the ball rotating velocities have been shown for different values of the blockage ratio. Our numerical results are in a good agreement with the Jeffery's solution for most values of the blockage ratio; but we can observe the wall influence on the rotating velocity for the largest value of the blockage ratio, $K = 0.3$, in Figure2.4.

2.5.2 Sedimentation of a single particle

In this section we have considered the terminal speed of a sedimenting ball in a vertical channel of infinite length fill led with a Newtonian fluid. The computational domain is $\Omega = (-1, 1) \times (-1, 1) \times (-1, 1)$. The ball radius is $a = 0.1$ and its mass center is initially located at (0,0,0). The fluid and particle densities are $\rho_f = 1$, $\rho_s = 1.5$, the fluid viscosity being $\mu = 1$. The mesh sizes for the velocity field is $h = 1/48$, $1/64$, or $1/80$ and the mesh size for the pressure is $2h$, the time step is $\Delta t = 0.001$. We have validated our numerical results (see Table 2.1) with the theoretical solution, e.g., in [18]. The terminal speed V of a segmenting ball in fluid is given by the following formula which is derived from Stokes' law:

$$V = \frac{2}{9}\frac{\rho_s - \rho_f}{\mu} g a^2 \tag{2.72}$$

where g is gravity. So for our case the terminal velocity is -1.0896 cm/sec.

Mesh Size h (cm)	Terminal Speed(cm/sec)	
	Collocation Method	Immersed Boundary Method
1/48	-1.0147	-0.9495
1/64	-1.0558	-0.9919
1/80	-1.0662	-1.0151

Table 2.1: The terminal speed in an infinite length vertical channel for two methods with three different mesh sizes.

2.5.3 Two balls interaction in an one-wall driven bounded shear flow

In this section, we consider the case of two balls of the same size interacting in an one wall-driven bounded shear flow fluid as visualized in Figure 2.5. The ball radii are $r = 0.1$. The fluid and ball densities are $\rho_f = \rho_s = 1$, the viscosity is $\mu = 1$. The computational domain is $\Omega = (-1.5, 1.5) \times (-1, 1) \times (-0.5, 0.5)$ (i.e. $L_1 = 3$, $L_2 = 2$, and $L_3 = 1$). The shear rate is fixed at $\dot{\gamma} = 1$ so the velocity of the top wall is $U = 1.0$, the bottom wall is $U = 0$. The mass centers of the two balls are initially located on the shear plane at $(-d_0, 0, \triangle s)$ and $(d_0, 0, -\triangle s)$, where $\triangle s$ varies and d_0 is 0.5. The mesh size for the velocity field is $h = 1/48$, the mesh size for the pressure is $2h$, The time step being $\triangle t = 0.001$. Then we consider six dimensionless initial vertical displacements $D = \triangle s/a$= 1, 0.5, 0.316,0.255, 0.194, and 0.122.

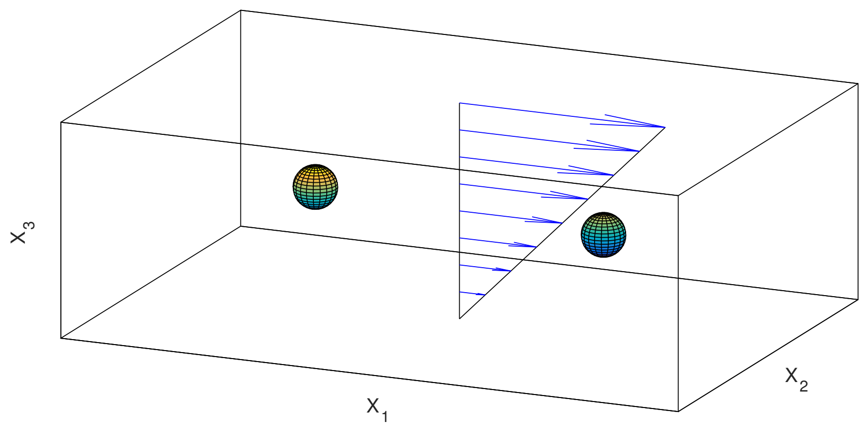

Figure 2.5: Two balls in an one wall driven shear flow.

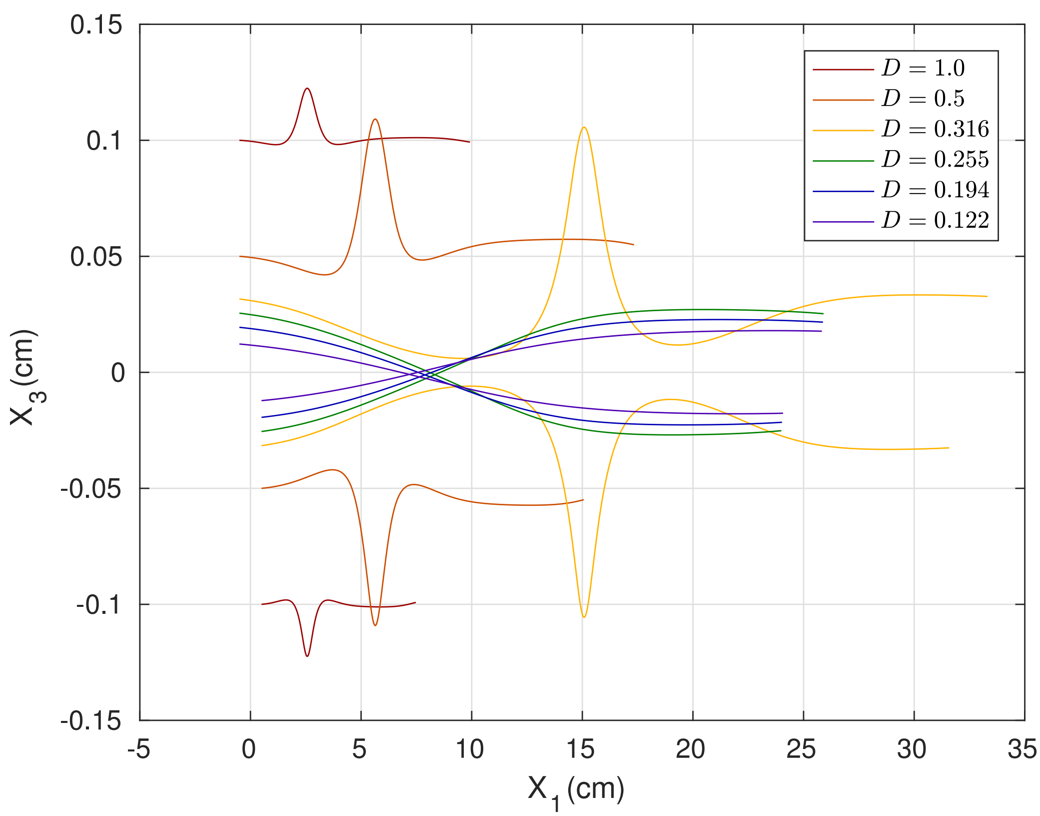

Figure 2.6: Trajectories of the ball mass center in an one wall driven shear flow: (a) the balls pass over/under for vertical displacements D = 1, 0.5, 0.316, and (b) the balls swap for vertical displacements D = 0.255, 0.194, and 0.122. D is a dimensionless number.

When two balls move in a bounded shear flow of a Newtonian fluid at Stokes regime with $D = 0.122$, 0.194, 0.255, 0.316, 0.5, 1 as in Figure 2.5, the higher ball takes over the lower one and then both return to their initial heights for those large vertical displacements $D = 1$, 0.5, and 0.316. These two particle paths are called pass (or open) trajectories. For $D = 0.255$, 0.194, and 0.122, the trajectories of two balls go cross and lead an exchange of vertical positions of two balls as in Figure 2.6. These two particle paths are called swapping.

2.5.4 Two balls interaction in a two-wall driven bounded shear flow

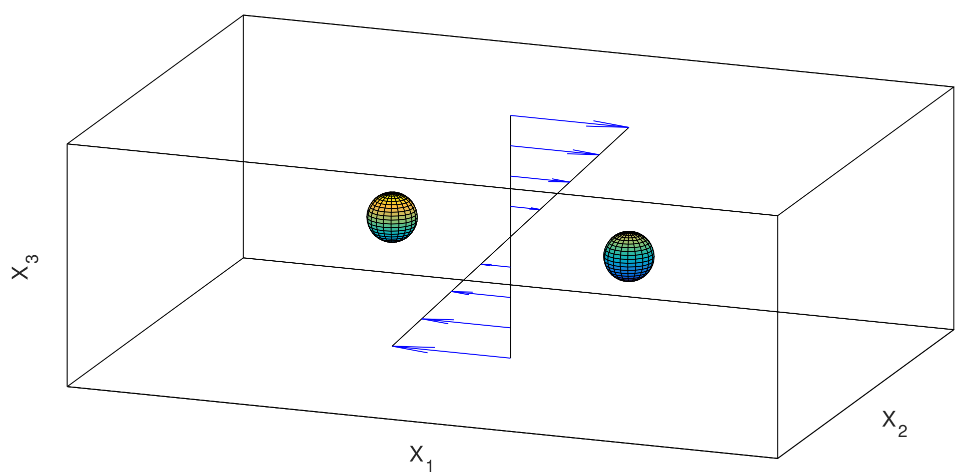

Figure 2.7: Two balls in a two wall driven shear flow.

In this section, we consider the cases of two balls of the same size interacting in a two-wall driven bounded shear flow fluid as visualized in Figure 2.7. The setup is the same as the one-wall driven case except for the velocity setting. For a two-wall driven bounded shear flow, the velocity of top wall is $U = 0.5$, and the bottom wall is $U = -0.5$. We have considered six different initial vertical displacements D= 1, 0.5, 0.316, 0.255, 0.194, and 0.122. The trajectories with respect to D are shown in Figure 2.8.

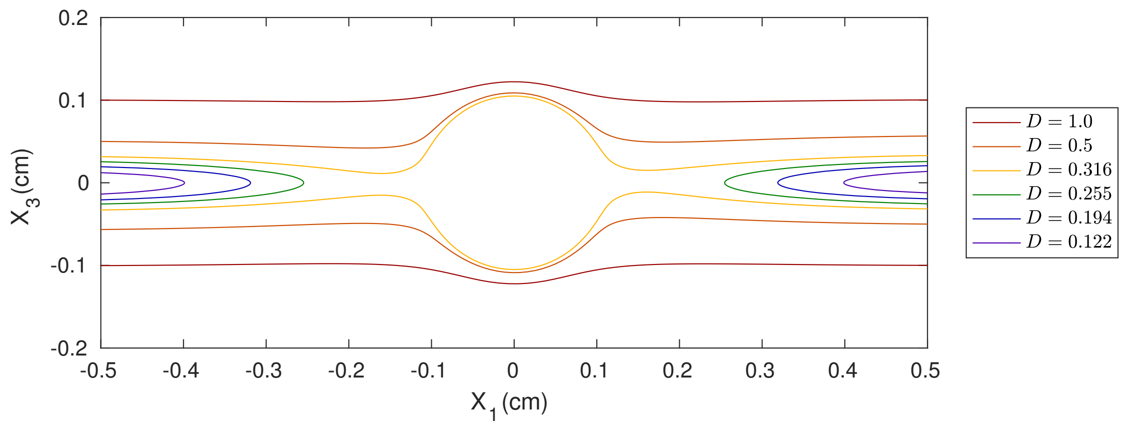

Figure 2.8: Trajectories of the ball mass center in a two wall driven shear flow: (a) the balls pass over/under for vertical displacements D = 1, 0.5, 0.316, and (b) the balls has return trajectories for vertical displacements D = 0.255, 0.194, and 0.122. D is a dimensionless number.

In Figure 2.8, the outer three pair trajectories are called passing over motion for D =1, 0.5, and 0.316. The higher ball goes from left to right and the lower ball goes from right to left and then both return to their initial heights. The inner three pair trajectories are called swapping or return motion for D = 0.255, 0.194, and 0.122. Two balls first approach each other and go cross the mid-plane $X_2 = 0$ then repel and reverse, respectively. Their trajectories are called return trajectories.

To link the computed trajectories in an one-wall driven shear flow mentioned in section 2.5.3 to those of two balls having the same initial configuration and moving in a two-wall driven shear flow with the same shear rate, we have plotted in Figure 2.9 the relative trajectories of the two-ball mass center via the graphs of $(x_{i,1} - \bar{x}_1, x_{i,3} - \bar{x}_3)$, for i =1, 2, the mass center of the two balls is $\mathbf{x}_i = (x_{i,1}, x_{i,2}, x_{i,3})$, i =1, 2; the midpoint between two ball mass center $\mathbf{x}_1$ and $\mathbf{x}_2$ is $\bar{\mathbf{x}} = \frac{1}{2}(\mathbf{x}_1 + \mathbf{x}_2) = (\bar{x}_1, \bar{x}_2, \bar{x}_3)^t$.

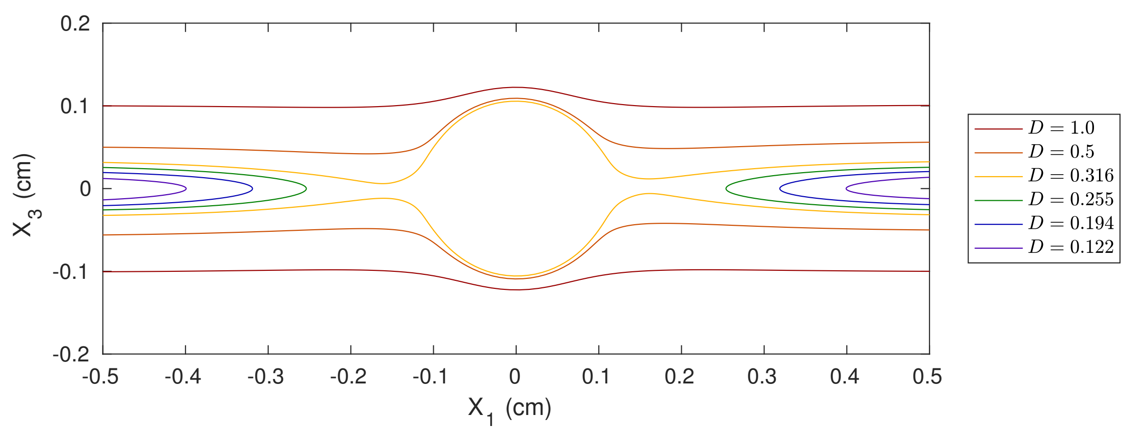

Figure 2.9: The relative trajectories of the ball mass center in an one wall driven shear flow: (a) the balls pass over/under for vertical displacements D = 1, 0.5, 0.316, and (b) the balls swap for vertical displacements D = 0.255, 0.194, and 0.122. D is a dimensionless number.

In Figure 2.9, the ball trajectories agree very well for both kinds of shear flow. It is worth mentioning that the ball trajectories visualized in Figure 2.9 closely resemble those reported in the Figure 3(b) of [42]. Actually these trajectories also resemble the streamlines around a freely suspended rotating ball (a torque-free ball) of the same radius centered at $(0, 0, 0)$ in a two-wall driven shear flow (e.g., see Figure 5.(b) of [42]). Thus, it is not surprising that there is circulation upstream and downstream from the ball centered at the origin due to the blockage of the ball and the existence of the two walls. Then, the swapping is exactly the motion of the two balls following the circulation upstream and downstream in a two-wall driven shear flow.

CHAPTER 3

Three-dimensional DLM/FD methods for simulating the motion of spheres in bounded shear flows of Oldroyd-B fluids

3.1 Several models of non-Newtonian fluid

3.1.1 Stokes equations

Consider the Stokes equations in $\Omega \times (0, T)$ describing a three-dimensional motion of an incompressible viscous fluid:

$$\begin{cases} -\nabla \cdot \sigma = \rho_f \mathbf{g}, \\ \nabla \cdot \mathbf{u} = 0. \end{cases} \tag{3.1}$$

where $\sigma = -p\mathbf{I} + \boldsymbol{\tau}$ with pressure, p, and stress tensor, $\boldsymbol{\tau}$, $\mathbf{u} = (u_1, u_2, u_3)$ is the flow velocity, $\mathbf{g}$ is the gravity, and ρ_f is the density of the fluid.

3.1.2 Newtonian model

The constitutive equation of the stress tensor is given by

$$\boldsymbol{\tau} = 2\mu\mathbf{D}(\mathbf{u}) \tag{3.2}$$

where μ is the fluid viscosity of the fluid and $\mathbf{D}(\mathbf{u})$ is the symmetric rate of strain tensor

$$2\mathbf{D}(\mathbf{u}) = \nabla\mathbf{u} + (\nabla\mathbf{u})^t, \tag{3.3}$$

with the Jacobian of the velocity, $\nabla\mathbf{u}$.

3.1.3 The UCM-model

In the Upper-Convected Maxwell model (UCM-model) (e.g., see [23]), the following constitutive equation was used to describe the viscoelastic stress tensor $\boldsymbol{\tau}_E$:

$$\lambda_1 \overset{\triangledown}{\boldsymbol{\tau}}_E + \boldsymbol{\tau}_E = 2\eta\mathbf{D}(\mathbf{u}), \tag{3.4}$$

where $\overset{\triangledown}{\boldsymbol{\tau}}_E$ is the upper-convected time derivative of $\boldsymbol{\tau}_E$ and defined by

$$\overset{\triangledown}{\boldsymbol{\tau}}_E = \frac{\partial \boldsymbol{\tau}_E}{\partial t} + (\mathbf{u} \cdot \nabla)\boldsymbol{\tau}_E - \boldsymbol{\tau}_E(\nabla\mathbf{u})^t - (\nabla\mathbf{u})\boldsymbol{\tau}_E, \tag{3.5}$$

where λ_1 is the relaxation time of the fluid, and η is the elastic viscosity of the fluid.

So, we have the constitutive equation for the UCM-model

$$\frac{\partial \boldsymbol{\tau}_E}{\partial t} + (\mathbf{u} \cdot \nabla)\boldsymbol{\tau}_E - \boldsymbol{\tau}_E(\nabla \mathbf{u})^t - (\nabla \mathbf{u})\boldsymbol{\tau}_E + \frac{1}{\lambda_1}\boldsymbol{\tau}_E = \frac{2\eta}{\lambda_1}\mathbf{D}(\mathbf{u}). \tag{3.6}$$

3.1.4 The Oldroyd-B model

In the more general model of Oldroyd-B fluid, we have considered the elastic-viscous split stress (EVSS) approach [35] in which the stress tensor $\boldsymbol{\tau}$ is split into a Newtonian component $\boldsymbol{\tau}_s$ and a viscoelastic component $\boldsymbol{\tau}_E$, i.e.

$$\boldsymbol{\tau} = \boldsymbol{\tau}_s + \boldsymbol{\tau}_E, \tag{3.7}$$

and $\boldsymbol{\tau}_s$ is governed by a Newtonian constitutive equation $\boldsymbol{\tau}_s = 2\mu\mathbf{D}(\mathbf{u})$, and $\boldsymbol{\tau}_E$ satisfies the UCM constitutive equation (3.6). Thus, the Oldroyd-B model can be seen as a linear combination of the UCM and the Newtonian models:

$$\begin{cases} -\nabla \cdot \sigma = \rho_f \mathbf{g}, \\ \nabla \cdot \mathbf{u} = 0, \\ \lambda_1 \overset{\nabla}{\boldsymbol{\tau}}_E + \boldsymbol{\tau}_E = 2\eta\mathbf{D}(\mathbf{u}), \end{cases} \tag{3.8}$$

where $\sigma = -p\mathbf{I} + \boldsymbol{\tau}_s + \boldsymbol{\tau}_E$. Therefore, equation (3.9) can be written more explicitly as follows:

$$\begin{cases} \nabla p - 2\mu\nabla\cdot\mathbf{D}(\mathbf{u}) - \nabla\cdot\boldsymbol{\tau}_E = \rho_f\mathbf{g}, \\ \nabla\cdot\mathbf{u} = 0, \\ \lambda_1\overset{\nabla}{\boldsymbol{\tau}}_E + \boldsymbol{\tau}_E = 2\eta\mathbf{D}(\mathbf{u}), \end{cases} \tag{3.9}$$

Remark 3.1. Using the definition of conformation tenser $\mathbf{C} = \dfrac{\lambda_1}{\eta}\boldsymbol{\tau}_E + \mathbf{I}$, we obtain the Oldroyd-B model in terms of $\mathbf{C}$:

$$\begin{cases} \nabla p - 2\mu\nabla\cdot\mathbf{D}(\mathbf{u}) - \dfrac{\eta}{\lambda_1}\nabla\cdot(\mathbf{C}-\mathbf{I}) = \rho_f\mathbf{g}, \\ \nabla\cdot\mathbf{u} = 0, \\ \dfrac{\partial\mathbf{C}}{\partial t} + (\mathbf{u}\cdot\nabla)\mathbf{C} - (\nabla\mathbf{u})\mathbf{C} - \mathbf{C}(\nabla\mathbf{u})^t + \dfrac{1}{\lambda_1}\mathbf{C} = \dfrac{1}{\lambda_1}\mathbf{I}, \end{cases} \tag{3.10}$$

and

$$\eta = \eta_1\left(1 - \frac{\lambda_2}{\lambda_1}\right), \tag{3.11}$$

$$\mu = \eta_1 - \eta, \tag{3.12}$$

where η is the fluid elastic viscosity, μ is the solvent viscosity, η_1 is the dynamic fluid viscosity, λ_1 is the relaxation time of the fluid, λ_2 is retardation time, and $\mathbf{I}$ is the identity matrix. The conformation tensor $\mathbf{C}$ is symmetric and positive definite (see [23]).

3.1.5 The Carreau model

We also consider Oldroyd-B fluids with the property of shear-thinning. In Oldroyd-B model, the fluid viscosity η_1 is constant in the given domain. To have a shear-thinning effect in an Oldroyd-B model, the Carreau model [4] has been considered. Under the Carreau model, the fluid viscosity $\eta_1(\dot{\gamma_e})$ depends on the fluid velocity and is defined by

$$\eta_1(\dot{\gamma_e}) = \frac{\eta_1}{\left(1 + (\lambda_1 \dot{\gamma_e})^2\right)^{\frac{1-n}{2}}}, \tag{3.13}$$

where η_1 is the fluid viscosity without shear thinning, $\dot{\gamma_e} = \sqrt{2\mathbf{D}(\mathbf{u}) : \mathbf{D}(\mathbf{u})}$ and n is a positive number less than 1. Then, the Oldroyd-B model with the property of shear-thinning is given by

$$\begin{cases} \nabla p - 2\mu \nabla \cdot \mathbf{D}(\mathbf{u}) - \nabla \cdot \left(\dfrac{\eta}{\lambda_1} (\mathbf{C} - \mathbf{I}) \right) = \rho_f \mathbf{g}, \\ \nabla \cdot \mathbf{u} = 0, \\ \dfrac{\partial \mathbf{C}}{\partial t} + (\mathbf{u} \cdot \nabla)\mathbf{C} - (\nabla \mathbf{u})\mathbf{C} - \mathbf{C}(\nabla \mathbf{u})^t + \dfrac{1}{\lambda_1}\mathbf{C} = \dfrac{1}{\lambda_1}\mathbf{I}, \end{cases} \tag{3.14}$$

3.2 DLM/FD methods for simulating fluid-particle interaction in Stokes flow

3.2.1 The governing equations

Fictitious domain formulations using distributed Lagrange multiplier for flow around freely moving particles at finite Reynolds numbers and their associated computational methods have been developed and tested in, e.g., [15, 16, 14, 27, 28, 26, 29]. For the cases of a neutrally buoyant particle in two-dimensional fluid flows of a Newtonian fluid at the Stokes regime, a similar DLM/FD method has been developed and validated in [31]. In this section, we discuss first the formulation of a ball and then the associated numerical treatments for simulating its motion in a three-dimensional bounded shear flow of Oldroyd-B fluids. Let $\Omega \subset \mathbb{R}^3$ be a rectangular parallelepiped filled with an Oldroyd-B fluid and containing N freely moving rigid spheres B_i centered at $\mathbf{G}_i = \{G_{i1}, G_{i2}, G_{i3}\}^t$ for $i = 1, 2, \cdots, N$.

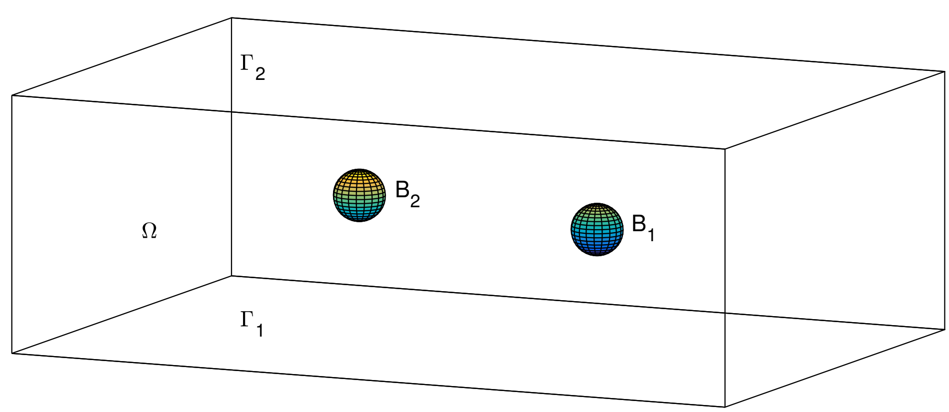

Figure 3.1: An example of a region Ω with two spheres.

Let ρ_f be the density of a viscoelasic fluid of Oldroyd-B type and ρ_s be density of particles. Let $B(t) = \bigcup_{i=1}^{N} B_i(t)$.We denote by $\gamma_i(t)$ the boundary $\partial B_i(t)$ of $B_i(t)$ for $i = 1, 2, \cdots, N$ and let $\gamma(t) = \bigcup_{i=1}^{N} \gamma_i(t)$.

For some $T > 0$, the governing equations for the fluid-particles system are as follows:

For the fluid flow, the Stokes equations for the Oldroyd-B model are

$$\nabla p - 2\mu\nabla \cdot \mathbf{D}(\mathbf{u}) - \frac{\eta}{\lambda_1}\nabla \cdot (\mathbf{C} - \mathbf{I}) = \rho_f \mathbf{g} \quad in\ \Omega \setminus \overline{B(t)}, t \in (0, T), \tag{3.15}$$

$$\nabla \cdot \mathbf{u} = 0 \quad in\ \Omega \setminus \overline{B(t)}, t \in (0, T), \tag{3.16}$$

$$\mathbf{u} = \mathbf{g_0} \quad on\ \Gamma \times (0, T), with\ \int_\Gamma \mathbf{g_0} \cdot \mathbf{n} d\Gamma = 0, \tag{3.17}$$

$$\mathbf{u}(\mathbf{x}, t) = \mathbf{V}_i(t) + \boldsymbol{\omega}_i(t) \times \overrightarrow{\mathbf{G}_i(t)\mathbf{x}}, \quad \forall \mathbf{x} \in \gamma_i(t),\ i = 1, 2, \cdots, N, \tag{3.18}$$

$$\frac{\partial \mathbf{C}}{\partial t} + (\mathbf{u} \cdot \nabla)\mathbf{C} - (\nabla \mathbf{u})\mathbf{C} - \mathbf{C}(\nabla \mathbf{u})^t + \frac{1}{\lambda_1}\mathbf{C} = \frac{1}{\lambda_1}\mathbf{I} \quad in\ \Omega \setminus \overline{B(t)}, t \in (0, T), \tag{3.19}$$

$$\mathbf{C}(\mathbf{x}, 0) = \mathbf{C}_0(\mathbf{x}), \quad \mathbf{x} \in \Omega \setminus \overline{B(0)}, \tag{3.20}$$

$$\mathbf{C} = \mathbf{C}_L \quad on\ \Gamma^-, \tag{3.21}$$

where $\mathbf{u}$ is the flow velocity, p is the pressure, $\mathbf{D}(\mathbf{u}) = (\nabla\mathbf{u} + (\nabla\mathbf{u})^{\mathbf{t}})/\mathbf{2}$ is the rate of deformation tensor, $\mathbf{C}$ is the conformation tensor, $\mu = \eta_1\lambda_2/\lambda_1$ is the solvent viscosity of fluid, ρ_f is the density of fluid, $\mathbf{g}$ denotes gravity, $\eta = \eta_1 - \mu$ is the elastic fluid viscosity, η_1 is the fluid viscosity λ_1 is the relaxation time of the fluid, λ_2 is the retardation time of the fluid. In (3.17), Γ is the union of the bottom boundary Γ_1 and top boundary Γ_2 as in Figure 3.1 and $\mathbf{n}$ is the unit normal vector pointing outward to the flow region, and $\Gamma^-(t)$ in (3.21) being the upstream portion of Γ at time t. The boundary conditions given in (3.17) are $\mathbf{g}_0 = \{-U, 0, 0\}^t$ on Γ_1 and $\mathbf{g}_0 = \{U, 0, 0\}^t$ on Γ_2 for a bounded shear flow. We assume also that the flow is periodic in the x_1 and x_2 directions with the periods L_1 and L_2, respectively, and in (3.18), a no-slip condition takes place on the boundary of particles $\gamma(t)$, namely

$$\mathbf{u}(\mathbf{x}, t) = \mathbf{V}_i(t) + \boldsymbol{\omega}_i(t) \times \overrightarrow{\mathbf{G}_i(t)\mathbf{x}}, \quad \forall \mathbf{x} \in \gamma_i(t),\ i = 1, 2, \cdots, N, \tag{3.22}$$

where $\mathbf{V}_i$ is the translation velocity, $\boldsymbol{\omega}_i$ is the angular velocity, $\mathbf{G}_i$ is the center of mass and $\mathbf{x}$ is a point on the surface of the particle with $\overrightarrow{\mathbf{G}_i(t)\mathbf{x}} = \{x_1 - G_{i,1}(t), x_2 - G_{i,2}(t), x_3 - G_{i,3}(t)\}^t$.

The motion of particle satisfies the following Euler-Newton's equations:

$$\mathbf{v}_i(\mathbf{x}, t) = \mathbf{V}_i(t) + \boldsymbol{\omega}_i(t) \times \overrightarrow{\mathbf{G}_i(t)\mathbf{x}}, \quad \forall \{\mathbf{x}, t\} \in \overline{B_i(t)} \times (0, T),\ i = 1, 2, \cdots, N, \tag{3.23}$$

$$\frac{\mathrm{d}\mathbf{G}_i}{\mathrm{d}t} = \mathbf{V}_i, \tag{3.24}$$

$$M_{p,i}\frac{\mathrm{d}\mathbf{V}_i}{\mathrm{d}t} = M_i\mathbf{g} + \mathbf{F}_i, \tag{3.25}$$

$$\frac{\mathrm{d}(\boldsymbol{I}_{p,i}\boldsymbol{\omega}_i)}{\mathrm{d}t} = \mathbf{T}_i, \tag{3.26}$$

$$\mathbf{G}_i(0) = \mathbf{G}_i^0,\ \mathbf{V}_i(0) = \mathbf{V}_i^0,\ \boldsymbol{\omega}_i(0) = \boldsymbol{\omega}_i^0, \tag{3.27}$$

for $i = 1, 2, \cdots, N$, where $M_{p,i}$ and $\mathbf{I}_{p,i}$ are the mass and the moment of inertia of the i-th particle, respectively; $\mathbf{F}_i$ and $\mathbf{T}_i$ are the hydrodynamic force and torque imposed on the i-th particle by the fluid. In equations (3.25) and (3.26), the hydrodynamic force, $\mathbf{F}_i$, and torque, $\mathbf{T}_i$ imposed on the i-th particle by the fluid are given by

$$\mathbf{F}_i = -\int_{\gamma_i} \sigma \mathbf{n} \, \mathrm{d}\gamma, \quad \mathbf{T}_i = -\int_{\gamma_i} \overrightarrow{\mathbf{G}_i \mathbf{x}} \times \sigma \mathbf{n} \, \mathrm{d}\gamma. \tag{3.28}$$

3.2.2 DLM/FD formulation

To obtain a distributed Lagrange multiplier/fictitious domain formulation for the above problem (3.15)-(3.28), we proceed as in [15, 16], namely: (i) we derive a global variational formulation of the virtual power type of problem (3.15)-(3.28), (ii) we then fill the region occupied by the rigid body by the surrounding fluid (i.e. embed $\Omega \setminus \overline{B(t)}$ in Ω) with the constraint that the fluid inside the rigid body region has a rigid body motion, and then (iii) we relax the rigid body motion constraint by using a distributed Lagrange multiplier, obtaining the following fictitious domain formulation over the entire region Ω.

For convenience of derivation, we assume there is only one ball in the fluid, $B(t)$ is a solid ball in the fluid, $\gamma(t)$ is the boundary of $B(t)$, and $\mathbf{G}(t)$ is the center of mass of this ball. In the equations of the motion of particle (3.15)-(3.21), we set $\mathbf{V}$, the translation velocity of the particle, $\boldsymbol{\omega}$ the angular velocity of the particle, M_p and $\mathbf{I_p}$ the mass and the moment of inertia of the particle, respectively; $\mathbf{F}$ and $\mathbf{T}$ the hydrodynamic force and torque imposed on the particle $B(t)$ by the fluid, respectively.

To obtain a variational formulation for above problem (3.15)-(3.21), we define the following function spaces

$$\mathbf{W}_{\mathbf{g}_0}(t) = \{\mathbf{v}|\mathbf{v} \in (H^1(\Omega \setminus \overline{B(t)}))^3,\ \mathbf{v} = \mathbf{V}(t) + \boldsymbol{\omega}(t) \times \overrightarrow{\mathbf{G}(t)\mathbf{x}} \quad on\ \partial B(t),$$
$$\mathbf{v} = \mathbf{g}_0(t) \quad \text{on}\, \Gamma,\ \mathbf{v} \text{ is periodic in the } x_1 \text{ and } x_2 \text{ directions with}$$
$$\text{periods } L_1 \text{ and } L_2\text{, respectively}\},$$

$$\mathbf{W}_0(t) = \{(\mathbf{v}, \mathbf{Y}, \boldsymbol{\theta})|(\mathbf{v}, \mathbf{Y}, \boldsymbol{\theta}) \in (H^1(\Omega \setminus \overline{B(t)}))^3 \times \mathbb{R}^3 \times \mathbb{R}^3, \mathbf{v} = 0 \quad \text{on}\, \Gamma,$$
$$\mathbf{v} = \mathbf{Y} + \boldsymbol{\theta} \times \overrightarrow{\mathbf{G}(t)\mathbf{x}} \quad on\ \partial B(t),\ \mathbf{v} \text{ is periodic in the } x_1 \text{ and } x_2$$
$$\text{directions with periods } L_1 \text{ and } L_2\text{, respectively}\},$$

$$L_0^2(\Omega \setminus \overline{B(t)}) = \left\{ q \,\middle|\, q \in L^2(\Omega \setminus \overline{B(t)}), \int_{\Omega \setminus \overline{B(t)}} q \, \mathrm{d}\mathbf{x} = 0 \right\},$$

and

$$\mathbf{W}(\Omega \setminus \overline{B(t)}) = \left\{ \mathbf{A} \,\middle|\, \mathbf{A} = [a_{ij}] \in M_{3\times 3}, a_{ij} \in H^1(\Omega \setminus \overline{B(t)}), i, j = 1, 2, 3 \right\},$$

$$\mathbf{W}_{\mathbf{C}_L}(\Omega \setminus \overline{B(t)}) = \left\{ \mathbf{A} \,\middle|\, \mathbf{A} \in \mathbf{W}(\Omega \setminus \overline{B(t)}), \mathbf{A} = \mathbf{C}_L(t)\ on\, \Gamma^- \right\},$$

$$\mathbf{W}_{\mathbf{C}_0}(\Omega \setminus \overline{B(t)}) = \left\{ \mathbf{A} \,\middle|\, \mathbf{A} \in \mathbf{W}(\Omega \setminus \overline{B(t)}), \mathbf{A} = \mathbf{0}\ on\, \Gamma^- \right\}.$$

The variational formulation of the system (3.15) – (3.21) is as follows:

For a.e. $t \in (0, T)$, find $\mathbf{u}(t) \in \mathbf{W}_{\mathbf{g}_0}(t)$, $p(t) \in L_0^2(\Omega \setminus \overline{B(t)})$, $\mathbf{C}(t) \in \mathbf{W}_{\mathbf{C}_L}$,$\mathbf{V}(t) \in \mathbb{R}^3$,

$\mathbf{G}(t) \in \mathbb{R}^3$, $\boldsymbol{\omega}(t) \in \mathbb{R}^3$, such that

$$\begin{cases} -\displaystyle\int_{\Omega\setminus\overline{B(t)}} p\nabla\cdot\mathbf{v}\mathrm{d}\mathbf{x} + 2\mu\int_{\Omega\setminus\overline{B(t)}} \mathbf{D}(\mathbf{u}):\mathbf{D}(\mathbf{v})\mathrm{d}\mathbf{x} \\ \quad -\dfrac{\eta}{\lambda_1}\displaystyle\int_{\Omega\setminus\overline{B(t)}} \mathbf{v}\cdot(\nabla\cdot(\mathbf{C}-\mathbf{I}))\mathrm{d}\mathbf{x} + \left(M_p\dfrac{\mathrm{d}\mathbf{V}}{\mathrm{d}t} - M_p\mathbf{g}\right)\cdot\mathbf{Y} \\ \quad +\dfrac{\mathrm{d}\left(\mathbf{I_p}\boldsymbol{\omega}\right)}{\mathrm{d}t}\cdot\boldsymbol{\theta} = \rho_f\displaystyle\int_{\Omega\setminus\overline{B(t)}} \mathbf{g}\cdot\mathbf{v}\,\mathrm{d}\mathbf{x} \quad \forall(\mathbf{v},\mathbf{Y},\boldsymbol{\theta})\in\mathbf{W}_0(t). \end{cases} \tag{3.29}$$

$$\int_{\Omega\setminus\overline{B(t)}} q\nabla\cdot\mathbf{u}\,\mathrm{d}\mathbf{x} = 0, \quad \forall q \in L^2(\Omega\setminus\overline{B(t)}), \tag{3.30}$$

$$\begin{cases} \displaystyle\int_{\Omega\setminus\overline{B(t)}} \left(\dfrac{\partial\mathbf{C}}{\partial t} + (\mathbf{u}\cdot\nabla)\mathbf{C} - (\nabla\mathbf{u})\mathbf{C} - \mathbf{C}(\nabla\mathbf{u})^t + \dfrac{1}{\lambda_1}\mathbf{C}\right):\mathbf{s}\,\mathrm{d}\mathbf{x} \\ \quad = \dfrac{1}{\lambda_1}\displaystyle\int_{\Omega\setminus\overline{B(t)}} \mathbf{I}:\mathbf{s}\,\mathrm{d}\mathbf{x}, \quad \forall\mathbf{s}\in\mathbf{W}, \end{cases} \tag{3.31}$$

$$\frac{\mathrm{d}\mathbf{G}}{\mathrm{d}t} = \mathbf{V}, \tag{3.32}$$

$$\mathbf{u}(\mathbf{x},0) = \widetilde{\mathbf{u}}_0(\mathbf{x}) = \begin{cases} \mathbf{u}_0(\mathbf{x}), \quad \forall\mathbf{x}\in\Omega\setminus\overline{B(0)}, \\ \mathbf{V}_0 + \boldsymbol{\omega}_0\times\overrightarrow{\mathbf{G}_0\mathbf{x}}, \quad \forall\mathbf{x}\in\overline{B(0)}. \end{cases} \tag{3.33}$$

$$\mathbf{C}(\mathbf{x},0) = \mathbf{C}_0(\mathbf{x}), \quad \forall\mathbf{x}\in\Omega, \tag{3.34}$$

$$\mathbf{G}(0) = \mathbf{G}_0, \quad \mathbf{V}(0) = \mathbf{V}_0, \quad \boldsymbol{\omega}(0) = \boldsymbol{\omega}_0. \tag{3.35}$$

To obtain an equivalent fictitious domain formulation, first we fill B with a fluid of density, ρ_f, and suppose that the fluid follows the same rigid body motion as B itself, which is

$$\mathbf{u}(\mathbf{x},t) = \mathbf{V}(t) + \boldsymbol{\omega}(t)\times\overrightarrow{\mathbf{G}(t)\mathbf{x}}, \quad \forall\mathbf{x}\in B(t). \tag{3.36}$$

Define a function space

$$\widetilde{\mathbf{W}}_0(t) = \left\{ (\mathbf{v}, \mathbf{Y}, \boldsymbol{\theta}) \,\middle|\, (\mathbf{v}|_{\Omega \setminus \overline{B(t)}}, \mathbf{Y}, \boldsymbol{\theta}) \in \mathbf{W}_0(t), \mathbf{v}(\mathbf{x}, t) = \mathbf{Y} + \boldsymbol{\theta} \times \overrightarrow{\mathbf{G}(t)\mathbf{x}} \quad \forall \mathbf{x} \in B(t) \right\}.$$

Suppose particle B is made of an homogeneous material of density ρ_f which follows

$$\rho_f \int_{B(t)} \mathbf{g} \cdot \mathbf{v} \, d\mathbf{x} = \frac{\rho_f}{\rho_s} M_p \mathbf{g} \cdot \mathbf{Y}, \quad \forall (\mathbf{v}, \mathbf{Y}, \boldsymbol{\theta}) \in \widetilde{\mathbf{W}}_0(t), \tag{3.37}$$

$$\nabla \cdot \mathbf{v} = 0 \;\; in \; B(t), \quad \forall (\mathbf{v}, \mathbf{Y}, \boldsymbol{\theta}) \in \widetilde{\mathbf{W}}_0(t), \tag{3.38}$$

$$\nabla \cdot \mathbf{u} = 0 \;\; in \; B(t) \;\; and \; \mathbf{D}(\mathbf{u}) = 0 \;\; in \; B(t). \tag{3.39}$$

To obtain a fictitious domain formulation, we define the following function spaces

$$\mathbf{V}_{\mathbf{g}_0}(t) = \left\{ \mathbf{v} \,\middle|\, \mathbf{v} \in (H^1(\Omega))^3, \mathbf{v} = \mathbf{g}_0(t) \; on \, \Gamma \right\},$$

$$L_0^2(\Omega) = \left\{ q \,\middle|\, q \in L^2(\Omega), \int_\Omega q \, d\mathbf{x} = 0 \right\},$$

and

$$\mathbf{V}_{\mathbf{C}_L}(\Omega) = \left\{ \mathbf{A} \,\middle|\, \mathbf{A} \in \mathbf{W}(\Omega), \mathbf{A} = \mathbf{C}_L(t) \; on \, \Gamma^- \right\},$$

$$\mathbf{V}_{\mathbf{C}_0}(\Omega) = \left\{ \mathbf{A} \,\middle|\, \mathbf{A} \in \mathbf{W}(\Omega), \mathbf{A} = 0 \; on \, \Gamma^- \right\}.$$

Combining (3.29)-(3.35) with (3.36)-(3.39), we obtain the fictitious domain formulation as follows:

For a.e. $t \in (0, T)$, find $\mathbf{u}(t) \in \mathbf{V}_{\mathbf{g}_0}(t)$, $p(t) \in L_0^2(\Omega)$, $\mathbf{C}(t) \in \mathbf{V}_{\mathbf{C}_L}$, $\mathbf{V}(t) \in \mathbb{R}^3$,

$\mathbf{G}(t) \in \mathbb{R}^3$, $\boldsymbol{\omega}(t) \in \mathbb{R}^3$, such that ($p = 0$, $\mathbf{D}(\mathbf{u}) = 0$, $\mathbf{C} = I$, $\nabla \cdot \mathbf{u} = 0$ in B(t))

$$\begin{cases} -\displaystyle\int_\Omega p \nabla \cdot \mathbf{v} \, \mathrm{d}\mathbf{x} + 2\mu \int_\Omega \mathbf{D}(\mathbf{u}) : \mathbf{D}(\mathbf{v}) \, \mathrm{d}\mathbf{x} \\ -\dfrac{\eta}{\lambda_1} \displaystyle\int_\Omega \mathbf{v} \cdot (\nabla \cdot (\mathbf{C} - \mathbf{I})) \, \mathrm{d}\mathbf{x} + M_p \frac{\mathrm{d}\mathbf{V}}{\mathrm{d}t} \cdot \mathbf{Y} + \frac{\mathrm{d}\,(\mathbf{I_p}\boldsymbol{\omega})}{\mathrm{d}t} \cdot \boldsymbol{\theta} \\ = \rho_f \displaystyle\int_\Omega \mathbf{g} \cdot \mathbf{v} \, \mathrm{d}\mathbf{x} + \left(1 - \frac{\rho_f}{\rho_s}\right) M_p \mathbf{g} \cdot \mathbf{Y}, \quad \forall (\mathbf{v}, \mathbf{Y}, \boldsymbol{\theta}) \in \widetilde{\mathbf{W}}_0(t), \end{cases} \tag{3.40}$$

$$\int_\Omega q \nabla \cdot \mathbf{u} \, \mathrm{d}\mathbf{x} = 0, \quad \forall q \in L^2(\Omega), \tag{3.41}$$

$$\begin{cases} \displaystyle\int_\Omega \left(\frac{\partial \mathbf{C}}{\partial t} + (\mathbf{u} \cdot \nabla)\mathbf{C} - (\nabla \mathbf{u})\mathbf{C} - \mathbf{C}(\nabla \mathbf{u})^t + \frac{1}{\lambda_1}\mathbf{C} \right) : \mathbf{s} \, \mathrm{d}\mathbf{x} \\ = \dfrac{1}{\lambda_1} \displaystyle\int_\Omega \mathbf{I} : \mathbf{s} \, \mathrm{d}\mathbf{x}, \quad \forall \mathbf{s} \in \mathbf{V}_{\mathbf{C}_0}, \mathbf{C} = \mathbf{I} \, in \, B(t), \end{cases} \tag{3.42}$$

$$\frac{\mathrm{d}\mathbf{G}}{\mathrm{d}t} = \mathbf{V}, \tag{3.43}$$

$$\mathbf{u}(\mathbf{x}, t) = \mathbf{V}(t) + \boldsymbol{\omega}(t) \times \overrightarrow{\mathbf{G}(t)\mathbf{x}}, \quad \forall \mathbf{x} \in B(t). \tag{3.44}$$

$$\mathbf{u}(\mathbf{x}, 0) = \widetilde{\mathbf{u}}_0(\mathbf{x}) \tag{3.45}$$

$$\mathbf{C}(\mathbf{x}, 0) = \mathbf{C}_0(\mathbf{x}), \quad \forall \mathbf{x} \in \Omega, \tag{3.46}$$

$$\mathbf{G}(0) = \mathbf{G}_0, \quad \mathbf{V}(0) = \mathbf{V}_0, \quad \boldsymbol{\omega}(0) = \boldsymbol{\omega}_0. \tag{3.47}$$

To relax the rigid body motion constraint (3.44), we introduce a Lagrange multiplier, $\boldsymbol{\lambda} \in \Lambda(t) = (H^1(B(t)))^3$, and a pairing for any $\boldsymbol{\mu} \in (H^1(B(t)))^3$ and $\mathbf{v} \in (H^1(\Omega))^3$ such that

$$\langle \boldsymbol{\mu}, \mathbf{v} \rangle_{\Lambda(t)} = \int_{B(t)} \left(\boldsymbol{\mu} \cdot \mathbf{v} + d^2 \nabla \boldsymbol{\mu} : \nabla \mathbf{v} \right) \, \mathrm{d}\mathbf{x},$$

where d is a scaling constant and, typically, has been used as the diameter of the particles.

Then, we obtain the fictitious domain formulation over the entire region Ω as follows:

For a.e. $t \in (0,T)$, find $\mathbf{u}(t) \in \mathbf{V}_{\mathbf{g}_0}(t)$, $p(t) \in L^2_0(\Omega)$, $\mathbf{C}(t) \in \mathbf{V}_{\mathbf{C}_L}$,$\mathbf{V}(t) \in \mathbb{R}^3$, $\mathbf{G}(t) \in \mathbb{R}^3$, $\boldsymbol{\omega}(t) \in \mathbb{R}^3$, $\boldsymbol{\lambda}(t) \in \Lambda(t)$ such that

$$\begin{cases} -\displaystyle\int_\Omega p\nabla\cdot\mathbf{v}\,\mathrm{d}\mathbf{x} + 2\mu_f\int_\Omega \mathbf{D}(\mathbf{u}):\mathbf{D}(\mathbf{v})\,\mathrm{d}\mathbf{x} - \frac{\eta}{\lambda_1}\int_\Omega \mathbf{v}\cdot(\nabla\cdot(\mathbf{C}-\mathbf{I}))\,\mathrm{d}\mathbf{x} \\ +M_p\dfrac{\mathrm{d}\mathbf{V}}{\mathrm{d}t}\cdot\mathbf{Y} + \dfrac{\mathrm{d}\,(\mathbf{I_p}\boldsymbol{\omega})}{\mathrm{d}t}\cdot\boldsymbol{\theta} - \left\langle \boldsymbol{\lambda}, \mathbf{v}-\mathbf{Y}-\boldsymbol{\theta}\times\overrightarrow{\mathbf{Gx}}\right\rangle_{\Lambda(t)} \\ = \rho_f\displaystyle\int_\Omega \mathbf{g}\cdot\mathbf{v}\,\mathrm{d}\mathbf{x} + \left(1-\frac{\rho_f}{\rho_s}\right)M_p\mathbf{g}\cdot\mathbf{Y}, \\ \forall(\mathbf{v},\mathbf{Y},\boldsymbol{\theta}) \in (H^1_0(\Omega))^3\times\mathbb{R}^3\times\mathbb{R}^3, \end{cases} \tag{3.48}$$

$$\int_\Omega q\nabla\cdot\mathbf{u}\,\mathrm{d}\mathbf{x} = 0, \quad \forall q \in L^2(\Omega), \tag{3.49}$$

$$\begin{cases} \displaystyle\int_\Omega \left(\frac{\partial\mathbf{C}}{\partial t} + (\mathbf{u}\cdot\nabla)\mathbf{C} - (\nabla\mathbf{u})\mathbf{C} - \mathbf{C}(\nabla\mathbf{u})^t + \frac{1}{\lambda_1}\mathbf{C}\right):\mathbf{s}\,\mathrm{d}\mathbf{x} \\ = \dfrac{1}{\lambda_1}\displaystyle\int_\Omega \mathbf{I}:\mathbf{s}\,\mathrm{d}\mathbf{x}, \quad \forall\mathbf{s}\in\mathbf{V}_{\mathbf{C}_0}, \mathbf{C}=\mathbf{I}\;in\,B(t), \end{cases} \tag{3.50}$$

$$\frac{\mathrm{d}\mathbf{G}}{\mathrm{d}t} = \mathbf{V}, \tag{3.51}$$

$$\mathbf{u}(\mathbf{x},0) = \widetilde{\mathbf{u}}_0(\mathbf{x}), \quad \forall\mathbf{x}\in\Omega, \tag{3.52}$$

$$\left\langle \boldsymbol{\mu}, \mathbf{u}(\mathbf{x},t) - \mathbf{V}(t) - \boldsymbol{\omega}(t)\times\overrightarrow{\mathbf{G(t)x}}\right\rangle_{\Lambda(t)} = 0, \forall\boldsymbol{\mu}\in\Lambda(t), \tag{3.53}$$

$$\mathbf{C}(\mathbf{x},0) = \mathbf{C}_0(\mathbf{x}), \quad \forall\mathbf{x}\in\Omega, \tag{3.54}$$

$$\mathbf{G}(0) = \mathbf{G}_0, \quad \mathbf{V}(0) = \mathbf{V}_0, \quad \boldsymbol{\omega}(0) = \boldsymbol{\omega}_0. \tag{3.55}$$

Remark 3.2. Since $\mathbf{u}$ is divergence free and satisfies the Dirichlet boundary conditions on Γ, we obtain

$$2\int_\Omega \mathbf{D}(\mathbf{u}) : \mathbf{D}(\mathbf{v})\,\mathrm{d}\mathbf{x} = \int_\Omega \nabla\mathbf{u} : \nabla\mathbf{v}\,\mathrm{d}\mathbf{x}, \quad \forall \mathbf{v} \in (H_0^1(\Omega))^3.$$

So in relation (3.48) we can replace $2\int_\Omega \mathbf{D}(\mathbf{u}) : \mathbf{D}(\mathbf{v})\,\mathrm{d}\mathbf{x}$ by $\int_\Omega \nabla\mathbf{u} : \nabla\mathbf{v}\,\mathrm{d}\mathbf{x}$. Also the gravity $\mathbf{g}$ in (3.48) can be absorbed into the pressure term.

3.3 Numerical methods

3.3.1 Finite element approximation

For the purpose of finding an approximation solution of problem (3.48)-(3.55) by finite element methods, we need a partition of the flow region $\Omega \in \mathbb{R}^3$. We used an uniform finite element mesh for Ω.

For the space discretization, we have chosen P_1-*iso*-P_2 finite element space for the velocity field and conformation tensor and P_1 finite element space for the pressure (like in Bristeau et al., (1987) [2] and Glowinski, (2003) [14]). Then we have the following function spaces:

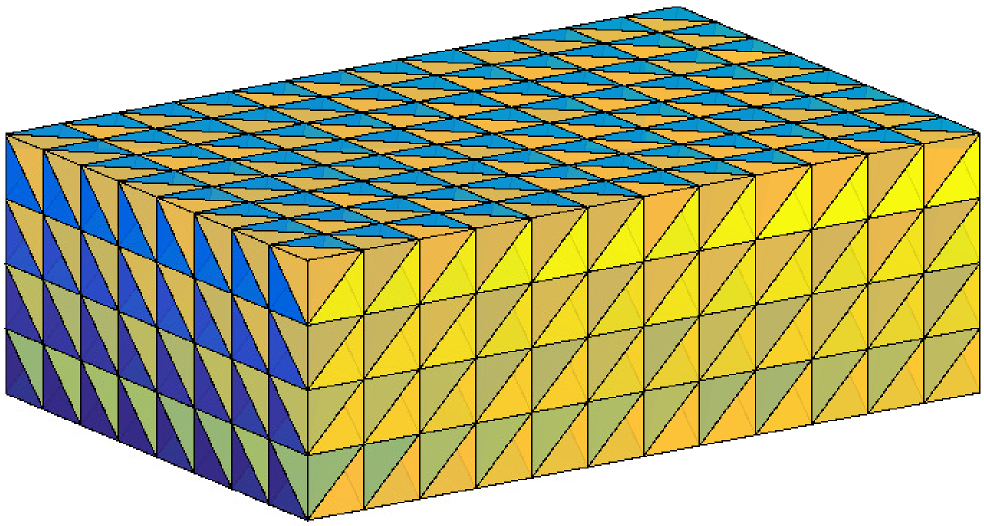

Figure 3.2: A tretrahedrization of a flow region in $\mathbb{R}^3$.

$$
\begin{aligned}
\mathbf{V}_h = \{\mathbf{v}_h \,\big|\, & \mathbf{v}_h \in \left(C^0(\bar{\Omega})\right)^3, \mathbf{v}_h|_T \in (P_1)^3, \forall T \in \mathcal{T}_h, \quad \mathbf{v}_h \text{ is periodic in the } x_1 \\
& \text{and } x_2 \text{ directions with period } L_1 \text{ and } L_2 \text{, respectively } \}, \\
\mathbf{V}_{\mathbf{g}_{0h}(t)} = \{\mathbf{v}_h | & \mathbf{v}_h \in \mathbf{V}_h, \mathbf{v}_h|_\Gamma = \mathbf{g}_{0h}(t)\}, \\
\mathbf{V}_{0h} = \{\mathbf{v}_h | & \mathbf{v}_h \in \mathbf{V}_h, \mathbf{v}_h|_\Gamma = 0\}, \\
L_h^2 = \{q_h | & q_h \in C^0(\bar{\Omega}), q_h|_T \in P_1, \forall T \in \mathcal{T}_{2h}, \quad q_h \text{ is periodic in the } x_1 \\
& \text{and } x_2 \text{ directions with period } L_1 \text{ and } L_2 \text{, respectively } \}, \\
L_{0h}^2 = \{q_h | & q_h \in L_h^2, \int_\Omega q_h \, \mathrm{d}\mathbf{x} = 0\},
\end{aligned}
$$

where h is the space mesh size, $\mathcal{T}_h$ is a regular tetrahedral mesh of Ω, $\mathcal{T}_{2h}$ is another tetrahedral mesh of Ω, twice coarser than $\mathcal{T}_h$, and P_1 is the space of the polynomials in three variables of degree ≤ 1 and $\mathbf{g}_{0h}(t)$ is an approximation of $\mathbf{g}_0(t)$ satisfying

$$\int_{\Gamma} \mathbf{g}_{0h}(t) \cdot \mathbf{n} d\Gamma = 0.$$

The finite dimensional spaces for approximating $\mathbf{V}_{\mathbf{C_{L(t)}}}$ and $\mathbf{V}_{\mathbf{C_0}}$, respectively, are defined by

$$\mathbf{V}_{\mathbf{C}_{L_h}} = \{\mathbf{s}_h | \mathbf{s}_h \in \left(C^0(\bar{\Omega})\right)^{3\times 3}, \mathbf{s}_h|_T \in (P_1)^{3\times 3}, \forall T \in \mathcal{T}_h, \mathbf{s}_h|_{\Gamma_h^-} = \mathbf{C}_{L_h(t)}\},$$
$$\mathbf{V}_{\mathbf{C}_{0h}} = \left\{\mathbf{s}_h \left| \mathbf{s}_h \in \left(C^0(\bar{\Omega})\right)^{3\times 3}, \mathbf{s}_h \right|_T \in (P_1)^{3\times 3}, \forall T \in \mathcal{T}_h, \mathbf{s}_h \left|_{\Gamma_h^-} = 0 \right. \right\},$$

where $\Gamma_h^- = \{\mathbf{x} \,|\mathbf{x} \in \Gamma, \mathbf{g}_{0h}(\mathbf{x}, t) \cdot \mathbf{n}(\mathbf{x}) < 0\}$. For simulating the particle motion in fluid flow, let us define the finite dimensional space to approach the space of Lagrange multiplier $\Lambda(t)$ (e.g., see [28], [30]). Let $\{\boldsymbol{\xi}_i\}_{i=1}^{N(t)}$ be a set of points from $\overline{B(t)}$ which cover $\overline{B(t)}$ evenly. The discrete Lagrange multiplier space is defined by

$$\Lambda_h(t) = \left\{ \boldsymbol{\mu}_h \left| \boldsymbol{\mu}_h = \sum_{i=1}^{N(t)} \boldsymbol{\mu}_i \delta(\mathbf{x} - \boldsymbol{\xi}_i), \boldsymbol{\mu}_i \in \mathbb{R}^3, \forall i = 1, \cdots, N(t) \right. \right\},$$

where $\mathbf{x} \to \delta(\mathbf{x} - \boldsymbol{\xi}_i)$ is the Dirac measure at $\mathbf{x} = \boldsymbol{\xi}_i$. Then we define a pairing over $\Lambda_h(t) \times \mathbf{V}_{\mathbf{g}_{0h}(t)}$ (or $\Lambda_h(t) \times \mathbf{V}_{0h}$) by

$$\langle \boldsymbol{\mu}_h, \mathbf{v}_h \rangle_{\Lambda_h(t)} = \sum_{i=1}^{N} \boldsymbol{\mu}_i \cdot \mathbf{v}_h(\boldsymbol{\xi}_i), \tag{3.56}$$

for $\boldsymbol{\mu}_h \in \boldsymbol{\Lambda}_h(t), \mathbf{v}_h \in \mathbf{V}_{\mathbf{g}_{0h}(t)}$ *or* $\mathbf{V}_{0h}$. A typical set $\{\boldsymbol{\xi}_i\}_{i=1}^{N(t)}$ of points from $\overline{B(t)}$ to be used in (3.56) is defined as

$$\{\boldsymbol{\xi}_i\}_{i=1}^{N(t)} = \{\boldsymbol{\xi}_i\}_{i=1}^{N_1(t)} \bigcup \{\boldsymbol{\xi}_i\}_{i=N_1(t)+1}^{N(t)},$$

where $\{\boldsymbol{\xi}_i\}_{i=1}^{N_1(t)}$ is the set of those vertices of the velocity grid $\mathcal{T}_h$ contained in $B(t)$ and the distance between those vertices and the boundary $\partial B(t)$ is greater than or equal to $\frac{h}{2}$, and selected points $\{\boldsymbol{\xi}_i\}_{i=N_1(t)+1}^{N(t)}$ from $\partial B(t)$.

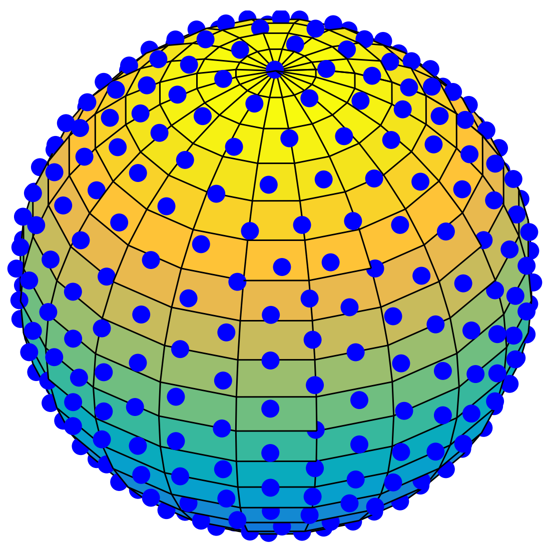

Figure 3.3: An example of collocation points on the sphere surface.

For simulating particle interactions in Stokes flow, we define a modified pairing as follows:

$$\langle \boldsymbol{\mu}_h, \mathbf{v}_h \rangle_{\Lambda_h(t)} = \sum_{i=1}^{N_1(t)} \boldsymbol{\mu}_i \cdot \mathbf{v}_h(\boldsymbol{\xi}_i) + \sum_{i=N_1(t)+1}^{N(t)} \sum_{j=1}^{M} \boldsymbol{\mu}_i \cdot \mathbf{v}_h(\boldsymbol{\xi}_i) D_h(\boldsymbol{\xi}_i - \mathbf{x}_j) h^3, \tag{3.57}$$

for $\boldsymbol{\mu}_h \in \Lambda_h(t), \mathbf{v}_h \in \mathbf{V}_{\mathbf{g}_{0h}(t)}$ *or* $\mathbf{V}_{0h}$ where $\{\mathbf{x}_j\}_{j=1}^{M}$ are the grid points of the finite elements for the velocity, and the function $D_h(\mathbf{X}-\boldsymbol{\xi}_i)$ is defined as

$$D_h(\mathbf{X}-\boldsymbol{\xi}_i)=\delta_h(X_1-\xi_{i1})\delta_h(X_2-\xi_{i2})\delta_h(X_3-\xi_{i3}),$$

with $\mathbf{X}=(X_1,X_2,X_3)^t$ and $\xi_i=(\xi_{i1},\xi_{i2},\xi_{i3})^t$, and the one-dimensional approximate Dirac measure δ_h being defined by

$$\delta_h(z)=\begin{cases}\dfrac{1}{8h}\left(3-\dfrac{2|z|}{h}+\sqrt{1+\dfrac{4|z|}{h}-4\left(\dfrac{|z|}{h}\right)^2}\right), & |z|\leq h,\\ \dfrac{1}{8h}\left(5-\dfrac{2|z|}{h}-\sqrt{-7+\dfrac{12|z|}{h}-4\left(\dfrac{|z|}{h}\right)^2}\right), & h\leq|z|\leq 2h,\\ 0, & \textit{otherwise.}\end{cases}$$

where the discrete Dirac measure D_h were developed by Peskin [34].

Applying the above finite dimensional spaces, we obtain the following semi-discretization of problem (3.48)- (3.55) :

For $0<t<T$, find $\mathbf{u}_h(t)\in\mathbf{V}_{\mathbf{g}_{0h}}(t)$, $p(t)\in L^2_{0h}$, $\mathbf{C}_h(t)\in\mathbf{V}_{\mathbf{C}_{L_h}(t)}$,$\mathbf{V}(t)\in\mathbb{R}^3$, $\mathbf{G}(t)\in\mathbb{R}^3$, $\boldsymbol{\omega}(t)\in\mathbb{R}^3$, $\boldsymbol{\lambda}_h\in\Lambda_h(t)$ such that

$$\begin{cases}-\displaystyle\int_\Omega p\nabla\cdot\mathbf{v}\,\mathrm{d}\mathbf{x}+\mu_f\int_\Omega\nabla\mathbf{u}_h:\nabla\mathbf{v}\,\mathrm{d}\mathbf{x}\\ \quad-\dfrac{\eta}{\lambda_1}\displaystyle\int_\Omega\mathbf{v}\cdot(\nabla\cdot(\mathbf{C}_h-\mathbf{I}))\,\mathrm{d}\mathbf{x}+M_p\dfrac{\mathrm{d}\mathbf{V}}{\mathrm{d}t}\cdot\mathbf{Y}+\dfrac{\mathrm{d}\left(\mathbf{I_p}\boldsymbol{\omega}\right)}{\mathrm{d}t}\cdot\boldsymbol{\theta}\\ \quad=\left(1-\dfrac{\rho_f}{\rho_s}\right)M_p\mathbf{g}\cdot\mathbf{Y}+\left\langle\boldsymbol{\lambda}_h,\mathbf{v}-\mathbf{Y}-\boldsymbol{\theta}\times\overrightarrow{\mathbf{Gx}}\right\rangle_{\Lambda_h(t)},\\ \quad\forall(\mathbf{v},\mathbf{Y},\boldsymbol{\theta})\in\mathbf{V}_{0h}\times\mathbb{R}^3\times\mathbb{R}^3,\end{cases}\tag{3.58}$$

$$\int_{\Omega} q\nabla \cdot \mathbf{u}_h \,\mathrm{d}\mathbf{x} = 0, \quad \forall q \in L_h^2, \tag{3.59}$$

$$\begin{cases} \displaystyle\int_{\Omega} \left(\frac{\partial \mathbf{C}_h}{\partial t} + (\mathbf{u}_h \cdot \nabla)\mathbf{C}_h - (\nabla \mathbf{u}_h)\mathbf{C}_h - \mathbf{C}_h(\nabla \mathbf{u}_h)^t + \frac{1}{\lambda_1}\mathbf{C}_h \right) : \mathbf{s}_h \,\mathrm{d}\mathbf{x} \\ \qquad = \displaystyle\frac{1}{\lambda_1}\int_{\Omega} \mathbf{I} : \mathbf{s}_h \,\mathrm{d}\mathbf{x}, \quad \forall \mathbf{s}_h \in \mathbf{V}_{\mathbf{C}_{0h}}; \mathbf{C}_h = \mathbf{I} \;\; in \;\; B_h(t), \end{cases} \tag{3.60}$$

$$\frac{\mathrm{d}\mathbf{G}}{\mathrm{d}t} = \mathbf{V}, \tag{3.61}$$

$$\mathbf{u}_h(\mathbf{x}, 0) = \widetilde{\mathbf{u}}_{0h}(\mathbf{x}), \quad \forall \mathbf{x} \in \Omega, \tag{3.62}$$

$$\left\langle \boldsymbol{\mu}_h, \mathbf{u}_h(t) - \mathbf{V}(t) - \boldsymbol{\omega}(t) \times \overrightarrow{\mathbf{G(t)x}} \right\rangle_{\Lambda_h(t)} = 0, \forall \mu_h \in \Lambda_h(t), \tag{3.63}$$

$$\mathbf{C}_h(\mathbf{x}, 0) = \mathbf{C}_{0h}(\mathbf{x}), \quad \forall \mathbf{x} \in \Omega, \tag{3.64}$$

$$\mathbf{G}(0) = \mathbf{G}_0, \quad \mathbf{V}(0) = \mathbf{V}_0, \quad \boldsymbol{\omega}(0) = \boldsymbol{\omega}_0, \tag{3.65}$$

where $\widetilde{\mathbf{u}}_{0h}$ is an approximation of $\widetilde{\mathbf{u}}_0$ such that

$$\int_{\Omega} q\nabla \cdot \widetilde{\mathbf{u}}_{0h} \mathrm{d}\mathbf{x} = 0, \quad \forall q \in L_h^2.$$

Remark 3.3. If we consider our particle as a sphere, then in relation (3.58) the term $\dfrac{\mathrm{d}\,(\mathbf{I}_\mathbf{p}\boldsymbol{\omega})}{\mathrm{d}t}$ can be written as $\mathbf{I}_\mathbf{p}\dfrac{\mathrm{d}\boldsymbol{\omega}}{\mathrm{d}t}$, which is much easier when solving it numerically (e.g., see [16]).

Remark 3.4. For the two ball interaction in a bounded shear flow, there is no lubrication force between the two balls under creeping flow conditions. Therefore, we are not allowed to apply an artificial repulsive force to prevent ball overlapping in numerical simulation since such force might alter the trajectories of the two ball mass centers. To deal with the interaction during the two ball interaction, we have to impose a minimal gap of size ch between the balls where c is some constant between 0 and 1, h being the mesh size of the velocity field. Then, when advancing the two ball mass centers in equation (3.24), we proceed as follows at each sub-cycling time step: (i) we do nothing if the gap between the two balls at the new position is greater or equal than ch, (ii) if the gap size of the two balls at the new position is less than ch, we do not advance the balls directly; but instead we first move the ball centers in the direction perpendicularly to the line joining the previous centers, and then move them in the direction parallel to the line joining the previous centers, and make sure that the gap size is no less than ch.

3.3.2 Operator splitting scheme

To fully discretize system (3.48)-(3.55), we first reduce it to a finite dimensional initial value problem using the above finite element spaces (after dropping most of the sub-scripts h's). Next, we combine the Lozinski-Owens factorization approach (see, e.g., [24], [17]) with the Lie scheme [7] to decouple the above finite element analogue of system, (3.48)-(3.55), into a sequence of subproblems and apply the backward Euler schemes to time-discretize some of these subproblems.

First we consider the following initial value problem:

$$\begin{cases} \dfrac{\mathrm{d}\phi}{\mathrm{d}t} + A(\phi) = 0 \quad on\ (0, T), \\ \phi(0) = \phi_0, \end{cases}$$

with $0 < T < +\infty$. We suppose that operator A has a decomposition such as

$A = \sum_{j=1}^{J} A_j$ with $J \geq 2$.

Let $\tau > 0$ be a time-discretization step, we denote $n\tau$ by t^n. Let ϕ^n be an approximation of $\phi(t^n)$, we can write down the Lie's scheme as follows:

Given $\phi^0 = \phi_0$.

For $n \geq 0$, ϕ^n is known and we compute ϕ^{n+1} via

$$\begin{cases} \dfrac{\mathrm{d}\phi}{\mathrm{d}t} + A_j(\phi) = 0 \quad \mathit{on}\ (t^n, t^{n+1}), \\ \phi(t^n) = \phi^{n+\frac{j-1}{J}}; \phi^{n+\frac{j}{J}} = \phi(t^{n+1}), \end{cases}$$

for $j = 1, \cdots, J$.

3.3.3 Operator splitting for using matrix factorization

Since the conformation tensor $\mathbf{C}$ is symmetric and positive definite, following the matrix factorization approach developed in [24], we have considered $\mathbf{C} = \mathbf{A}\mathbf{A}^t$, where $\mathbf{A}^t$ is the transpose matrix of $\mathbf{A}$. After splitting the constitutive equation of the conformation tensor, we first have the following three subproblems:

$$\begin{cases} \dfrac{\partial \mathbf{C}}{\partial t} + (\mathbf{u} \cdot \nabla)\mathbf{C} = \mathbf{0}, \quad \mathit{on}\ (t^n, t^{n+1}), \\ \mathbf{C}(t^n) = \mathbf{C}^n; \quad \mathbf{C}^{n+\frac{1}{3}} = \mathbf{C}(t^{n+1}), \end{cases} \tag{3.66}$$

$$\begin{cases} \dfrac{\partial \mathbf{C}}{\partial t} + \dfrac{1}{\lambda_1}\mathbf{C} - (\nabla \mathbf{u})\mathbf{C} - \mathbf{C}(\nabla \mathbf{u})^t = \mathbf{0}, \quad \mathit{on}\ (t^n, t^{n+1}), \\ \mathbf{C}(t^n) = \mathbf{C}^{n+\frac{1}{3}}; \quad \mathbf{C}^{n+\frac{2}{3}} = \mathbf{C}(t^{n+1}), \end{cases} \tag{3.67}$$

$$\begin{cases} \dfrac{\partial \mathbf{C}}{\partial t} = \dfrac{1}{\lambda_1}\mathbf{I}, \quad on\ (t^n, t^{n+1}), \\ \mathbf{C}(t^n) = \mathbf{C}^{n+\frac{2}{3}}; \quad \mathbf{C}^{n+1} = \mathbf{C}(t^{n+1}), \end{cases} \tag{3.68}$$

Now we derive equivalent equations of (3.66) and (3.67) in the following.

Lemma 3.5. *For a matrix $\mathbf{A}$, a given $\mathbf{u} \in \mathbb{R}^3$ and a positive constant λ_1, we have*

(i) if $\mathbf{A}$ satisfies the equation

$$\frac{\partial \mathbf{A}}{\partial t} + (\mathbf{u} \cdot \nabla)\mathbf{A} = \mathbf{0}, \tag{3.69}$$

then $\mathbf{C} = \mathbf{A}\mathbf{A}^t$ satisfies the equation $\dfrac{\partial \mathbf{C}}{\partial t} + (\mathbf{u} \cdot \nabla)\mathbf{C} = \mathbf{0}$;

(ii) if $\mathbf{A}$ satisfies the equation

$$\frac{\partial \mathbf{A}}{\partial t} + \frac{1}{2\lambda_1}\mathbf{A} - (\nabla \mathbf{u})\mathbf{A} = \mathbf{0}, \tag{3.70}$$

then $\mathbf{C} = \mathbf{A}\mathbf{A}^t$ satisfies the equation
$\dfrac{\partial \mathbf{C}}{\partial t} + \dfrac{1}{\lambda_1}\mathbf{C} - (\nabla \mathbf{u})\mathbf{C} - \mathbf{C}(\nabla \mathbf{u})^t = \mathbf{0}.$

Proof. (i) Given $\dfrac{\partial \mathbf{A}}{\partial t} + (\mathbf{u} \cdot \nabla)\mathbf{A} = \mathbf{0}$, multiplying the equation by $\mathbf{A}^t$ to the right, we obtain

$$\frac{\partial \mathbf{A}}{\partial t}\mathbf{A}^t + (\mathbf{u} \cdot \nabla)\mathbf{A}\mathbf{A}^t = \mathbf{0}. \tag{3.71}$$

Multiplying the transpose of the equation by $\mathbf{A}$ to the left, we obtain

$$\mathbf{A}\frac{\partial \mathbf{A}^t}{\partial t} + \mathbf{A}(\mathbf{u} \cdot \nabla)\mathbf{A}^t = \mathbf{0}. \tag{3.72}$$

Adding (3.71) and (3.72) gives

$$\frac{\partial\left(\mathbf{A}\mathbf{A}^t\right)}{\partial t} + (\mathbf{u}\cdot\nabla)\left(\mathbf{A}\mathbf{A}^t\right) = \mathbf{0}.$$

Thus, we get

$$\frac{\partial \mathbf{C}}{\partial t} + (\mathbf{u}\cdot\nabla)\mathbf{C} = \mathbf{0}.$$

(ii) Given $\frac{\partial \mathbf{A}}{\partial t} + \frac{1}{2\lambda_1}\mathbf{A} - (\nabla\mathbf{u})\mathbf{A} = \mathbf{0}$, multiplying the equation by $\mathbf{A}^t$ to the right, we obtain

$$\frac{\partial \mathbf{A}}{\partial t}\mathbf{A}^t + \frac{1}{2\lambda_1}\mathbf{A}\mathbf{A}^t - (\nabla\mathbf{u})\mathbf{A}\mathbf{A}^t = \mathbf{0}. \tag{3.73}$$

Multiplying the transpose of the equation by $\mathbf{A}$ to the left, we obtain

$$\mathbf{A}\frac{\partial \mathbf{A}^t}{\partial t} + \frac{1}{2\lambda_1}\mathbf{A}\mathbf{A}^t - \mathbf{A}\mathbf{A}^t(\nabla\mathbf{u})^t = \mathbf{0} \tag{3.74}$$

Adding (3.73) and (3.74) gives

$$\frac{\partial\left(\mathbf{A}\mathbf{A}^t\right)}{\partial t} + \frac{1}{\lambda_1}\mathbf{A}\mathbf{A}^t - (\nabla\mathbf{u})\mathbf{A}\mathbf{A}^t - \mathbf{A}\mathbf{A}^t(\nabla\mathbf{u})^t = \mathbf{0}.$$

Thus, we obtain

$$\frac{\partial \mathbf{C}}{\partial t} + \frac{1}{\lambda_1}\mathbf{C} - (\nabla\mathbf{u})\mathbf{C} - \mathbf{C}(\nabla\mathbf{u})^t = \mathbf{0}.$$

□

Therefore, we can solve the equations (3.69) and (3.70) for $\mathbf{A}$ instead of the equations (3.66) and (3.67) for $\mathbf{C}$ and the resulting matrix $\mathbf{C} = \mathbf{A}\mathbf{A}^t$ is , at least semi-positive definite at the discrete level. The finite dimensional subspaces $\mathbf{V}_{\mathbf{A}_{L_h}(t)}$ and $\mathbf{V}_{\mathbf{A}_{0h}}$ for $\mathbf{A}$ can be defined by the way similar to the spaces $\mathbf{V}_{\mathbf{C}_{L_h}(t)}$ and $\mathbf{V}_{\mathbf{C}_{0h}}$.

Applying the Lie's scheme in [7] to the discrete analogue of the problem (3.58)-(3.65) with $\mathbf{C} = \mathbf{A}\mathbf{A}^t$ and using the backward Euler's method to some subproblems, we obtain:

Given $\mathbf{u}^0 = \mathbf{u}_{0h}, \mathbf{C}^0 = \mathbf{C}_{0h}, \mathbf{G}^0 = \mathbf{G}_0, \mathbf{V}^0 = \mathbf{V}_0, \boldsymbol{\omega}^0 = \boldsymbol{\omega}_0$.

For $n \geq 0$, $\mathbf{u}^n, \mathbf{C}^n, \mathbf{G}^n, \mathbf{V}^n, \boldsymbol{\omega}^n$ are known, we compute the approximate solution at $t = t^{n+1}$ via the following steps:

1. We first predict the position and the translation velocity of the center of mass as follows.

$$\frac{d\mathbf{G}}{dt} = \mathbf{V}(t), \tag{3.75}$$

$$M_p \frac{d\mathbf{V}}{dt} = 0 \tag{3.76}$$

$$\mathbf{I_p} \frac{d\boldsymbol{\omega}}{dt} = 0, \tag{3.77}$$

$$\mathbf{V}(t^n) = \mathbf{V}^n, \boldsymbol{\omega}(t^n) = \boldsymbol{\omega}^n, \mathbf{G}(t^n) = \mathbf{G}^n, \tag{3.78}$$

   for $t^n < t < t^{n+1}$. Then set $\mathbf{V}^{n+\frac{1}{4}} = \mathbf{V}(t^{n+1})$, $\boldsymbol{\omega}^{n+\frac{1}{4}} = \boldsymbol{\omega}(t^{n+1})$, and $\mathbf{G}^{n+\frac{1}{4}} = \mathbf{G}(t^{n+1})$. With the center $\mathbf{G}^{n+\frac{1}{4}}$ we get in the above step, the region of $B_h^{n+\frac{1}{4}}$ occupied by the particle is determined. Set $\mathbf{C}^{n+\frac{1}{4}} = \mathbf{I}$ in $B_h^{n+\frac{1}{4}}$ and $\mathbf{C}^{n+\frac{1}{4}} = \mathbf{C}^n$ otherwise.

2. Then we enforce the rigid body motion in $B_h^{n+\frac{1}{4}}$ and solve $\mathbf{u}^{n+\frac{2}{4}}$ and $p^{n+\frac{2}{4}}$

simultaneously as follows:

Find $\mathbf{u}^{n+\frac{2}{4}} \in \mathbf{V}^{n+1}_{\mathbf{g}_{0h}}$, $p^{n+\frac{2}{4}} \in L^2_{0h}$, $\boldsymbol{\lambda}^{n+\frac{2}{4}} \in \Lambda_h^{n+\frac{1}{4}}$, $\mathbf{V}^{n+\frac{2}{4}} \in \mathbb{R}^3$, $\boldsymbol{\omega}^{n+\frac{2}{4}} \in \mathbb{R}^3$ such that

$$\begin{cases} -\displaystyle\int_\Omega p^{n+\frac{2}{4}} \nabla \cdot \mathbf{v} \, \mathrm{d}\mathbf{x} + \mu_f \int_\Omega \nabla \mathbf{u}^{n+\frac{2}{4}} : \nabla \mathbf{v} \, \mathrm{d}\mathbf{x} \\ -\dfrac{\eta}{\lambda_1} \displaystyle\int_\Omega \mathbf{v} \cdot \left(\nabla \cdot \left(\mathbf{C}^{n+\frac{1}{4}} - \mathbf{I} \right) \right) \mathrm{d}\mathbf{x} \\ +M_p \dfrac{\mathbf{V}^{n+\frac{2}{4}} - \mathbf{V}^{n+\frac{1}{4}}}{\triangle t} \cdot \mathbf{Y} + \mathbf{I_p} \dfrac{\boldsymbol{\omega}^{n+\frac{2}{4}} - \boldsymbol{\omega}^{n+\frac{1}{4}}}{\Delta t} \cdot \boldsymbol{\theta} \\ = \left(1 - \dfrac{\rho_f}{\rho_s} \right) M_p \mathbf{g} \cdot \mathbf{Y} + \left\langle \boldsymbol{\lambda}^{n+\frac{2}{4}}, \mathbf{v} - \mathbf{Y} - \boldsymbol{\theta} \times \overrightarrow{\mathbf{G}^{n+\frac{1}{4}} \mathbf{x}} \right\rangle_{\Lambda_h^{n+\frac{1}{4}}}, \\ \forall \; (\mathbf{v}, \mathbf{Y}, \boldsymbol{\theta}) \in \mathbf{V}_{0h} \times \mathbb{R}^3 \times \mathbb{R}^3, \end{cases} \tag{3.79}$$

$$\int_\Omega q \nabla \cdot \mathbf{u}^{n+\frac{2}{4}} \, \mathrm{d}\mathbf{x} = 0, \quad \forall q \in L^2_h, \tag{3.80}$$

$$\left\langle \boldsymbol{\mu}, \mathbf{u}^{n+\frac{2}{4}} - \mathbf{V}^{n+\frac{2}{4}} - \boldsymbol{\omega}^{n+\frac{2}{4}} \times \overrightarrow{\mathbf{G}^{n+\frac{1}{4}} \mathbf{x}} \right\rangle_{\Lambda_h^{n+\frac{1}{4}}} = 0, \quad \forall \boldsymbol{\mu} \in \Lambda_h^{n+\frac{1}{4}}, \tag{3.81}$$

and set $\mathbf{C}^{n+\frac{2}{4}} = \mathbf{C}^{n+\frac{1}{4}}$.

3. We first find the matrix factor of $\mathbf{C}^{n+\frac{2}{4}}$ such that $\mathbf{A}^{n+\frac{2}{4}}(\mathbf{A}^{n+\frac{2}{4}})^t = \mathbf{C}^{n+\frac{2}{4}}$ and compute $\mathbf{A}^{n+\frac{3}{4}}$ via the solution of

$$\begin{cases} \displaystyle\int_\Omega \frac{\mathrm{d}\mathbf{A}(t)}{\mathrm{d}t} : \mathbf{s} \, \mathrm{d}\mathbf{x} + \int_\Omega \left(\mathbf{u}^{n+\frac{2}{4}} \cdot \nabla \right) \mathbf{A}(t) : \mathbf{s} \, \mathrm{d}\mathbf{x} = \mathbf{0}, \forall \mathbf{s} \in \mathbf{V}_{\mathbf{A}_{0h}} \\ \mathbf{A}(t^n) = \mathbf{A}^{n+\frac{2}{4}}; \\ \mathbf{A}(t) \in \mathbf{V}^{n+1}_{\mathbf{A}_{L_h}}, t \in [t^n, t^{n+1}], \end{cases} \tag{3.82}$$

and set $\mathbf{A}^{n+\frac{3}{4}} = \mathbf{A}(t^{n+1})$.

4. We compute $\mathbf{A}^{n+1}$ via the solution of

$$\begin{cases} \displaystyle\int_\Omega \left[\frac{\mathbf{A}^{n+1} - \mathbf{A}^{n+\frac{3}{4}}}{\Delta t} - \left(\nabla \mathbf{u}^{n+\frac{2}{4}}\right) \mathbf{A}^{n+1} + \frac{1}{2\lambda_1} \mathbf{A}^{n+1} \right] : \mathbf{s}\, d\mathbf{x} = \mathbf{0}, \\ \forall \mathbf{s} \in \mathbf{V}_{\mathbf{A}_{0h}}; \mathbf{A}^{n+1} \in \mathbf{V}^{n+1}_{\mathbf{A}_{L_h}}, \end{cases} \tag{3.83}$$

and set

$$\mathbf{C}^{n+1} = \mathbf{A}^{n+1}(\mathbf{A}^{n+1})^t + \frac{\triangle t}{\lambda_1}\mathbf{I}. \tag{3.84}$$

Finally, we set $\mathbf{u}^{n+1} = \mathbf{u}^{n+\frac{2}{4}}$, $\mathbf{G}^{n+1} = \mathbf{G}^{n+\frac{1}{4}}$, $\mathbf{V}^{n+1} = \mathbf{V}^{n+\frac{2}{4}}$, and $\boldsymbol{\omega}^{n+1} = \boldsymbol{\omega}^{n+\frac{2}{4}}$. In the above,$\mathbf{V}^{n+1}_{\mathbf{A}_{L_h}} = \mathbf{V}_{\mathbf{A}_{L_h}(t^{n+1})}$, $\mathbf{V}^{n+1}_{\mathbf{g}_{0h}} = \mathbf{V}_{\mathbf{g}_{0h}(t^{n+1})}$, $\Lambda_h^{n+\frac{1}{4}} = \Lambda_h(t^{n+\frac{1}{4}})$, and $B_h^{n+s} = B_h(t^{n+s})$.

3.3.4 Operator splitting scheme for having Carreau model

The operator splitting scheme for having the Carreau model, we have modified Step 2 in Section 3.3.3 as follows:

2'. We first compute

$$\left(\dot{\gamma}^n\right)^2 = 2\mathbf{D}(\mathbf{u}^n) : \mathbf{D}(\mathbf{u}^n), \tag{3.85}$$

and then obtain the viscosity η_1, the solvent viscosity μ and the elastic viscosity η by

$$\eta_1\left(\dot{\gamma}^n\right) = \frac{\eta_1}{\left(1 + (\lambda_1 \dot{\gamma}^n)^2\right)^{\frac{1-n}{2}}}, \tag{3.86}$$

$$\mu\left(\dot{\gamma}^{n}\right)=\eta_1\left(\dot{\gamma}^{n}\right)\frac{\lambda_2}{\lambda_1}, \tag{3.87}$$

$$\eta\left(\dot{\gamma}^{n}\right)=\eta_1\left(\dot{\gamma}^{n}\right)-\mu\left(\dot{\gamma}^{n}\right). \tag{3.88}$$

Then we enforce the rigid body motion in $B_h^{n+\frac{1}{4}}$ and solve the stokes problem simultaneously as follows

Find $\mathbf{u}^{n+\frac{2}{4}} \in \mathbf{V}_{\mathbf{g}_{0h}}^{n+1}$, $p^{n+\frac{2}{4}} \in L_{0h}^2$, $\boldsymbol{\lambda}^{n+\frac{1}{4}} \in \Lambda_h^{n+\frac{2}{4}}$, $\mathbf{V}^{n+\frac{2}{4}} \in \mathbb{R}^3$, $\boldsymbol{\omega}^{n+\frac{2}{4}} \in \mathbb{R}^3$ such that

$$\begin{cases} -\int_\Omega p^{n+\frac{2}{4}}\nabla\cdot\mathbf{v}\,\mathrm{d}\mathbf{x}+\mu_f\int_\Omega \nabla\mathbf{u}^{n+\frac{2}{4}}:\nabla\mathbf{v}\,\mathrm{d}\mathbf{x} \\ +M_p\dfrac{\mathbf{V}^{n+\frac{2}{4}}-\mathbf{V}^{n+\frac{1}{4}}}{\triangle t}\cdot\mathbf{Y}+\mathbf{I_p}\dfrac{\boldsymbol{\omega}^{n+\frac{2}{4}}-\boldsymbol{\omega}^{n+\frac{1}{4}}}{\triangle t}\cdot\boldsymbol{\theta} \\ =2\int_\Omega\left(\mu_f-\mu\left(\dot{\gamma}^{n}\right)\right)\left(\mathbf{D}(\mathbf{u}^n):\nabla\mathbf{v}\right)\,\mathrm{d}\mathbf{x} \\ +\int_\Omega \mathbf{v}\cdot\left(\nabla\cdot\dfrac{\eta\left(\dot{\gamma}^{n}\right)}{\lambda_1}\left(\mathbf{C}^{n+\frac{1}{4}}-\mathbf{I}\right)\right)\,\mathrm{d}\mathbf{x} \\ +\left(1-\dfrac{\rho_f}{\rho_s}\right)M_p\mathbf{g}\cdot\mathbf{Y}+\left\langle\boldsymbol{\lambda}^{n+\frac{2}{4}},\mathbf{v}-\mathbf{Y}-\boldsymbol{\theta}\times\overrightarrow{\mathbf{G}^{n+\frac{1}{4}}\mathbf{x}}\right\rangle_{\Lambda_h^{n+\frac{1}{4}}}, \\ \quad\forall\,(\mathbf{v},\mathbf{Y},\boldsymbol{\theta})\in\mathbf{V}_{0h}\times\mathbb{R}^3\times\mathbb{R}^3, \end{cases} \tag{3.89}$$

$$\int_\Omega q\nabla\cdot\mathbf{u}^{n+\frac{2}{4}}\,\mathrm{d}\mathbf{x}=0,\quad \forall q\in L_h^2, \tag{3.90}$$

$$\left\langle\boldsymbol{\mu},\mathbf{u}^{n+\frac{2}{4}}-\mathbf{V}^{n+\frac{2}{4}}-\boldsymbol{\omega}^{n+\frac{2}{4}}\times\overrightarrow{\mathbf{G}^{n+\frac{2}{4}}\mathbf{x}}\right\rangle_{\Lambda_h^{n+\frac{1}{4}}}=0,\quad \forall\boldsymbol{\mu}\in\Lambda_h^{n+\frac{1}{4}}. \tag{3.91}$$

and set $\mathbf{C}^{n+\frac{2}{4}}=\mathbf{C}^{n+\frac{1}{4}}$.

Remark 3.6. In order to use faster solver to solve above system (3.89)-(3.91), we have chosen to keep constant viscosity and move the difference to the right hand side of (3.89) with the velocity obtained at the previous time step.

3.3.5 Operator splitting for using logarithm conformation tensor

Besides matrix factorization approach, we have considered the log-conformation representation for the conformation tensor which is the technique first developed in [13].

We consider two decoupled subproblems of constitutive equation by using operator splitting scheme:

$$\frac{\partial \mathbf{C}}{\partial t} + (\mathbf{u} \cdot \nabla)\mathbf{C} = \mathbf{0}, \tag{3.92}$$

$$\frac{\partial \mathbf{C}}{\partial t} + \frac{1}{\lambda_1}\mathbf{C} - (\nabla \mathbf{u})\mathbf{C} - \mathbf{C}(\nabla \mathbf{u})^t = \frac{1}{\lambda_1}\mathbf{I}. \tag{3.93}$$

To keep the conformation tensor $\mathbf{C}$ positive definite and resolve the exponential behavior of $\mathbf{C}$, we have used the following the log-conformation representation for the conformation tensor to solve the above subproblems (3.92)-(3.93). In [13], it was shown that with $\mathbf{u}$ being a divergence-free velocity field and $\mathbf{C}$ a symmetric positive definite tensor field, the velocity gradient $\nabla \mathbf{u}$ can be decomposed as

$$\nabla \mathbf{u} = \mathbf{O} + \mathbf{S} + \mathbf{N}\mathbf{C}^{-1}, \tag{3.94}$$

where $\mathbf{O}$ and $\mathbf{N}$ are skew-symmetric, and $\mathbf{S}$ is symmetric, trace free, and commutes with $\mathbf{C}$.

Solving the subproblems (3.92) – (3.93) by using these matrices, we obtain the scheme as follows:

$$\frac{\partial \mathbf{C}}{\partial t} + (\mathbf{u} \cdot \nabla)\mathbf{C} = \mathbf{0}, \tag{3.95}$$

$$\frac{\partial \mathbf{C}}{\partial t} - (\mathbf{OC} - \mathbf{CO}) - 2\mathbf{SC} = \frac{1}{\lambda_1}(\mathbf{I} - \mathbf{C}). \tag{3.96}$$

Remark 3.7. Given the decomposition of $\nabla \mathbf{u}$ in (3.94) and assume $\mathbf{O}$ and $\mathbf{N}$ are skew-symmetric, and $\mathbf{S}$ is symmetric, trace free, and commutes with $\mathbf{C}$. We get equation (3.96) from (3.93) as follows:

First we replace $\nabla \mathbf{u}$ by $\mathbf{O} + \mathbf{S} + \mathbf{N}\mathbf{C}^{-1}$ and get

$$\frac{\partial \mathbf{C}}{\partial t} + \frac{1}{\lambda_1}\mathbf{C} - (\mathbf{O} + \mathbf{S} + \mathbf{N}\mathbf{C}^{-1})\mathbf{C} - \mathbf{C}(\mathbf{O} + \mathbf{S} + \mathbf{N}\mathbf{C}^{-1})^t = \frac{1}{\lambda_1}\mathbf{I}. \tag{3.97}$$

Since $\mathbf{O}$ and $\mathbf{N}$ are skew-symmetric, and $\mathbf{S}$ is symmetric and commutes with $\mathbf{C}$, we obtain

$$\frac{\partial \mathbf{C}}{\partial t} + \frac{1}{\lambda_1}\mathbf{C} - \mathbf{OC} - \mathbf{SC} - \mathbf{N} - \mathbf{CO}^t - \mathbf{CS}^t - \mathbf{C}(\mathbf{C}^{-1})^t\mathbf{N}^t = \frac{1}{\lambda_1}\mathbf{I}, \tag{3.98}$$

then

$$\frac{\partial \mathbf{C}}{\partial t} + \frac{1}{\lambda_1}\mathbf{C} - \mathbf{OC} - \mathbf{SC} - \mathbf{N} + \mathbf{CO} - \mathbf{SC} + \mathbf{C}(\mathbf{C}^{-1})^t\mathbf{N} = \frac{1}{\lambda_1}\mathbf{I}, \tag{3.99}$$

Since $\mathbf{C}$ is symmetric, $\mathbf{C}(\mathbf{C}^{-1})^t = (\mathbf{C})^t(\mathbf{C}^{-1})^t = \mathbf{I}$, we obtain

$$\frac{\partial \mathbf{C}}{\partial t} + \frac{1}{\lambda_1}\mathbf{C} - \mathbf{OC} - \mathbf{N} + \mathbf{CO} - 2\mathbf{SC} + \mathbf{N} = \frac{1}{\lambda_1}\mathbf{I}, \tag{3.100}$$

After simplifying (3.100), we get (3.96) as follows

$$\frac{\partial \mathbf{C}}{\partial t} - (\mathbf{OC} - \mathbf{CO}) - 2\mathbf{SC} = \frac{1}{\lambda_1}(\mathbf{I} - \mathbf{C}). \tag{3.101}$$

Remark 3.8. To compute $\mathbf{O}$, $\mathbf{S}$, and $\mathbf{N}$ from a divergence-free velocity field $\mathbf{u}$ for a three-dimensional case, we can derive then as follows:

(i) If the conformation tensor C is proportional to unit tensor, then set $\mathbf{S} = \dfrac{\nabla\mathbf{u} + (\nabla\mathbf{u})^T}{2}$ and $\mathbf{O} = \mathbf{0}$.

(ii) Otherwise, diagonalize C via

$$\mathbf{C} = R\begin{bmatrix} \lambda_1 & 0 & 0 \\ 0 & \lambda_2 & 0 \\ 0 & 0 & \lambda_3 \end{bmatrix} R^t,$$

and set

$$\begin{bmatrix} m_{11} & m_{12} & m_{13} \\ m_{21} & m_{22} & m_{23} \\ m_{31} & m_{32} & m_{33} \end{bmatrix} = R^t(\nabla\mathbf{u})R,$$

where λ_1, λ_2, λ_3 are eigenvalues of $\mathbf{C}$ with respect to the eigenvectors in R. Then we obtain

$$\mathbf{S} = R\begin{bmatrix} m_{11} & 0 & 0 \\ 0 & m_{22} & 0 \\ 0 & 0 & m_{33} \end{bmatrix}R^t, \quad \mathbf{O} = R\begin{bmatrix} 0 & \omega_{12} & \omega_{13} \\ -\omega_{12} & 0 & \omega_{23} \\ -\omega_{13} & -\omega_{23} & 0 \end{bmatrix}R^t \tag{3.102}$$

with $\omega_{12} = \dfrac{\lambda_2 m_{12} + \lambda_1 m_{21}}{\lambda_2 - \lambda_1}$, $\omega_{13} = \dfrac{\lambda_3 m_{13} + \lambda_1 m_{31}}{\lambda_3 - \lambda_1}$, and $\omega_{23} = \dfrac{\lambda_3 m_{23} + \lambda_2 m_{32}}{\lambda_3 - \lambda_2}$.

Remark 3.9. Since the conformation tensor C is a symmetric positive definite matrix, it can always be diagonalized as $C = R\Lambda R^t$, and then we have $\log C = R\log(\Lambda)R^t$ where R is an orthogonal matrix.

Assume $\boldsymbol{\psi} = \log C$. Solving the subproblems (3.95) – (3.96) by using the logarithm of conformation tensor $\boldsymbol{\psi}$, we obtain the scheme as follows:

$$\frac{\partial \boldsymbol{\psi}}{\partial t} + (\mathbf{u}\cdot\nabla)\boldsymbol{\psi} = \mathbf{0}, \tag{3.103}$$

$$\frac{\partial \boldsymbol{\psi}}{\partial t} - (\mathbf{O}\boldsymbol{\psi} - \boldsymbol{\psi}\mathbf{O}) - 2\mathbf{S} = \frac{1}{\lambda_1}(e^{-\boldsymbol{\psi}} - \mathbf{I}). \tag{3.104}$$

To get the conformation tensor $\mathbf{C}$ by using constitutive equation for $\log \mathbf{C}$, we replace (3.82)-(3.84) by (3.105)-(3.107) when solving the constitutive equation:

3'. We set $\boldsymbol{\psi}^{n+\frac{2}{4}} = log\left(\mathbf{C}^{n+\frac{2}{4}}\right)$ and compute $\boldsymbol{\psi}^{n+\frac{3}{4}}$ via the solution of

$$\begin{cases} \displaystyle\int_\Omega \frac{\partial \boldsymbol{\psi}(t)}{\partial t} : \mathbf{s}\,\mathrm{d}\mathbf{x} + \int_\Omega \left(\mathbf{u}^{n+\frac{2}{4}}\cdot\nabla\right)\boldsymbol{\psi}(t) : \mathbf{s}\,\mathrm{d}\mathbf{x} = \mathbf{0}, \forall \mathbf{s} \in \mathbf{V}_{\mathbf{C}_{0h}} \\ \boldsymbol{\psi}(t^n) = \boldsymbol{\psi}^{n+\frac{2}{4}}, \\ \boldsymbol{\psi}(t) \in \mathbf{V}^{n+1}_{\log(\mathbf{C}_{L_h})}, t \in [t^n, t^{n+1}], \end{cases} \tag{3.105}$$

and set $\boldsymbol{\psi}^{n+\frac{3}{4}} = \boldsymbol{\psi}(t^{n+1})$ and $\mathbf{u}^{n+\frac{3}{4}} = \mathbf{u}^{n+\frac{2}{4}}$.

4'. We set $\mathbf{C}^{n+\frac{3}{4}} = e^{\boldsymbol{\psi}^{n+\frac{3}{4}}}$ and $\mathbf{O}^{n+\frac{3}{4}} + \mathbf{S}^{n+\frac{3}{4}} + \mathbf{N}^{n+\frac{3}{4}}\left(\mathbf{C}^{n+\frac{3}{4}}\right)^{-1} = \nabla \mathbf{u}^{n+\frac{3}{4}}$ and compute $\boldsymbol{\psi}^{n+1}$ via the solution of

$$\begin{cases} \dfrac{\partial \boldsymbol{\psi}(t)}{\partial t} - \left(\mathbf{O}^{n+\frac{3}{4}}\boldsymbol{\psi}(t) - \boldsymbol{\psi}(t)\mathbf{O}^{n+\frac{3}{4}}\right) - 2\mathbf{S}^{n+\frac{3}{4}} = \mathbf{0}, \\ \boldsymbol{\psi}(t^n) = \boldsymbol{\psi}^{n+\frac{3}{4}}, \\ \boldsymbol{\psi}(t) \in \mathbf{V}^{n+1}_{\log(\mathbf{C}_{L_h})}, t \in [t^n, t^{n+1}], \end{cases} \tag{3.106}$$

and set $\boldsymbol{\psi}^{n+1} = \boldsymbol{\psi}(t^{n+1})$ and $\widetilde{\mathbf{C}}^{n+1} = e^{\boldsymbol{\psi}^{n+1}}$. Then we solve

$$\begin{cases} \dfrac{\partial \mathbf{C}}{\partial t} = \dfrac{1}{\lambda_1}(\mathbf{I} - \mathbf{C}), \\ \mathbf{C}(t^n) = \widetilde{\mathbf{C}}^{n+1}, \\ \mathbf{C}(t) \in \mathbf{V}^{n+1}_{\mathbf{C}_{L_h}}, t \in [t^n, t^{n+1}];\ \textit{set}\ \mathbf{C}^{n+1} = \mathbf{C}(t^{n+1}) \end{cases} \tag{3.107}$$

In (3.106), it is better to use exact solution, which is available, instead of solving it numerically.

3.4 On the solution of the subproblems from operator splitting

3.4.1 Solution of the advection subproblems

We solve the advection problem (3.82) by a wave-like equation method as in, e.g., [10, 14]. After translation and dilation on the time axis, each component of the velocity vector $\mathbf{u}$ and of the tensor $\mathbf{A}$ is solution of a transport equation of the following type:

$$\begin{cases} \dfrac{\partial \varphi}{\partial t} + (\mathbf{U} \cdot \nabla)\varphi = 0 in\ \Omega \times (t^n, t^{n+1}), \\ \varphi(t^n) = \varphi_0, \ \ \varphi = \mathbf{g} on\ \Gamma^- \times (t^n, t^{n+1}), \end{cases} \tag{3.108}$$

where $\nabla \cdot \mathbf{U} = 0$ and $\dfrac{\partial \mathbf{U}}{\partial t} = 0$ on $\Omega \times (t^n, t^{n+1})$. Thus, (3.108) is equivalent to the well-posed problem:

$$\begin{cases} \dfrac{\partial^2 \varphi}{\partial t^2} - \nabla \cdot ((\mathbf{U} \cdot \nabla\varphi)\mathbf{U}) = 0 in\ \Omega \times (t^n, t^{n+1}), \\ \varphi(t^n) = \varphi_0, \ \ \dfrac{\partial \varphi}{\partial t}(0) = -\mathbf{U} \cdot \nabla\varphi_0, \ \ \varphi = \mathbf{g} on\ \Gamma^- \times (t^n, t^{n+1}), \\ (\mathbf{U} \cdot \mathbf{n}) \left(\dfrac{\partial \varphi}{\partial t} + (\mathbf{U} \cdot \nabla)\varphi \right) = 0 on\ \Gamma \setminus \Gamma^- \times (t^n, t^{n+1}). \end{cases} \tag{3.109}$$

Solving the wave-like equation (3.109) by a classical finite element/ time stepping method, a variational formulation of (3.109) is given by

$$\begin{cases} \displaystyle\int_\Omega \frac{\partial^2 \varphi}{\partial t^2} v \mathrm{d}\mathbf{x} + \int_\Omega (\mathbf{U} \cdot \nabla\varphi)(\mathbf{U} \cdot \nabla v) \mathrm{d}\mathbf{x} + \\ \displaystyle\int_{\Gamma \setminus \Gamma^-} \mathbf{U} \cdot \mathbf{n} \frac{\partial \varphi}{\partial t} v \mathrm{d}\Gamma = 0, \forall v \in W_0, \\ \varphi(t^n) = \varphi_0, \ \ \dfrac{\partial \varphi}{\partial t}(t^n) = -\mathbf{U} \cdot \nabla\varphi_0, \ \ \varphi = \mathbf{g} on\ \Gamma^- \times (t^n, t^{n+1}), \end{cases} \tag{3.110}$$

with the test function space W_0 defined by $W_0 = \{v | v \in H^1(\Omega), v = 0 on\ \Gamma^-\}$.

Let H_h^1 be a C^0-conforming finite element subspace of $H^1(\Omega)$. We define $W_{0h} = H_h^1 \cap W_0$. We suppose that $\lim_{h \to 0} W_{0h} = W_0$ in the usual finite element sense. Next, we define $\tau_1 > 0$ by $\tau_1 = \dfrac{\triangle t}{Q}$ where Q is a positive integer, and we discretize problem (3.110) by

$$\begin{cases} \varphi^0 = \varphi_0, \\ \int_\Omega (\varphi^{-1} - \varphi^1) v \mathrm{d}\mathbf{x} = 2\tau_1 \int_\Omega (\mathbf{U_h} \cdot \nabla \varphi^0) v \mathrm{d}\mathbf{x}, \ \forall v \in W_{0h}, \ \varphi^{-1} - \varphi^1 \in W_{0h}, \end{cases} \tag{3.111}$$

and for $q = 0, 1, 2, \cdots, Q-1$,

$$\begin{cases} \varphi^{q+1} \in H_h^1, \varphi^{q+1} = \mathbf{g}_h \, on \ \Gamma^-, \\ \int_\Omega \dfrac{\varphi^{q+1} + \varphi^{q-1} - 2\varphi^q}{\tau^2} v \mathrm{d}\mathbf{x} + \int_\Omega (\mathbf{U_h} \cdot \nabla \varphi^q)(\mathbf{U_h} \cdot \nabla v) \mathrm{d}\mathbf{x} \\ \quad + \int_{\Gamma \backslash \Gamma^-} \mathbf{U_h} \cdot \mathbf{n} \left(\dfrac{\varphi^{q+1} - \varphi^{q-1}}{\tau} \right) v \mathrm{d}\Gamma = 0, \ \ \forall v \in W_0, \end{cases} \tag{3.112}$$

where $\mathbf{U}_h$ and $\mathbf{g}_h$ are the approximates of $\mathbf{U}$ and $\mathbf{g}$, respectively.

Remark 3.10. Scheme (3.111)-(3.112) is a centered scheme which is formally second order accurate with respect to space and time discretizations. To be stable, scheme $(3.111) - (3.112)$ has to verify a condition such as $\tau_1 \leq ch$, which c of order of $\dfrac{1}{\|\mathbf{U}\|}$. Since the advection problem is decoupled from the other ones, we can choose proper time step here so that the above condition is satisfied. If one uses the trapezoidal rule to compute the first and the third integrals in (3.112), the above scheme becomes explicit and φ^{q+1} is obtained via the solution of a linear system with diagonal matrix.

Remark 3.11. Scheme $(3.111) - (3.112)$ does not introduce numerical dissipation, unlike the upwinding schemes commonly used to solve transport problems like (3.108).

3.4.2 Solution of the system (3.106)

Given matrices $\mathbf{O}$, $\mathbf{S}$, and $\boldsymbol{\psi}_0$ in $\Omega \times (t^n, t^{n+1})$. In the system (3.106), we solve tensor $\boldsymbol{\psi}$ via an initial value problem of ordinary differential equation as follows:

$$\begin{cases} \dfrac{\mathrm{d}\boldsymbol{\psi}(t)}{\mathrm{d}t} - (\mathbf{O}\boldsymbol{\psi}(t) - \boldsymbol{\psi}(t)\mathbf{O}) - 2\mathbf{S} = 0, \, in \; \Omega \times (t^n, t^{n+1}), \\ \qquad\qquad \boldsymbol{\psi}(t^n) = \boldsymbol{\psi}_0, \end{cases} \tag{3.113}$$

For the tensor, $\boldsymbol{\psi}(t)$, satisfying equation (3.113), we actually have its exact solution

$$\boldsymbol{\psi}(t^{n+1}) = e^{\mathbf{O}\triangle t}\boldsymbol{\psi}(t^n)e^{-\mathbf{O}\triangle t} + 2\mathbf{S}\triangle t, \tag{3.114}$$

where $\triangle t = t^{n+1} - t^n$. Therefore, we do not need to solve it numerically.

3.4.3 Solution of the rigid body motion enforcement problems

In the system (3.79)-(3.81), there are two multipliers, p and $\boldsymbol{\lambda}$. We have solved this system via an Uzawa conjugate gradient method [15], which is driven by both multipliers. The general problem of system (3.79)-(3.81) is given as follows:

Find $\mathbf{u} \in \mathbf{V}_{\mathbf{g}_{0h}}$, $p \in L^2_{0h}$, $\boldsymbol{\lambda} \in \Lambda_h$, $\mathbf{V} \in \mathbb{R}^3$, $\boldsymbol{\omega} \in \mathbb{R}^3$ such that

$$\begin{cases} -\int_\Omega p\nabla \cdot \mathbf{v}\,\mathrm{d}\mathbf{x} + \mu_f \int_\Omega \nabla\mathbf{u} : \nabla\mathbf{v}\,\mathrm{d}\mathbf{x} - \dfrac{\eta}{\lambda_1}\int_\Omega \mathbf{v}\cdot(\nabla\cdot(\mathbf{C}-\mathbf{I}))\,\mathrm{d}\mathbf{x} \\ +M_p\dfrac{\mathbf{V}-\mathbf{V}_0}{\triangle t}\cdot\mathbf{Y} + \mathbf{I_p}\dfrac{\boldsymbol{\omega}-\boldsymbol{\omega}_0}{\triangle t}\cdot\boldsymbol{\theta} \\ = \left(1-\dfrac{\rho_f}{\rho_s}\right)M_p\mathbf{g}\cdot\mathbf{Y} + \left\langle \boldsymbol{\lambda}, \mathbf{v}-\mathbf{Y}-\boldsymbol{\theta}\times\overrightarrow{\mathbf{Gx}}\right\rangle_{\Lambda_h}, \\ \quad \forall\ (\mathbf{v},\mathbf{Y},\boldsymbol{\theta}) \in \mathbf{V}_{0h}\times\mathbb{R}^3\times\mathbb{R}^3, \end{cases} \tag{3.115}$$

$$\int_\Omega q\nabla\cdot\mathbf{u}\,\mathrm{d}\mathbf{x} = 0, \quad \forall q \in L^2_h, \tag{3.116}$$

$$\left\langle \boldsymbol{\mu}, \mathbf{u}-\mathbf{V}-\boldsymbol{\omega}\times\overrightarrow{\mathbf{Gx}}\right\rangle_{\Lambda_h} = 0, \quad \forall\boldsymbol{\mu}\in\Lambda_h. \tag{3.117}$$

We solve the system, (3.115)-(3.117), by the following Uzawa conjugate gradient algorithm operating in the space $L^2_{0h}\times\Lambda_h$:

Assume $p^0 \in L^2_{0h}$ and $\boldsymbol{\lambda}^0 \in \Lambda_h$ are given.

We solve the problem:

Find $\mathbf{u}^0 \in \mathbf{V}_{\mathbf{g}_{0h}}$, $\mathbf{V}^0 \in \mathbb{R}^3$, $\boldsymbol{\omega}^0 \in \mathbb{R}^3$ satisfying

$$\begin{cases} \mu_f \int_\Omega \nabla\mathbf{u}^0 : \nabla\mathbf{v}\,d\mathbf{x} = \int_\Omega p\nabla\cdot\mathbf{v}\,d\mathbf{x} + \dfrac{\eta}{\lambda_1}\int_\Omega \mathbf{v}\cdot(\nabla\cdot(\mathbf{C}-\mathbf{I}))\,d\mathbf{x} + \left\langle\boldsymbol{\lambda}^0,\mathbf{v}\right\rangle_{\Lambda_h}, \\ \forall\ \mathbf{v}\in\mathbf{V}_{0h}; \mathbf{u}^0 \in \mathbf{V}_{\mathbf{g}_{0h}}, \end{cases} \tag{3.118}$$

$$M_p\frac{\mathbf{V}^0-\mathbf{V}_0}{\triangle t}\cdot\mathbf{Y} = \left(1-\frac{\rho_f}{\rho_s}\right)M_p\mathbf{g}\cdot\mathbf{Y} - \left\langle\boldsymbol{\lambda}^0,\mathbf{Y}\right\rangle_{\Lambda_h}, \quad \forall\ \mathbf{Y}\in\mathbb{R}^3, \tag{3.119}$$

$$\mathbf{I_p}\frac{\boldsymbol{\omega}^0 - \boldsymbol{\omega}_0}{\triangle t} \cdot \boldsymbol{\theta} = -\left\langle \boldsymbol{\lambda}^0, \boldsymbol{\theta} \times \overrightarrow{\mathbf{Gx}} \right\rangle_{\Lambda_h}, \quad \forall\, \boldsymbol{\theta} \in \mathbb{R}^3, \tag{3.120}$$

and then compute

$$\mathrm{g}_1^0 = \nabla \cdot \mathbf{u}^0; \tag{3.121}$$

next find $\mathbf{g}_2^0 \in \Lambda_h$ *satisfying*

$$\left\langle \boldsymbol{\mu}, \mathbf{g}_2^0 \right\rangle_{\Lambda_h} = \left\langle \boldsymbol{\mu}, \mathbf{u}^0 - \mathbf{V}^0 - \boldsymbol{\omega}^0 \times \overrightarrow{\mathbf{Gx}} \right\rangle_{\Lambda_h}, \quad \forall\, \boldsymbol{\mu} \in \Lambda_h, \tag{3.122}$$

and set

$$\mathrm{w}_1^0 = \mathrm{g}_1^0, \quad \mathbf{w}_2^0 = \mathbf{g}_2^0. \tag{3.123}$$

Then for $k \geq 0$, *assuming that* p^k, $\boldsymbol{\lambda}^k$, $\mathbf{u}^k$, $\mathbf{V}^k$, $\boldsymbol{\omega}^k$, $\mathrm{g}_1^{\mathrm{k}}$, $\mathbf{g}_2^k$, w_1^k *and* $\mathbf{w}_2^k$ *are known, compute* p^{k+1}, $\boldsymbol{\lambda}^{k+1}$, $\mathbf{u}^{k+1}$, $\mathbf{V}^{k+1}$, $\boldsymbol{\omega}^{k+1}$, $\mathrm{g}_1^{\mathrm{k+1}}$, $\mathbf{g}_2^{k+1}$, ${\mathrm{w}_1}^{k+1}$ *and* $\mathbf{w}_2^{k+1}$ *as follows:*

$$\begin{cases} \mu_f \displaystyle\int_\Omega \nabla \overline{\mathbf{u}}^k : \nabla \mathbf{v}\, d\mathbf{x} = \int_\Omega \mathrm{w}_1^k \nabla \cdot \mathbf{v}\, d\mathbf{x} + \left\langle \mathbf{w}_2^k, \mathbf{v} \right\rangle_{\Lambda_h}, \\ \forall\, \mathbf{v} \in \mathbf{V}_{0h}; \overline{\mathbf{u}}^k \in \mathbf{V}_{\mathbf{g}_{0h}}, \end{cases} \tag{3.124}$$

$$M_p \frac{\overline{\mathbf{V}}^k}{\triangle t} \cdot \mathbf{Y} = -\left\langle \mathbf{w}_2^k, \mathbf{Y} \right\rangle_{\Lambda_h}, \quad \forall\, \mathbf{Y} \in \mathbb{R}^3, \tag{3.125}$$

$$\mathbf{I_p}\frac{\overline{\boldsymbol{\omega}}^k}{\triangle t} \cdot \boldsymbol{\theta} = -\left\langle \mathbf{w}_2^k, \boldsymbol{\theta} \times \overrightarrow{\mathbf{Gx}} \right\rangle_{\Lambda_h}, \quad \forall\, \boldsymbol{\theta} \in \mathbb{R}^3, \tag{3.126}$$

and then compute

$$\overline{\mathrm{g}}_1^{\mathrm{k}} = \nabla \cdot \overline{\mathbf{u}}^{\mathrm{k}}; \tag{3.127}$$

next find $\overline{\mathbf{g}}_2^k \in \Lambda_h$ *satisfying*

$$\langle \boldsymbol{\mu}, \overline{\mathbf{g}}_2^k \rangle_{\Lambda_h} = \left\langle \boldsymbol{\mu}, \overline{\mathbf{u}}^k - \overline{\mathbf{V}}^k - \overline{\boldsymbol{\omega}}^k \times \overrightarrow{\mathbf{Gx}} \right\rangle_{\Lambda_h}, \quad \forall\, \boldsymbol{\mu} \in \Lambda_h, \tag{3.128}$$

and compute

$$\rho_k = \frac{\displaystyle\int_\Omega \left|\mathrm{g}_1^{\mathrm{k}}\right|^2 d\mathbf{x} + \langle \mathbf{g}_2^k, \mathbf{g}_2^k \rangle_{\Lambda_h}}{\displaystyle\int_\Omega \overline{\mathbf{g}}_1^k \mathrm{w}_1^k\, d\mathbf{x} + \langle \overline{\mathbf{g}}_2^k, \mathbf{w}_2^k \rangle_{\Lambda_h}}, \tag{3.129}$$

and

$$p^{k+1} = p^k - \rho_k {\mathrm{w}_1}^k, \tag{3.130}$$

$$\boldsymbol{\lambda}^{k+1} = \boldsymbol{\lambda}^k - \rho_k \mathbf{w}_2^k, \tag{3.131}$$

$$\mathbf{u}^{k+1} = \mathbf{u}^k - \rho_k \overline{\mathbf{u}}^k, \tag{3.132}$$

$$\mathbf{V}^{k+1} = \mathbf{V}^k - \rho_k \overline{\mathbf{V}}^k, \tag{3.133}$$

$$\boldsymbol{\omega}^{k+1} = \boldsymbol{\omega}^k - \rho_k \overline{\boldsymbol{\omega}}^k, \tag{3.134}$$

$$\mathrm{g}_1^{k+1} = \mathrm{g}_1^k - \rho_k \overline{\mathrm{g}}_1^k, \tag{3.135}$$

$$\mathbf{g}_2^{k+1} = \mathbf{g}_2^k - \rho_k \overline{\mathbf{g}}_2^k. \tag{3.136}$$

If

$$\frac{\displaystyle\int_\Omega \left|\mathrm{g}_1^{\mathrm{k+1}}\right|^2 d\mathbf{x} + \langle \mathbf{g}_2^{k+1}, \mathbf{g}_2^{k+1} \rangle_{\Lambda_h}}{\displaystyle\int_\Omega \left|\mathrm{g}_1^0\right|^2 d\mathbf{x} + \langle \mathbf{g}_2^0, \mathbf{g}_2^0 \rangle_{\Lambda_h}} \le \varepsilon, \tag{3.137}$$

then take $p = p^{k+1}$, $\boldsymbol{\lambda} = \boldsymbol{\lambda}^{k+1}$, $\mathbf{u} = \mathbf{u}^{k+1}$, $\mathbf{V} = \mathbf{V}^{k+1}$, *and* $\boldsymbol{\omega} = \boldsymbol{\omega}^{k+1}$. *Otherwise,* *compute*

$$\gamma_k = \frac{\displaystyle\int_\Omega \left|\mathrm{g}_1^{\mathrm{k}+1}\right|^2 d\mathbf{x} + \left\langle \mathbf{g}_2^{k+1}, \mathbf{g}_2^{k+1} \right\rangle_{\Lambda_h}}{\displaystyle\int_\Omega \left|\mathrm{g}_1^{\mathrm{k}}\right|^2 d\mathbf{x} + \left\langle \mathbf{g}_2^{k}, \mathbf{g}_2^{k} \right\rangle_{\Lambda_h}}, \tag{3.138}$$

and set

$$\mathrm{w}_1^{k+1} = \mathrm{g}_1^{k+1} + \gamma_k {\mathrm{w}_1}^k, \tag{3.139}$$

$$\mathbf{w}_2^{k+1} = \mathbf{g}_2^{k+1} + \gamma_k \mathbf{w}_2^k. \tag{3.140}$$

Then do $m = m + 1$ and go back to (3.124).

For Oldroyd-B fluid with the property of shear-thinning, the system (3.89)-(3.91) can also be solved by the same algorithm. The only difference are that there is an extra term

$$2 \int_\Omega \left(\mu_f - \mu \left(\dot{\gamma}^n \right) \right) \left(\mathbf{D}(\mathbf{u}^n) : \nabla \mathbf{v} \right) \mathrm{d}\mathbf{x},$$

and the elastic viscosity is not a constant any more.

3.5 Numerical results

3.5.1 Rotation of a single particle

We have considered the cases of a single neutrally buoyant ball placed at the middle between two walls initially with different values of the relaxation time λ_1 in a bounded shear flow of Oldroyd-B fluids. The densities of the fluid and that of the particle are $\rho_f = \rho_s = 1$ and the viscosity $\eta_1 = 1$. The computational domain is $\Omega =$

$(-a, a) \times (-b, b) \times (-c, c)$ (i.e. $L_1 = 2a, L_2 = 2b$, and $L_3 = 2c$). The shear rate $\dot{\gamma} = 1$ sec^{-1} so the speed of the top wall is $U = c$ and that of the bottom wall is $-U = -c$. For all the numerical simulations, we assume that all dimensional quantities are in the CGS units. We have obtained the rotating angular velocity with respect to the x_2-axis for different values of λ_1.

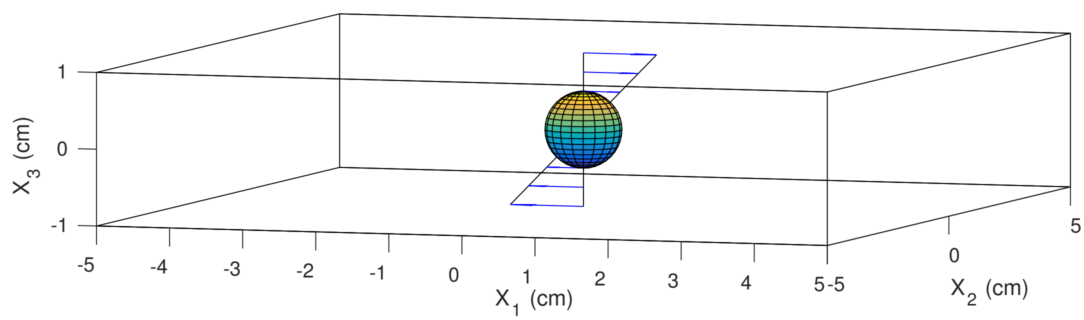

Figure 3.4: Single ball in a two-wall driven bounded shear flow as r=1/2 and L=10.

First, to study the wall effect on the particle rotating angular velocity, we consider the mass center of the ball is fixed at $(0, 0, 0)$ with three different λ_1 and define the blockage ratio $K = 2r/L_3$ with five particle radii $r = 1/10, 1/5, 1/3, 2/5, 1/2$. The retardation time is $\lambda_2 = \lambda_1/8$. The associated values of the Weissenberg number Wi $(= \lambda_1\dot{\gamma})$ are $0.5, 0.75$, and 1.0. In order to assure the unperturbed conditions, the computational domain is $\Omega = (-L/2, L/2) \times (-L/2, L/2) \times (-1, 1)$ where $L = 20r$ and $L_3 = 2$. The three different blockage ratios K as same as those cases in [8] (see Figure 3.5) for the validation are considered in this section.

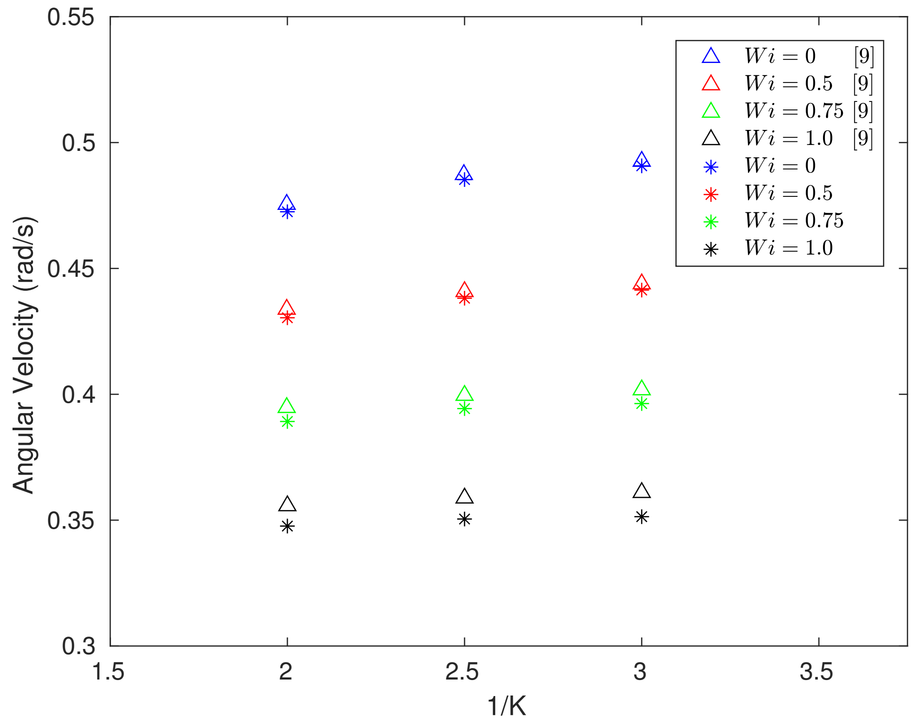

Figure 3.5: The angular velocity of the particles with respect to the ratio 1/K for four different Weissenberg numbers Wi. K and Wi are dimensionless numbers. The numerical results in Maxwell fluid (denoted by △) are taken from in [8] and the results we have obtained in Oldroyd-B fluid are denoted by "*".

As Wi < 0.5 and 1/K > 2.5, the angular velocity we have obtained is very close to the result in [8]. But as Wi > 0.5, our angular velocity is smaller then the one in Maxwell fluid.

Second, to study the effect of viscoelasticity on the particle angular velocity, we consider fixed mass center with six different ratios $\beta = \frac{\lambda_1}{\lambda_2}$. The mass center of the ball is fixed at $(0, 0, 0)$ all the time. The particle radius r is 0.1. The computational domain is $\Omega = (-1.5, 1.5) \times (-1.5, 1.5) \times (-1.5, 1.5)$. We have obtained the rotating angular velocity with respect to the x_2-axis for ten different values of the relaxation time λ_1. The associated values of the Weissenberg number Wi ($= \lambda_1 \dot{\gamma}$) are 0.01, 0.1, 0.25, 0.5, 1, 1.6, 2.6, 3.56, 4.2, and 5.5. The ratios β are 1.7, 1.8, 1.9, 2, 4, and 8. In Figure 3.7, when Wi > 1 we also get the numerical results which are smaller than the experimental results in [37] but the numerical results are getting larger and closer to the experimental results as β is getting smaller.

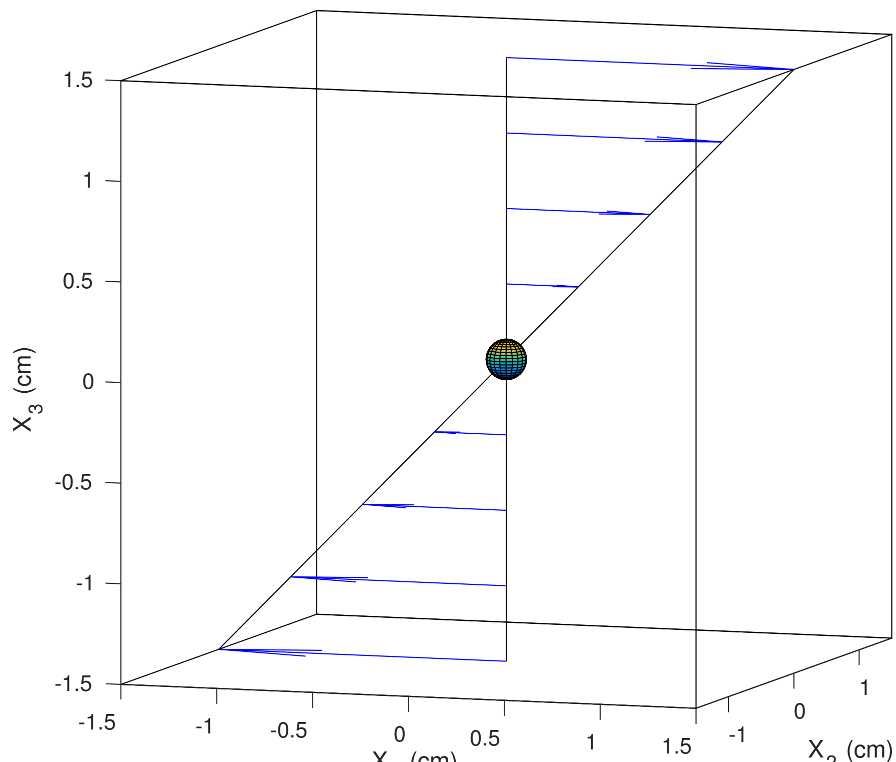

Figure 3.6: Single ball in a two-wall driven bounded shear flow as r=1/10 and L=3.

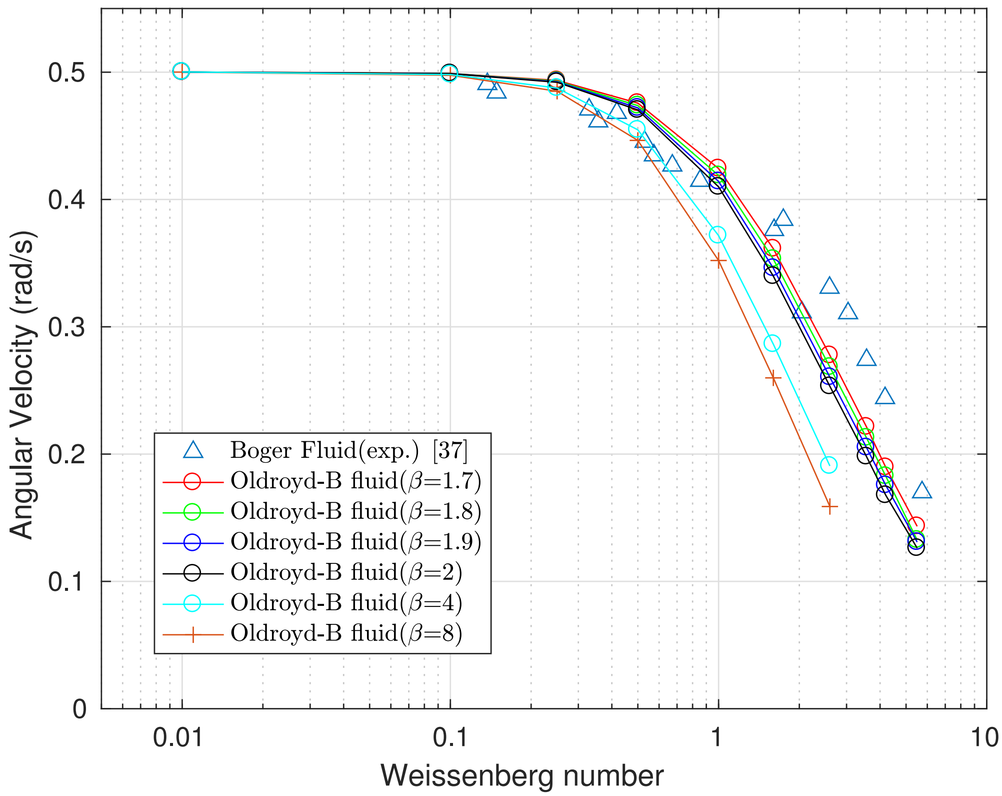

Figure 3.7: The angular velocity of the particles with respect to ten different Weissenberg numbers Wi in log-scale. The experimental results in Boger fluid are taken from [37] and our numerical results in Oldroyd-B fluid are obtained for the ball with fixed mass center for six β. Wi and β are dimensionless numbers.

3.5.2 Migration of a single particle in an one-wall driven bounded shear flow

It is known that particles migrate toward moving wall in shear flow of viscoelastic fluids (e.g., see[11]). To study the Migration of a single particle in an one-wall driven bounded shear flow, we have considered the cases of a single ball placed at the middle between two walls initially with respect to five relaxation times λ_1 in a bounded shear flow of Oldroyd-B fluids. The associated values of the Weissenberg number Wi are $0.01, 0.1, 0.5$, and 1.0. The ball radii are $r = 0.1$. The fluid and ball densities are $\rho_f = \rho_s = 1$, the viscosity being $\eta_1 = 1$. The computational domain is $\Omega = (-1.5, 1.5) \times (-1, 1) \times (-0.5, 0.5)$ The shear rate is fixed at $\dot{\gamma} = 1$ so the velocity of the top wall is $U = 1$, the bottom wall being $U = 0$. The mesh size for the velocity field and the conformation tensor is $h = 1/48$, the mesh size for the pressure is $2h$, The time step being $\triangle t = 0.001$. The mass center of the ball is located at $(0, 0, 0)$ initially. The results we have with respect to five different Wi are in Figure 3.8. Besides translating along the flow direction, the ball migrations along the gradient direction toward the moving (top) wall.

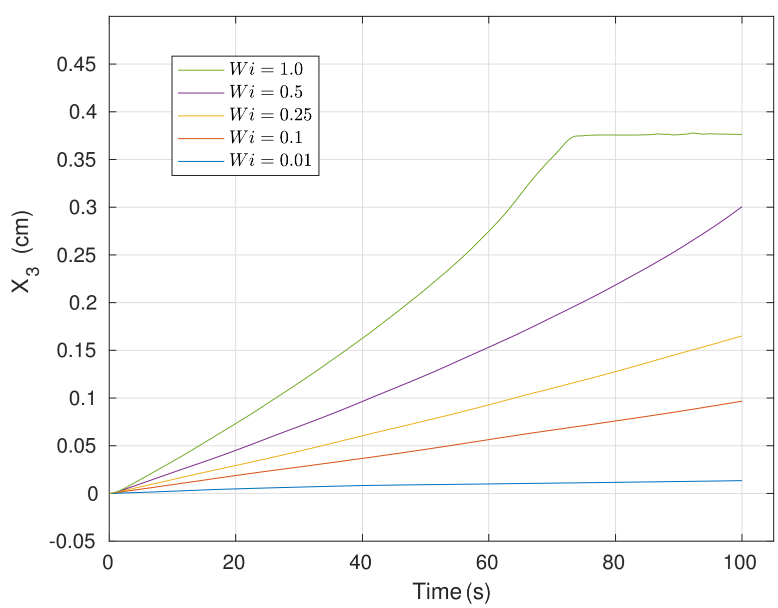

Figure 3.8: Heights of the single ball mass center in an one-wall driven bounded shear flow for five Wi form 0.01 to 1. As Wi increases, the particle migrates faster to the moving top wall. Wi is a dimensionless number.

As mentioned in [11, 12], the fluid viscoelasticity is the major factor affecting the migration toward the moving wall. The migration dynamics is amplified by the higher fluid viscoelasticity. In Oldroyd-B fluid flow, the fluid elasticity is controlled by the Weissenberg number Wi. Figure 3.8 shows that the particle moves toward the top moving wall in one-wall driven shear flows. The particle under higher Wi goes up more rapidly than the particle under lower Wi. As Wi= 1, the particle goes up to the wall with a small gap in limited time and then stays and moves forward along the wall. These results at least, qualitatively agrees with the experimental observations reported in [38].

3.5.3 Two ball interacting with large initial distance in a two-wall driven bounded shear flow

In this section, we consider the cases of two balls of the same size interacting in a bounded shear flow of Oldroyd-B fluids as visualized in Figure 3.9. The ball radii are $r = 0.1$. The fluid and ball densities are $\rho_f = \rho_s = 1$, the viscosity being $\eta_1 = 1$. The computational domain is $\Omega = (-1.5, 1.5) \times (-1, 1) \times (-0.5, 0.5)$ (i.e. $L_1 = 3$, $L_2 = 2$, and $L_3 = 1$). The shear rate is fixed at $\dot{\gamma} = 1$ so the velocity of the top wall is $U = 0.5$, that of the bottom wall being -0.5. The mass centers of the two balls are located on the shear plane at $(-d_0, 0, \triangle s)$ and $(d_0, 0, -\triangle s)$ initially, where $\triangle s$ varies and d_0 is 0.5. The time step being $\triangle t = 0.001$. Then we have considered six to seven dimensionless initial vertical displacements $D = \triangle s/a$.

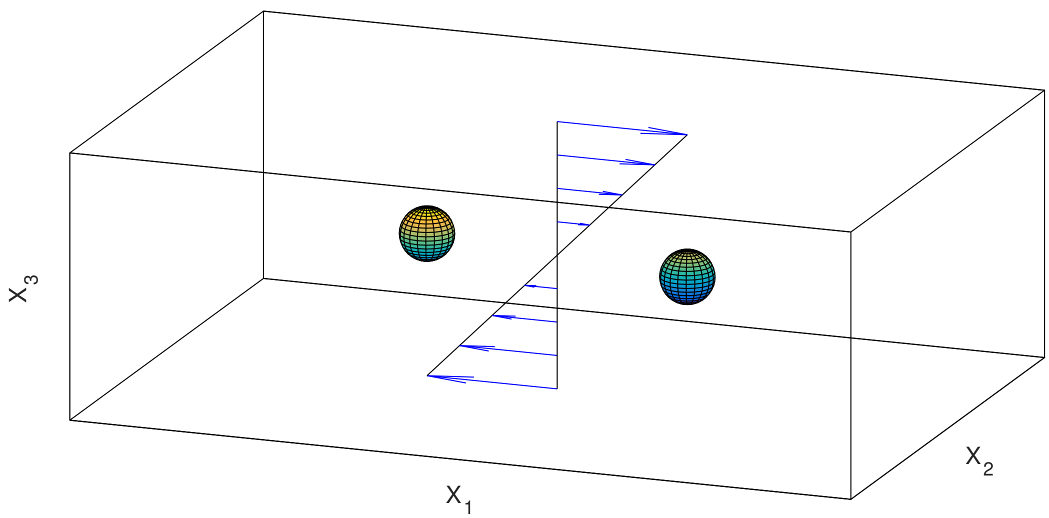

Figure 3.9: Two balls in a two-wall driven bounded shear flow.

When two balls move in a bounded shear flow of a Newtonian fluid at Stokes regime with D = 0.122, 0.194, 0.255, 0.316, 0.5, 1 as in Figure 3.10, the higher ball takes over the lower one and then both return to their initial heights for those large vertical displacements D = 1, 0.5, and 0.316. These two particle paths are called pass (or open) trajectories. But for smaller vertical displacements, D = 0.255, 0.194, 0.122, they first come close to each other and to the mid-plane between the two horizontal walls, then, the balls move away from each other and from the above mid-plane. These two particle paths are called return trajectories. Both kinds are on the shear plane as shown in Figure 3.10 for Wi=0 (Newtonian case) and they are consistent with the results obtained in [42].

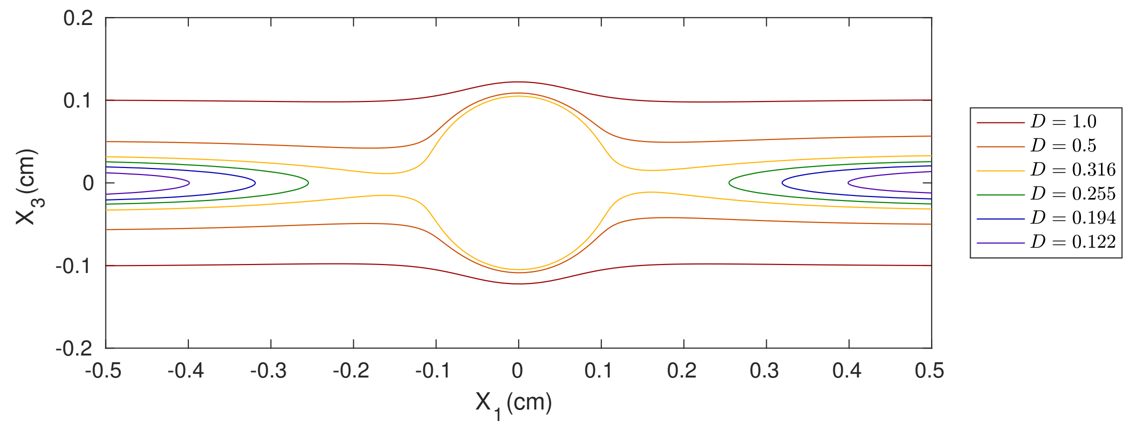

Figure 3.10: Trajectories of the two ball mass centers in a two-wall driven bounded shear flow for Wi=0 where the higher ball (initially located above $x_3 = 0$ and at $x_1 = -0.5$) moves from the left to the right and the lower ball (initially located below $x_3 = 0$ and at $x_1 = 0.5$) moves from the right to the left: (a) the balls pass over/under for vertical displacements $D = 1$, 0.5, and 0.316, and (b) the balls return for vertical displacements $D = 0.255$, 0.194, 0.122. D is a dimensionless number.

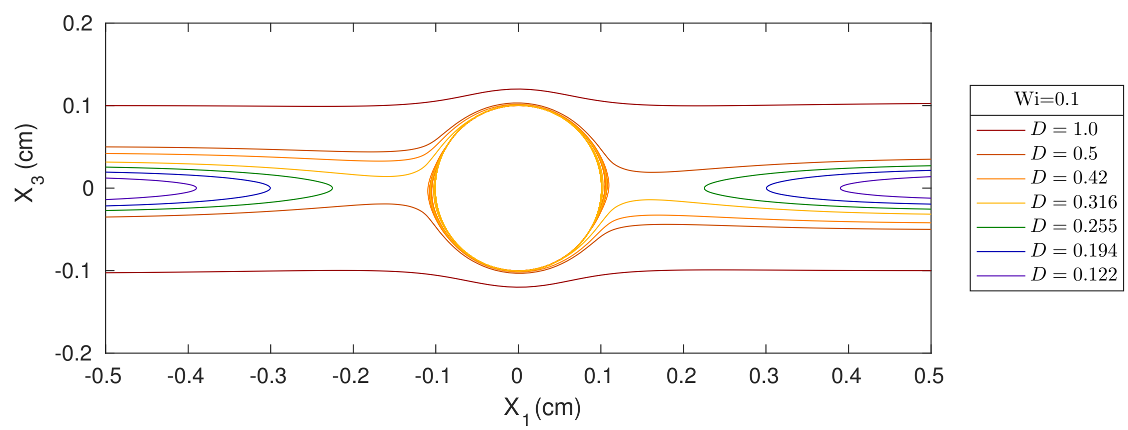

Figure 3.11: Trajectories of the two ball mass centers in a two-wall driven bounded shear flow for Wi=0.1 where the higher ball (initially located above $x_3 = 0$ and at $x_1 = -0.5$) moves from the left to the right and the lower ball (initially located below $x_3 = 0$ and at $x_1 = 0.5$) moves from the right to the left: (a) the balls pass over/under for vertical displacements $D = 1$, 0.5, (b) the balls return for vertical displacements $D = 0.42$, 0.316, and (c) the balls tumble for vertical displacements $D = 0.255$, 0.194, 0.122. D is a dimensionless number.

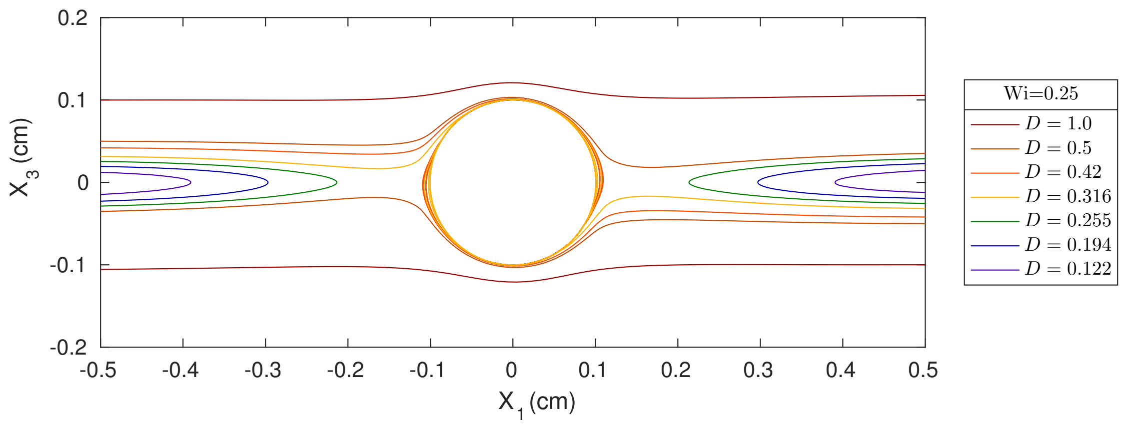

Figure 3.12: Trajectories of the two ball mass centers in a two-wall driven bounded shear flow for Wi=0.25 where the higher ball (initially located above $x_3 = 0$ and at $x_1 = -0.5$) moves from the left to the right and the lower ball (initially located below $x_3 = 0$ and at $x_1 = 0.5$) moves from the right to the left: (a) the balls pass over/under for vertical displacements $D = 1$, 0.5, (b) the balls return for vertical displacements $D = 0.42$, 0.316, and (c) the balls tumble for vertical displacements $D = 0.255$, 0.194, 0.122. D is a dimensionless number.

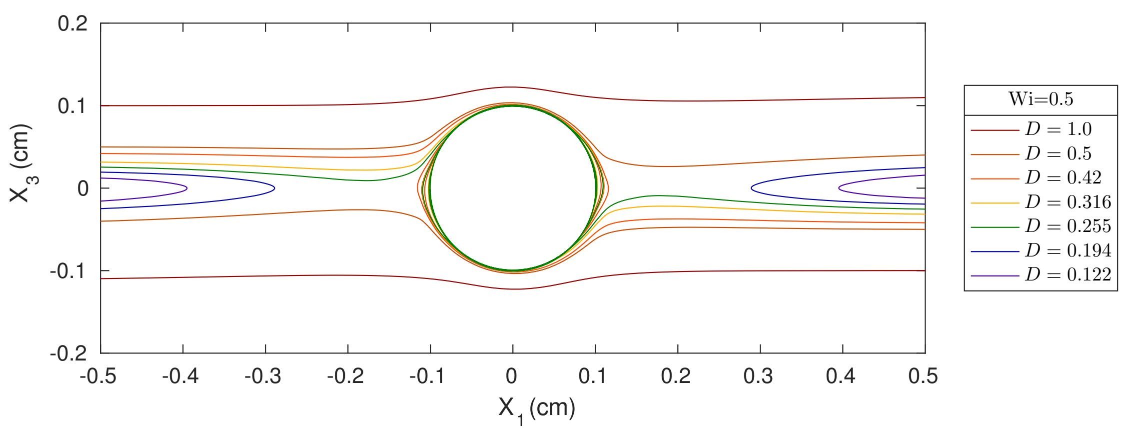

Figure 3.13: Trajectories of the two ball mass centers in a two wall driven bounded shear flow for Wi=0.5 where the higher ball (initially located above $x_3 = 0$ and at $x_1 = -0.5$) moves from the left to the right and the lower ball (initially located below $x_3 = 0$ and at $x_1 = 0.5$) moves from the right to the left: (a) the balls pass over/under for vertical displacements $D = 1$, 0.5, (b) the balls return for vertical displacements $D = 0.42$, 0.316, 0.255, and (c) the balls tumble for vertical displacements $D = 0.194$, 0.122. D is a dimensionless number.

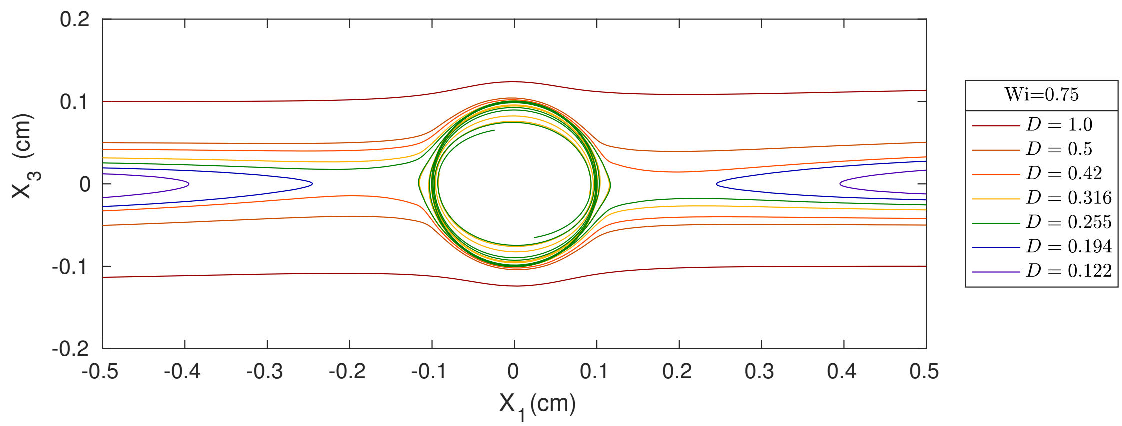

Figure 3.14: Trajectories of the two ball mass centers in a two wall driven bounded shear flow for Wi=0.75 where the higher ball (initially located above $x_3 = 0$ and at $x_1 = -0.5$) moves from the left to the right and the lower ball (initially located below $x_3 = 0$ and at $x_1 = 0.5$) moves from the right to the left: (a) the balls pass over/under for vertical displacements $D = 1, 0.5, 0.42$, (b) the balls return for vertical displacements $D = 0.316, 0.255$, and (c) the balls tumble for vertical displacements $D = 0.194, 0.122$. D is a dimensionless number.

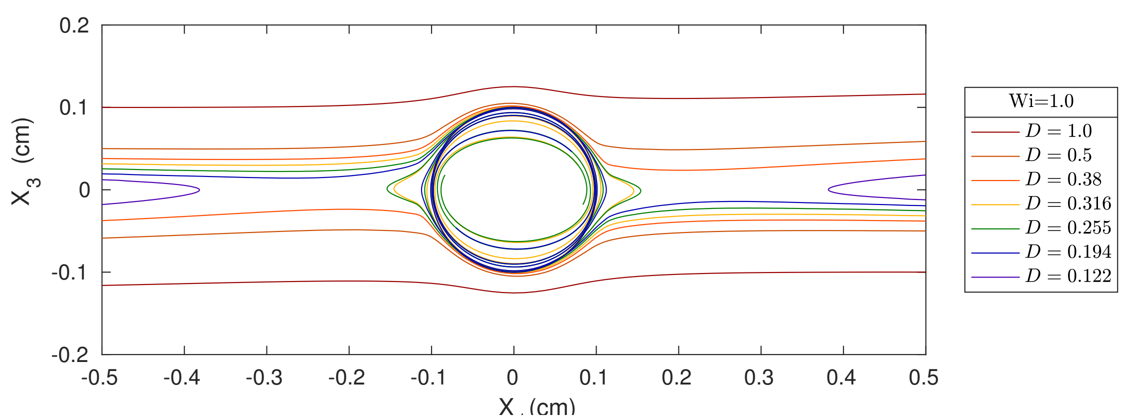

Figure 3.15: Trajectories of the two ball mass centers in a two-wall driven bounded shear flow for Wi=1 where the higher ball (initially located above $x_3 = 0$ and at $x_1 = -0.5$) moves from the left to the right and the lower ball (initially located below $x_3 = 0$ and at $x_1 = 0.5$) moves from the right to the left: (a) the balls pass over/under for $D = 1, 0.5, 0.38$, (b) the balls return for $D = 0.316, 0.255, 0.194$, and (c) the balls tumble for $D = 0.122$. D is a dimensionless number.

For the two balls interacting in an Oldroyd-B fluid with $D = 0.122$, 0.194, 0.255, 0.316, 0.42, 0.5, 1, we have summarized the results for Wi=0.1, 0.25, 0.5, 0.75, and 1 in Figure 3.21 to 3.25.

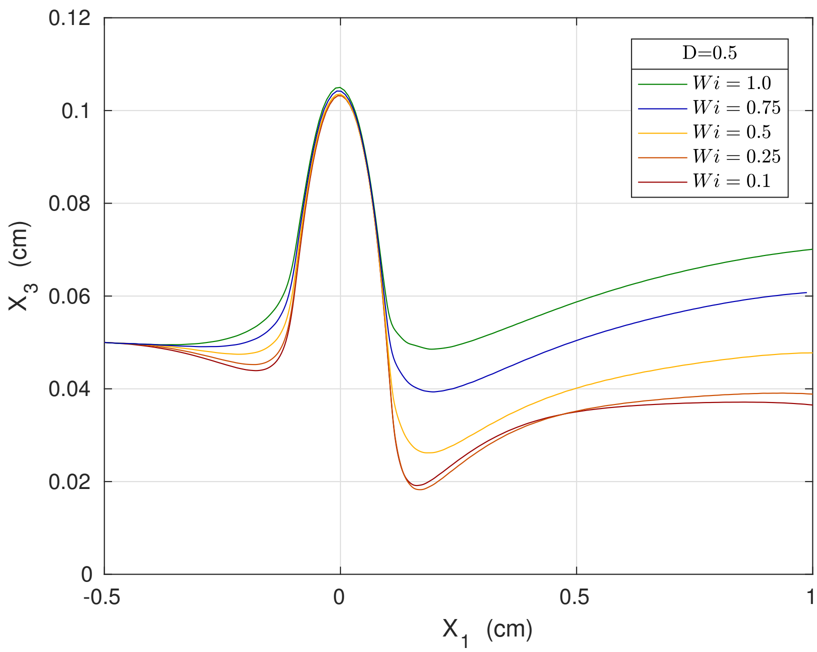

Figure 3.16: Trajectories of one ball mass center started above the mid-plane in a two-wall driven bounded shear flow for vertical displacements D=0.5. After two balls pass over/under each other, the trajectories first go toward the mid-plane then lift up but don't return to the initial vertical position like the case in a Newtonian fluid. D is a dimensionless number.

As in a Newtonian fluid, there are results of pass and return trajectories concerning two ball encounters; but the the trajectories of the two ball mass centers loose the symmetry due to the effect of elastic force arising from viscoelastic fluids. For example, in Figure 3.16 there are open trajectories of the ball started above the mid-plane associated with $D = 0.5$ for Wi=0.1, 0.25, 0.5, 0.75, and 1. These trajectories are much closer to the mid-plane after two balls pass over/under each other. The fluid elastic force is not strong enough to hold them together during passing over/under, but it already pulls the balls toward each other and then change the shape of the trajectories.

Another series of passing over trajectories as shown in Figure 3.17. There are the open trajectories the ball started above the mid-plane associated with $D = 1$ for Wi=0.1, 0.25, 0.5, 0.75, and 1. Instead of elastic force between two balls, the force from the moving wall effect is stronger and it leads the ball migrates toward the moving wall. As mentioned in section 3.5.2, the ball migrates faster under a higher Wi.

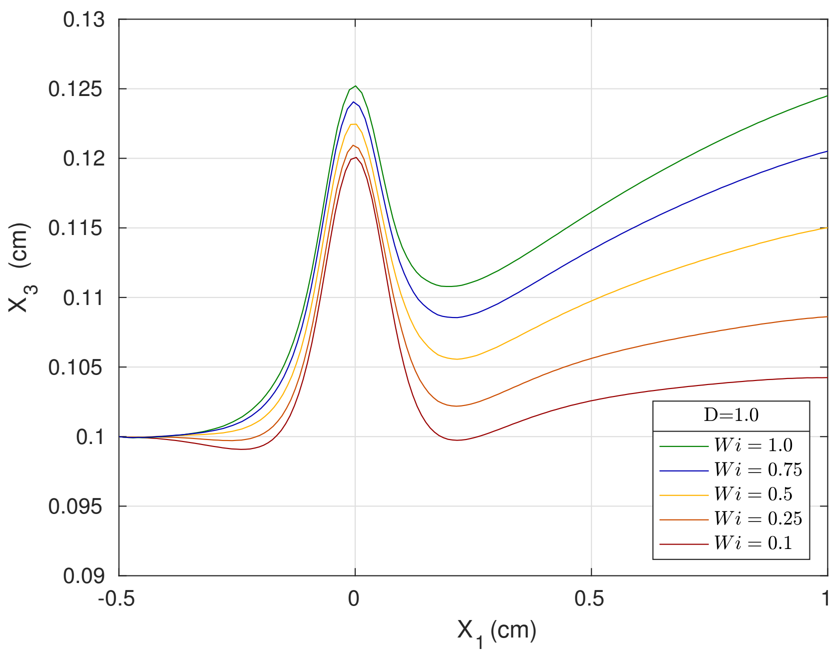

Figure 3.17: Trajectories of one ball mass center started above the mid-plane in a two-wall driven bounded shear flow for vertical displacements D=1. D is a dimensionless number.

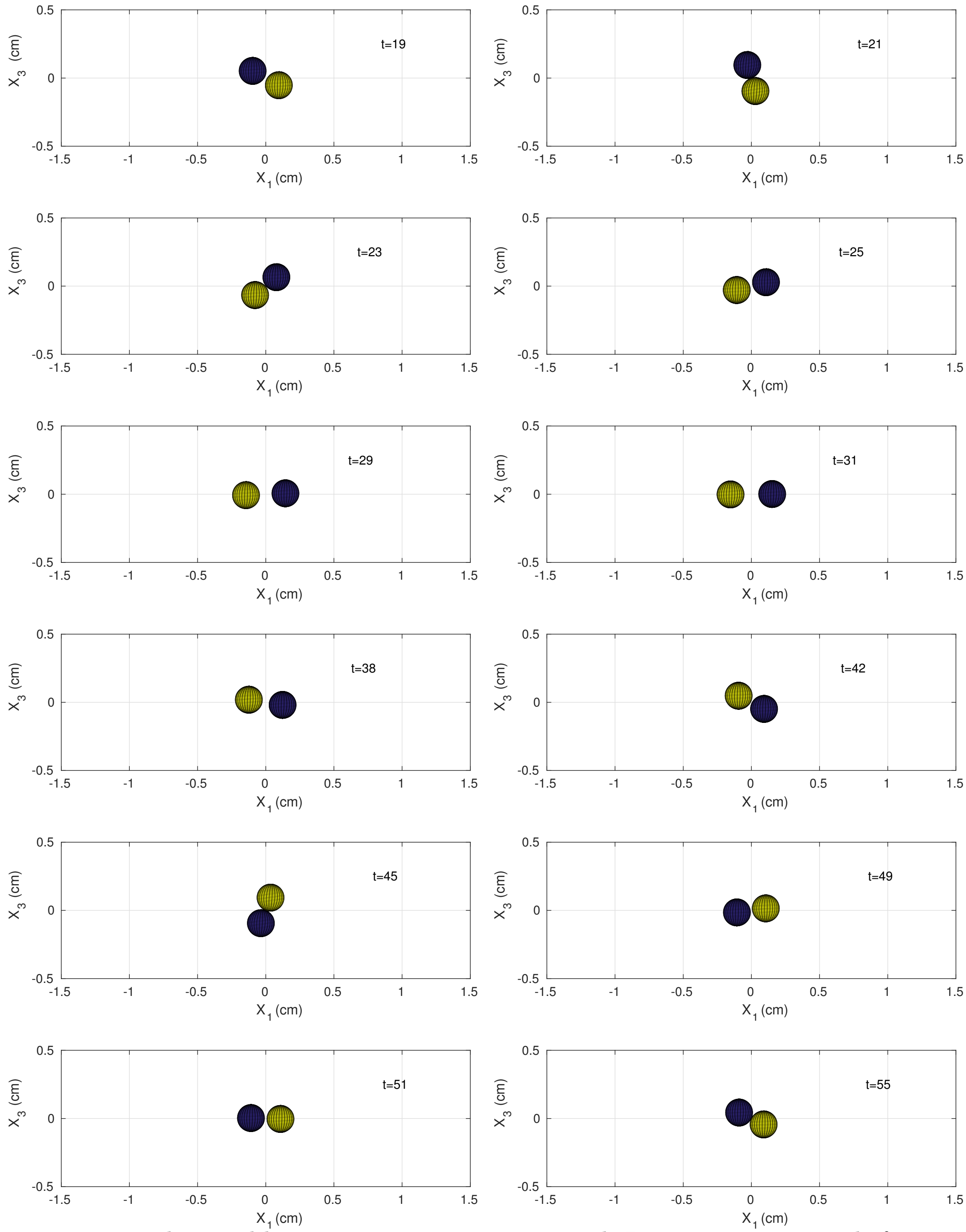

Figure 3.18: The tumbling motion as $Wi = 1.0$ and $D = 0.255$. For each frame, the horizontal direction is X_1 axis and vertical direction is X_3 axis. Wi and D are dimensionless numbers.

For higher values of Wi considered in this section, there are less return trajectories; instead it is easier to obtain the two ball chain once they run into each other. Actually depending on the Weissenberg number Wi and the initial vertical displacement $\triangle s$, a chain of two balls can be formed in a bounded shear flow, and then such chain tumbles. For example, for $D = 0.316$, the two balls come to each other, form a chain and then rotate with respect to the midpoint between two mass centers for Wi=0.1, 0.25, 0.5, 0.75, and 1. In Figure 3.18 it is a series of time frames of tumbling motion as Wi= 1.0 and D=0.255

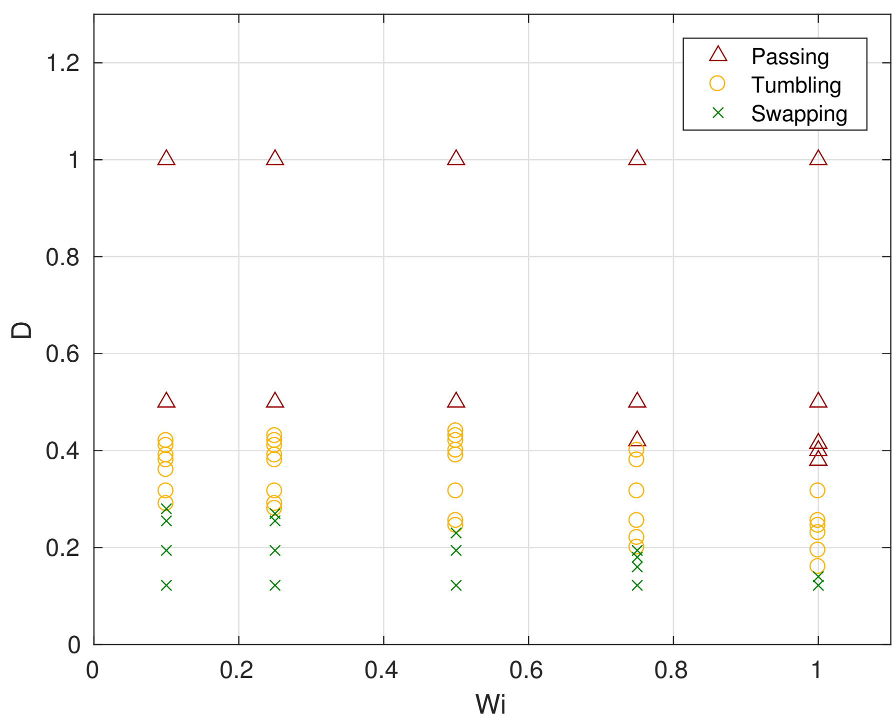

Figure 3.19: Phase diagram for the motion of two balls based on the initial vertical displacement D and Weissenberg number Wi in a two-wall driven bounded bounded shear flow. Wi and D are dimensionless numbers.

The details of the phase diagram of pass, return, and tumbling are shown in

Figure 3.19. The range of the vertical distance for the passing over becomes bigger for higher Weissenberg numbers. For the shear flow considered in this article, the increasing of the value of the Wi with a fixed shear rate is same as to increase the shear rate with a fixed relaxation time. This explains why, for Wi=1, two balls can have bigger gap between them while rotating with respect to the middle point between two mass centers since the two balls are kind of moving under higher shear rate. Those tumbling trajectories are actually associated with the closed streamlines around a freely rotating ball centred at the origin.

3.5.4 Two ball interacting with small initial distance in a two-wall driven bounded shear flow

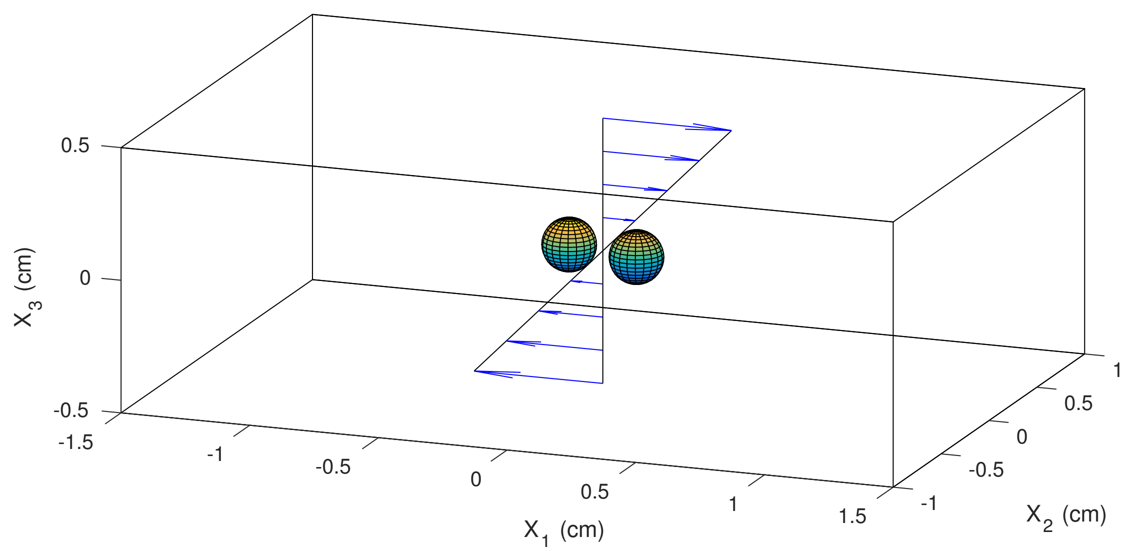

Figure 3.20: Two balls in a two-wall driven bounded shear flow.

In this section, we have considered the cases of two balls of the same size interacting in a bounded shear flow driven by walls as visualized in Figure 3.20. The ball radii are $r = 0.1$. The fluid and ball densities are $\rho_f = \rho_s = 1$, the viscosity being $\eta_1 = 1$. The computational domain is $\Omega = (-1.5, 1.5) \times (-1, 1) \times (-0.5, 0.5)$. The shear rate is fixed at $\dot{\gamma} = 1$ but the velocity of the top wall is $U = 1$, the bottom wall being $U = 0$. The mesh size for the velocity field and the conformation tensor is $h = 1/48$, the mesh size for the pressure is $2h$, The time step being $\triangle t = 0.001$.

In order to study the interactions of two balls besides passing and swapping behaviors (e.g., see [20], [21], [41]), we have considered the mass centers of the two balls are located on the shear plane at $(-x_0, 0, z_0)$ and $(x_0, 0, -z_0)$ initially such that the angle between the mid-plane $x_3 = 0$ and the line segment of two initial locations of mass center of particle is $175°$ counterclockwise. We define the gap size $= d - 2r$ where d is the distance between two mass centers of particle and r is 0.1.

For the two balls interacting in Oldroyd-B fluid with gap= $h/2$, h, $2h$, and $3h$ where h is the mesh size, we have summarized the results for Wi=0.1, 0.25, 0.5, 0.75, and 1 in Figure 3.21 to Figure 3.25. We have plotted in Figure 3.21 to 3.25 the relative trajectories of the two ball mass centers via the graphs of $(x_{i,1} - \bar{x_1}, x_{i,3} - \bar{x_3})$, for i =1, 2, the mass center of the two balls being $\mathbf{x}_i = (x_{i,1}, x_{i,2}, x_{i,3})$, i =1, 2; the midpoint between two ball mass center $\mathbf{x}_1$ and $\mathbf{x}_2$ is $\bar{\mathbf{x}} = \frac{1}{2}(\mathbf{x}_1 + \mathbf{x}_2) = (\bar{x_1}, \bar{x_2}, \bar{x_3})^t$.

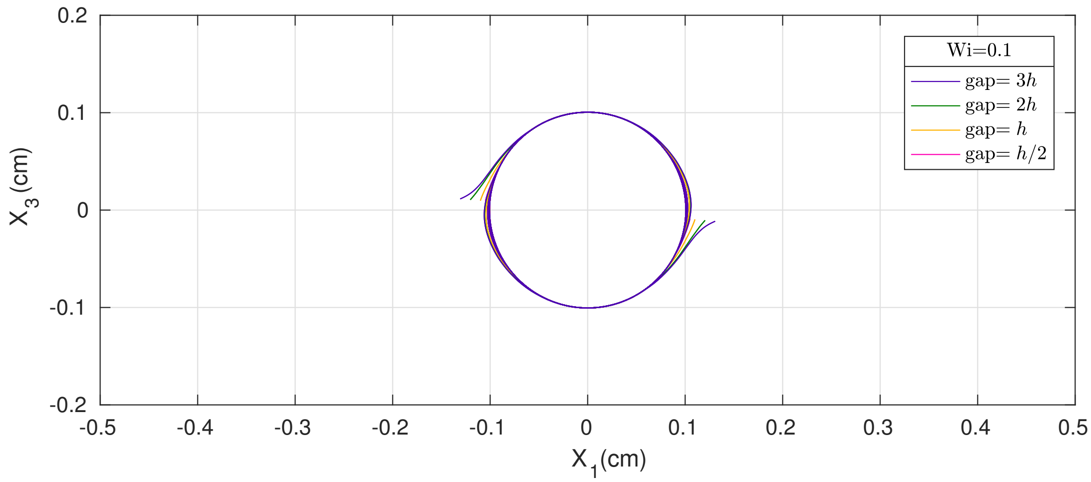

Figure 3.21: Trajectories of the two ball mass centers in a two-wall driven bounded shear flow for Wi=0.1 where the higher ball (initially located above $x_3 = 0$) moves from the left to the right and the lower ball (initially located below $x_3 = 0$) moves from the right to the left: all the balls tumble for gap = 3h, 2h, h, h/2. The unit of mesh size h is centimeter and Wi is a dimensionless number.

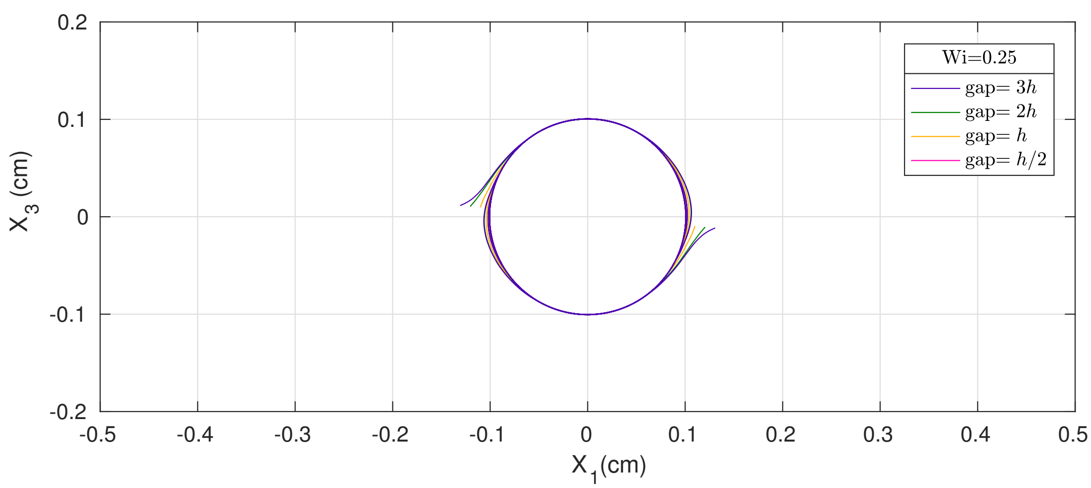

Figure 3.22: Trajectories of the two ball mass centers in a two-wall driven bounded shear flow for Wi=0.25 where the higher ball (initially located above $x_3 = 0$) moves from the left to the right and the lower ball (initially located below $x_3 = 0$) moves from the right to the left: all the balls tumble as gap = 3h, 2h, h, h/2. The unit of mesh size h is centimeter and Wi is a dimensionless number.

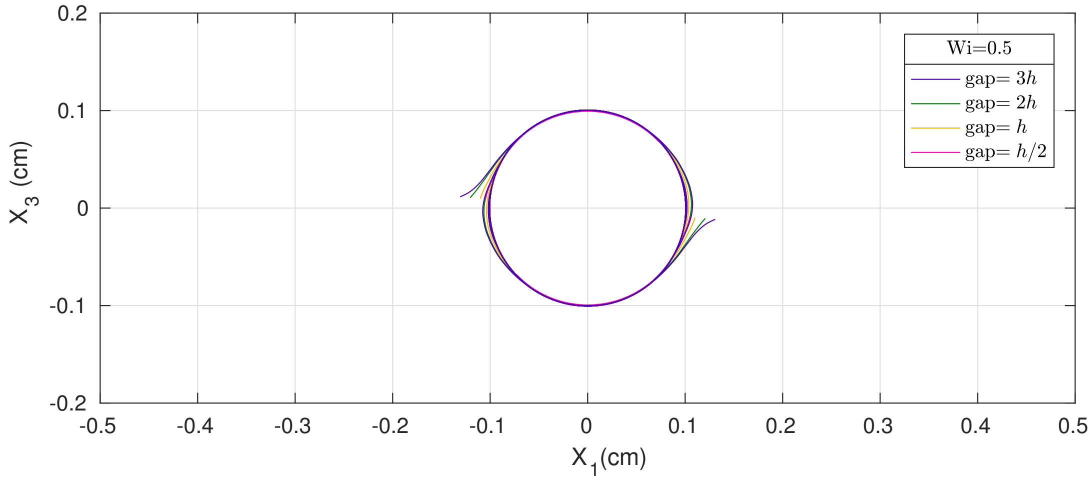

Figure 3.23: Trajectories of the two ball mass centers in a two-wall driven bounded shear flow for Wi=0.5 where the higher ball (initially located above $x_3 = 0$) moves from the left to the right and the lower ball (initially located below $x_3 = 0$) moves from the right to the left: the balls tumble for *gap* = 3h, 2h, h, h/2. The unit of mesh size h is centimeter and Wi is a dimensionless number.

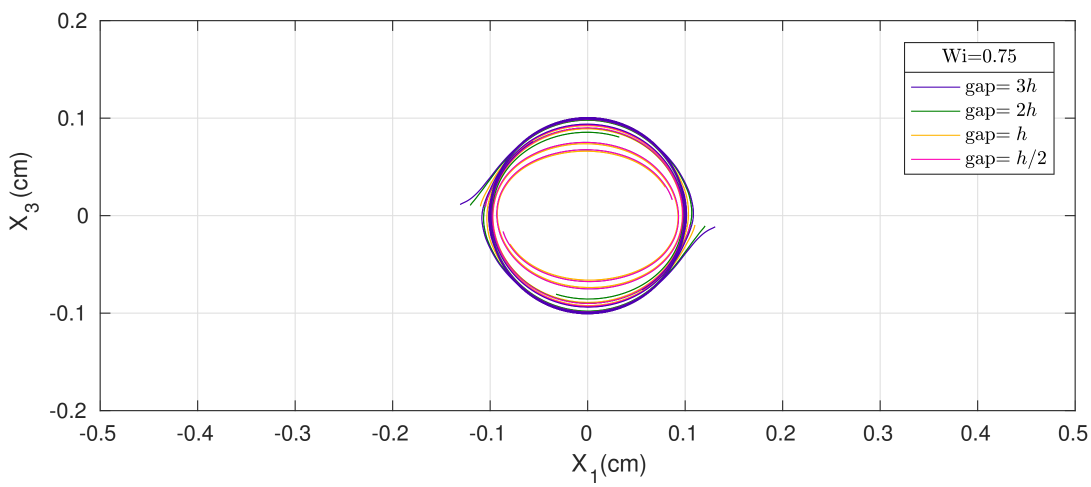

Figure 3.24: Trajectories of the two ball mass centers in a two-wall driven bounded shear flow for Wi=0.75 where the higher ball (initially located above $x_3 = 0$) moves from the left to the right and the lower ball (initially located below $x_3 = 0$) moves from the right to the left: the balls tumble then kayaking for *gap* = 3h, 2h, h, h/2. The unit of mesh size h is centimeter and Wi is a dimensionless number.

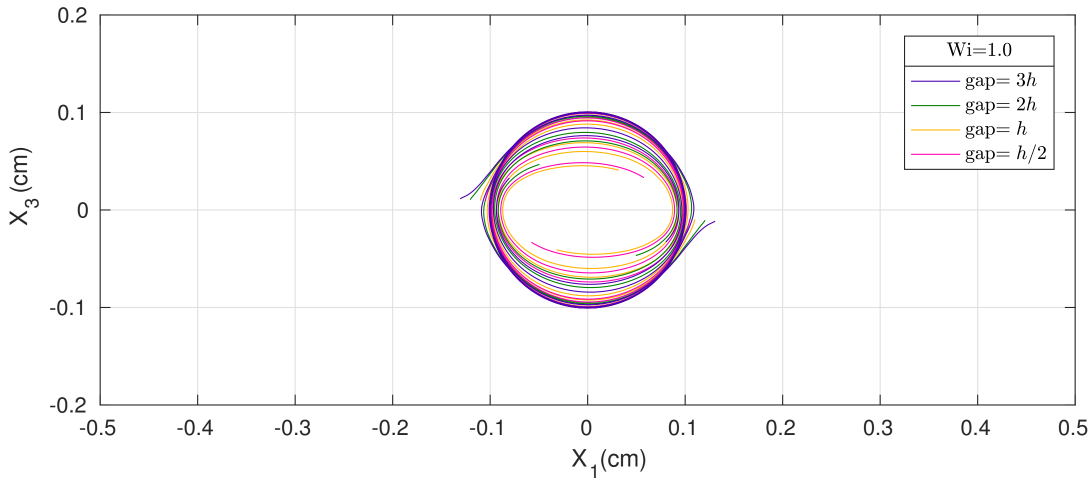

Figure 3.25: Trajectories of the two ball mass centers in a two-wall driven bounded shear flow for Wi=1 where the higher ball (initially located above $x_3 = 0$) moves from the left to the right and the lower ball (initially located below $x_3 = 0$) moves from the right to the left: the balls tumbling then kayaking for gap = 3h, 2h, h, h/2. The unit of mesh size h is centimeter and Wi is a dimensionless number.

For all cases we have considered in Figure 3.21 to 3.25, all the behaviors are tumbling for gap = 3h, 2h, h, h/2. Besides balls rotating around one another with a fixed axis, there is also a behavior that the two balls rotate but not around a fixed axis as Wi = 1 and gap = 3h, 2h, h, h/2. The behavior is similar to the motion of kayaking for a long body. As seen in Figure 3.26, it is a series of frames of kayaking behavior of the two balls for Wi = 1.0 and $gap = 3h$. To describe this behavior, two balls first chain and tumble while the two ball mass centers are on the shear plane $X_2 = 0$. Then two balls still rotate around one another but the two ball mass centers are not on the shear plane.

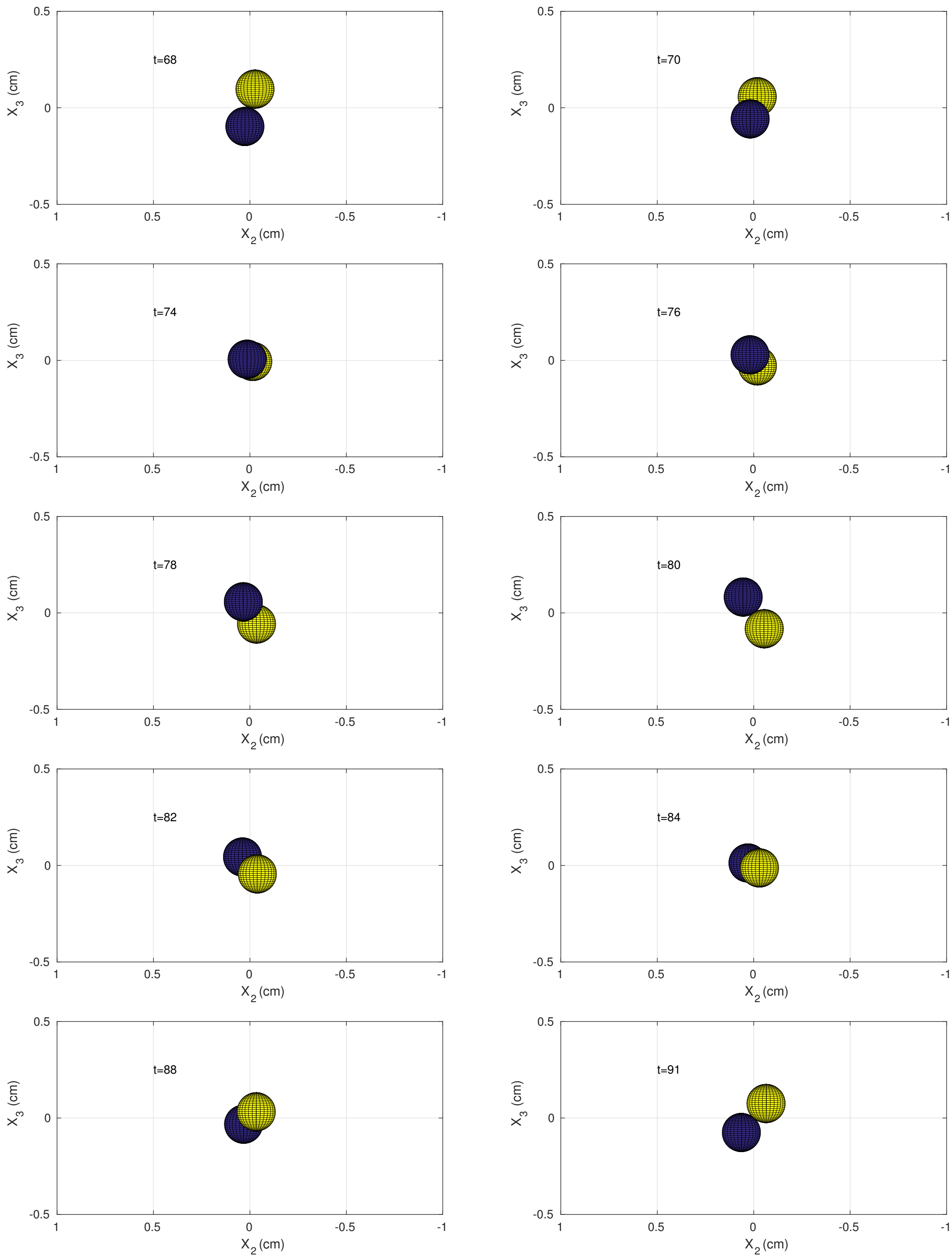

Figure 3.26: The kayaking motion as $Wi = 1.0$: the initial distance between two particles is 2r+gap where $r = 0.1$, gap=$3h$. For each frame, the horizontal direction is X_2 axis and vertical direction is X_3 axis. The unit of mesh size h is centimeter and Wi is a dimensionless number.

3.5.5 Two ball interacting with small initial distance in an one-wall driven bounded shear flow

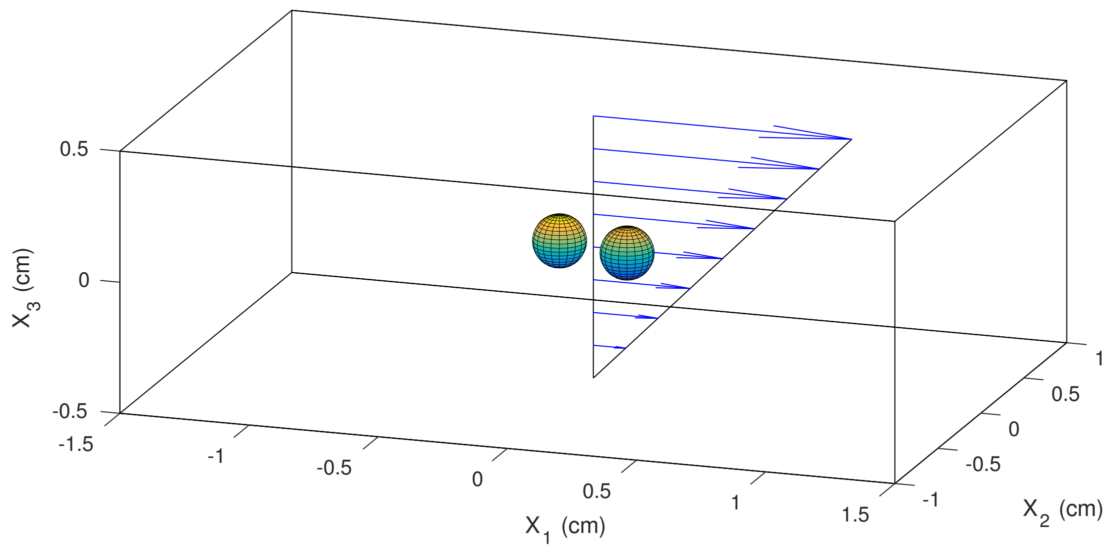

Figure 3.27: Two balls in an one-wall driven bounded shear flow.

In this section, we have considered the cases of two balls of the same size interacting in a bounded shear flow driven by the upper wall as visualized in Figure 3.27. The ball radii are $r = 0.1$. The fluid and ball densities are $\rho_f = \rho_s = 1$, the viscosity being $\eta_1 = 1$. The computational domain is $\Omega = (-1.5, 1.5) \times (-1, 1) \times (-0.5, 0.5)$. The shear rate is fixed at $\dot{\gamma} = 1$ but the velocity of the top wall is $U = 1$, the bottom wall being $U = 0$. The mesh size for the velocity field and the conformation tensor is $h = 1/48$, the mesh size for the pressure is $2h$, The time step being $\triangle t = 0.001$.

In order to study the interactions of two balls besides passing and swapping behaviors (e.g., see [20], [21], [41]), we have considered the mass centers of the two balls are located on the shear plane at $(-x_0, 0, z_0)$ and $(x_0, 0, -z_0)$ initially such that the angle between the mid-plane $x_3 = 0$ and the line segment of two initial locations of mass center of particle is 175° counterclockwise. We define the gap size $= d - 2r$ where d is the distance between two mass centers of particle and radius r is 0.1.

For the two balls interacting in Oldroyd-B fluid with gap= $h/8$, $h/4$, $h/2$, h, $2h$, and $3h$ where h is the mesh size, we have summarized the results for Wi=0.1, 0.25, 0.5, 0.75, and 1 in Figure 3.28 to Figure 3.32. We have plotted in Figure 3.28 to 3.32 the relative trajectories of the two ball mass centers via the graphs of $(x_{i,1} - \bar{x_1}, x_{i,3} - \bar{x_3})$, for i =1, 2, the mass center of the two balls being $\mathbf{x}_i = (x_{i,1}, x_{i,2}, x_{i,3})$, i =1, 2; the midpoint between two ball mass center $\mathbf{x}_1$ and $\mathbf{x}_2$ is $\bar{\mathbf{x}} = \frac{1}{2}(\mathbf{x}_1 + \mathbf{x}_2) = (\bar{x_1}, \bar{x_2}, \bar{x_3})^t$.

As seen in Figure 3.29, we show the passing behaviors for $gap = 3h$ which is different from the case under a two-wall driven fluid flow. But two-ball chain tumbles around a fixed axis in the middle of the two ball mass centers for gap = 2h, h, h/2, h/4, h/8. It is worthy to mention the tumbling behavior for $gap = 2h$. Two balls first approach with each other then chain and rotate in a while, then two balls still rotate but they rotate separately in a short time, but after the distance between two balls approaches a certain maximum separation distance, the two balls start to rebound then chain rotate again. This behavior is called kissing-tumbling-separation phenomena which has also obtained in an Oldroyd-B fluid in [20].

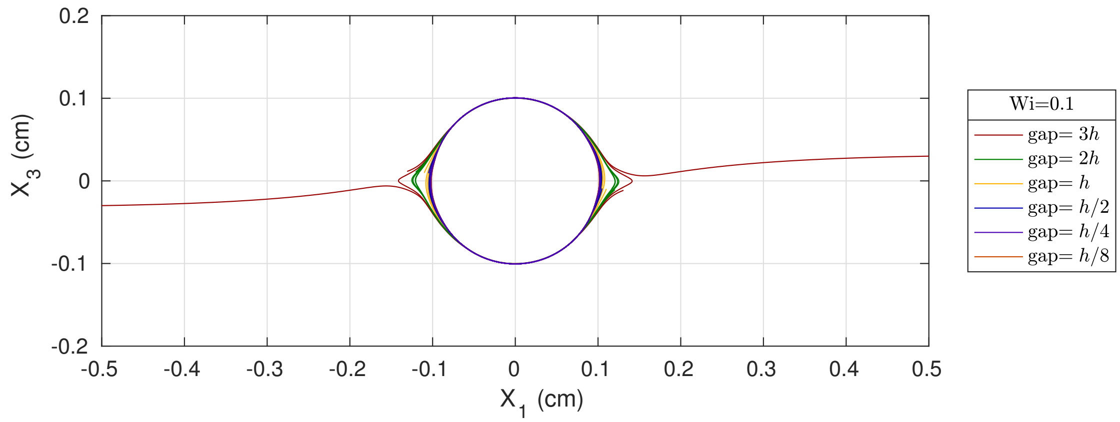

Figure 3.28: Trajectories of the two ball mass centers in an one-wall driven bounded shear flow for Wi=0.1 where the higher ball (initially located above $x_3 = 0$) moves from the left to the right and the lower ball (initially located below $x_3 = 0$) moves from the right to the left: (a) the balls pass over/under for *gap* = 3h, and (b) the balls tumble for *gap* = 2h, h, h/2, h/4, h/8. The unit of mesh size h is centimeter and Wi is a dimensionless number.

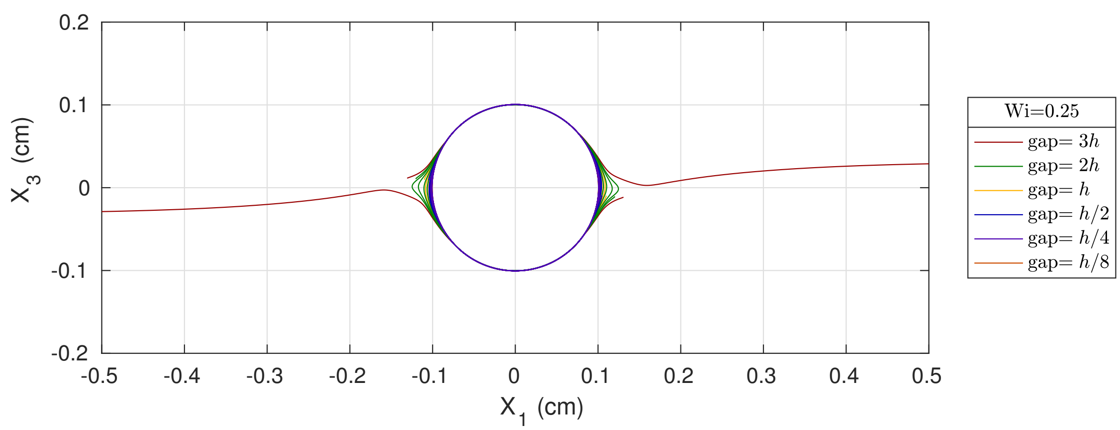

Figure 3.29: Trajectories of the two ball mass centers in an one-wall driven bounded shear flow for Wi=0.25 where the higher ball (initially located above $x_3 = 0$) moves from the left to the right and the lower ball (initially located below $x_3 = 0$) moves from the right to the left: (a) the balls pass over/under for *gap* = 3h, and (b) the balls tumble for *gap* = 2h, h, h/2, h/4, h/8. The unit of mesh size h is centimeter and Wi is a dimensionless number.

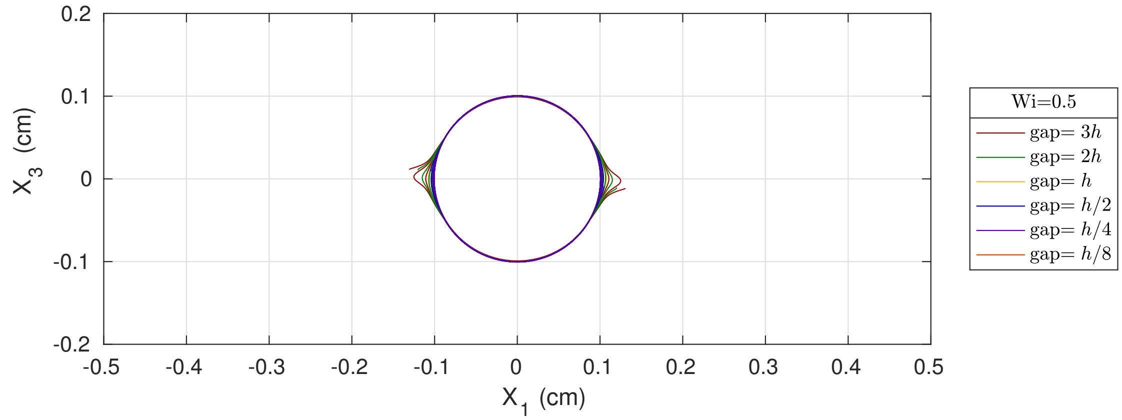

Figure 3.30: Trajectories of the two ball mass centers in an one-wall driven bounded shear flow for Wi=0.5 where the higher ball (initially located above $x_3 = 0$) moves from the left to the right and the lower ball (initially located below $x_3 = 0$) moves from the right to the left: the balls tumble for gap = 3h, 2h, h, h/2, h/4, h/8. The unit of mesh size h is centimeter and Wi is a dimensionless number.

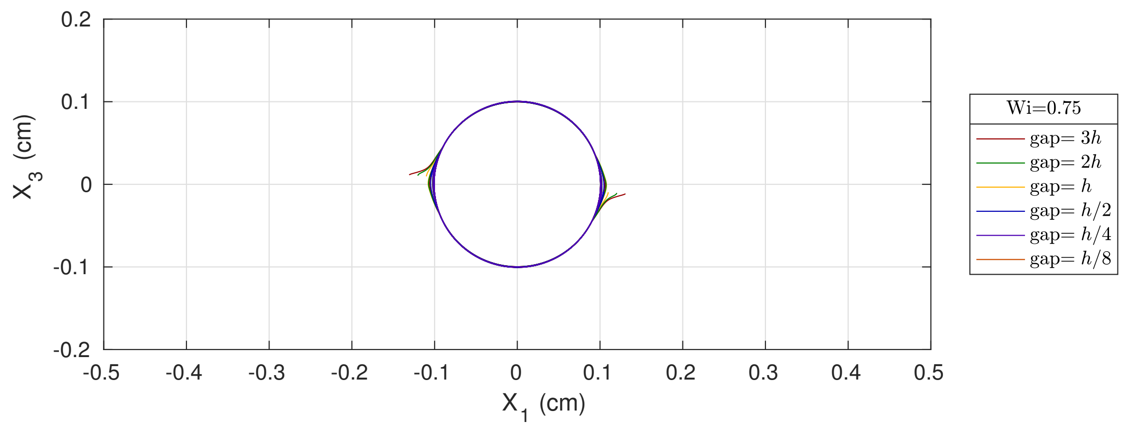

Figure 3.31: Trajectories of the two ball mass centers in an one-wall driven bounded shear flow for Wi=0.75 where the higher ball (initially located above $x_3 = 0$) moves from the left to the right and the lower ball (initially located below $x_3 = 0$) moves from the right to the left: the balls tumble for gap = 3h, 2h, h, h/2, h/4, h/8. The unit of mesh size h is centimeter and Wi is a dimensionless number.

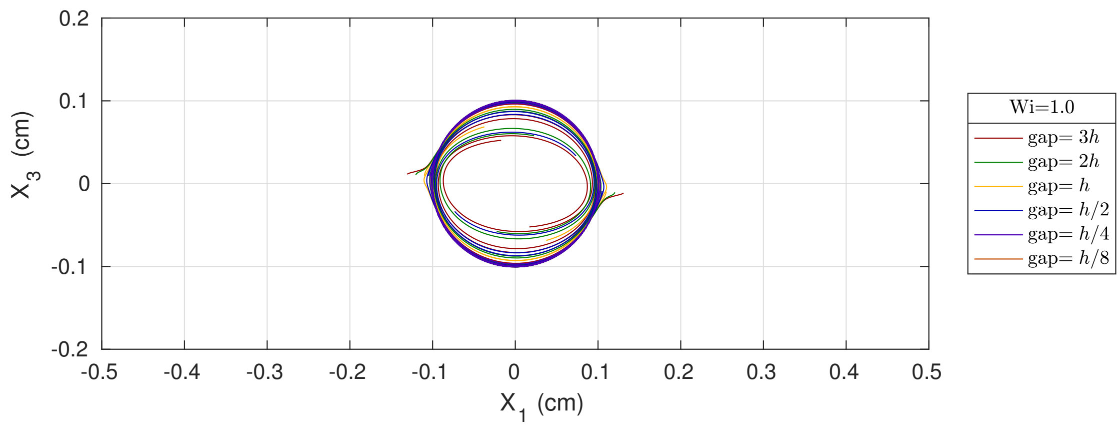

Figure 3.32: Trajectories of the two ball mass centers in an one-wall driven bounded shear flow for Wi=1 where the higher ball (initially located above $x_3 = 0$) moves from the left to the right and the lower ball (initially located below $x_3 = 0$) moves from the right to the left: (a) the balls tumble for gap = h/4, h/8, and (b) the balls tumbling then kayaking for gap = 3h, 2h, h, h/2. The unit of mesh size h is centimeter and Wi is a dimensionless number.

For higher Wi $= 0.5, 0.75, 1.0$ in Figure 3.30 to 3.32, all the behaviors are tumbling for gap = 3h, 2h, h, h/2, h/4, h/8. In Figure 3.33 is a series of frames of the two-ball tumbling behavior for Wi = 0.5 and $gap = 3h$. The kissing-tumbling-separation phenomena have been seen for higher gap sizes. Besides tumbling motions, the kayaking motion have been observed as Wi= 1. As seen in Figure 3.34, it is a series of frames of the two-ball kayaking behavior for Wi = 1 and $gap = 3h$. For a long body like a prolate ellipsoid, we say that it tumbles on the shear plane if its long axis rotates on the shear plane (i.e. rotating on the shear plane with respect to one of its short axis perpendicular to the shear plane). Such tumbling motion is not a stable state for higher values of Wi. Two ball chain can been seen as a loosely connected long body so that it should behave like a long body. Its long axis migrates away from the shear plane for high values of Wi so the motion changes from tumbling to kayaking.

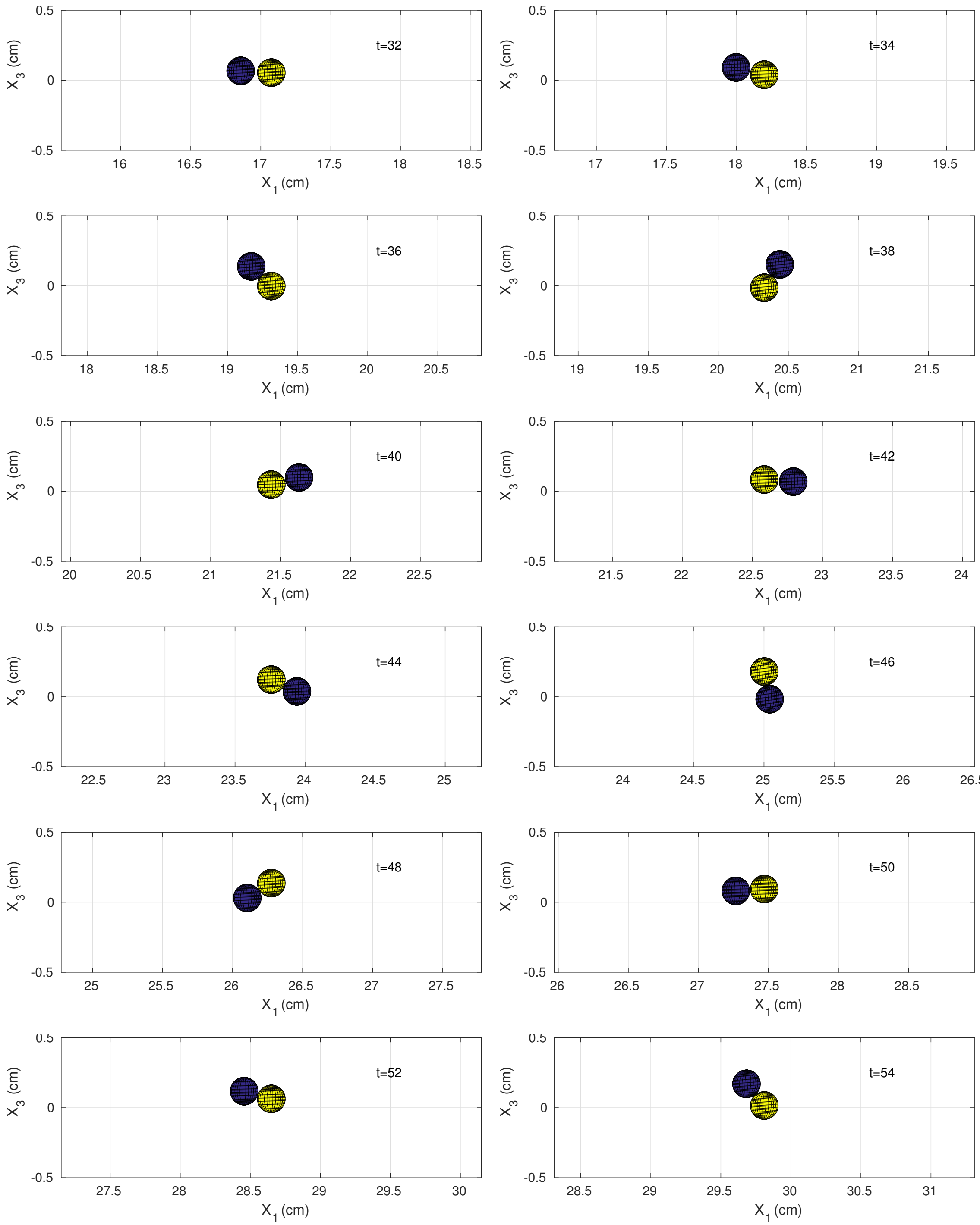

Figure 3.33: The tumbling motion as $Wi = 0.5$: the initial distance between two particles is 2r+gap where $r = 0.1$, gap=$3h$.For each frame, the horizontal direction is X_1 axis and vertical direction is X_3 axis. The unit of mesh size h is centimeter and Wi is a dimensionless number.

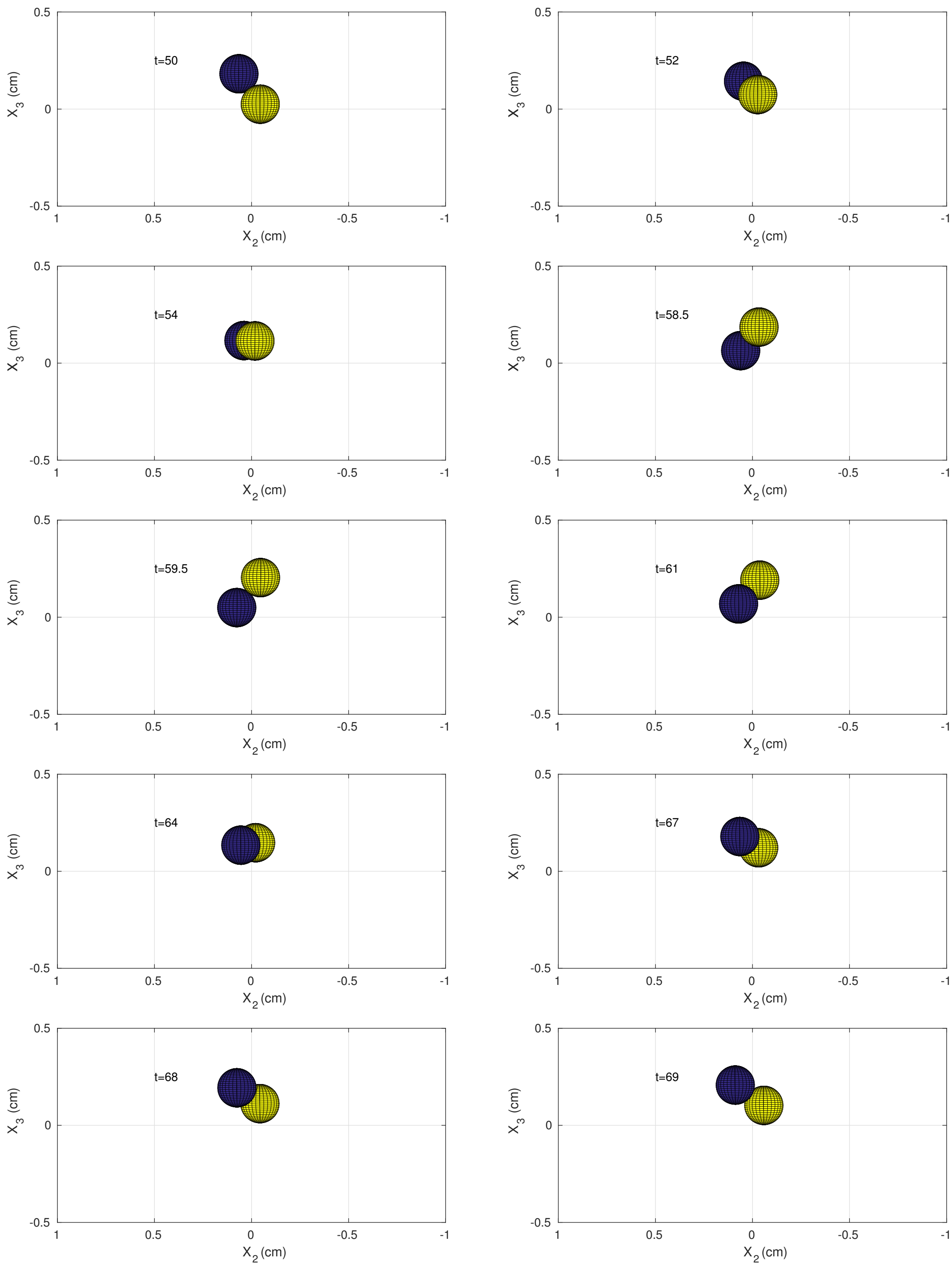

Figure 3.34: The kayaking motion as $Wi = 1.0$: the initial distance between two particles is 2r+gap where $r = 0.1$, gap=$3h$. For each frame, the horizontal direction is X_2 axis and vertical direction is X_3 axis. The unit of mesh size h is centimeter and Wi is a dimensionless number.

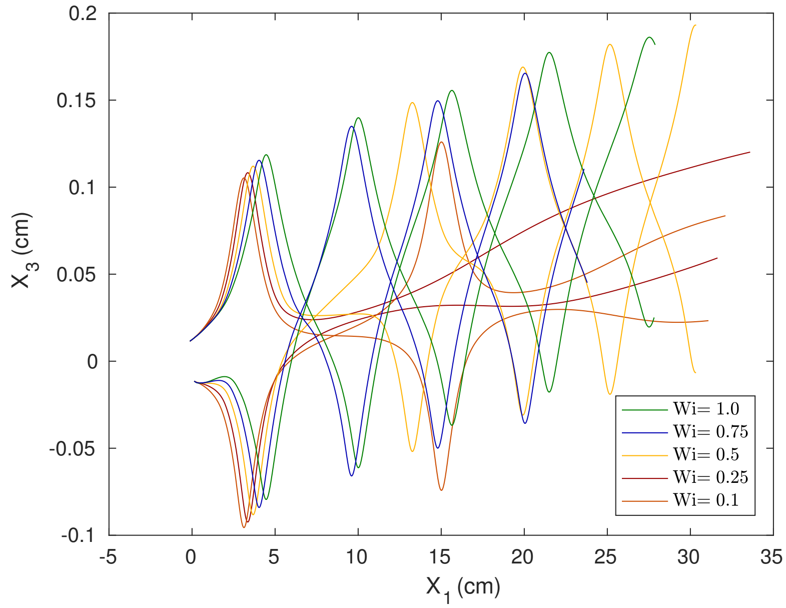

Figure 3.35: Trajectories of two ball mass centers in an one-wall driven bounded shear flow for *gap* =3h. The unit of mesh size h is centimeter and Wi is a dimensionless number.

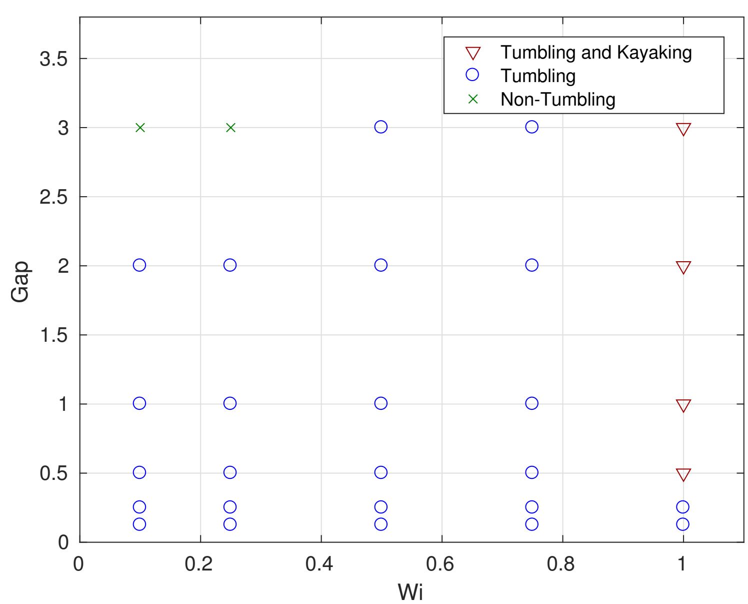

Figure 3.36: Phase diagram for the motion of two balls based on the initial gap size *gap* and Weissenberg number Wi in an one-wall driven bounded shear flow. The unit of mesh size h is centimeter and Wi is a dimensionless number.

For *gap* =3h and five considered Wi, trajectories of two ball mass centers are shown in Figure 3.35. For Wi= 0.1 and 0.25, the higher one takes over the lower one and both migrate toward the top moving wall. For Wi= $0.5, 0.75$, and 1, the higher first catch up the lower one to form a chain and they rotate around one another and migrate toward the moving wall as a cluster.

The details of the phase diagram of pass, tumbling, and tumbling then kayaking are shown in Figure 3.36. There are more tumbling-kayaking behaviors for a larger Weissenberg numbers.

CHAPTER 4

Conclusions and Future work

4.1 Conclusions

In this dissertation, we presented a new distributed Lagrange multiplier/fictitious domain method for simulating fluid-particle interaction in three-dimensional Stokes flow. A conjugate gradient method driven by both pressure and distributed Lagrange multiplier, called a one-shot method, has been developed to solve the discrete Stokes problem while enforcing the rigid body motion within the region occupied by the particle. The methodology is validated by comparing the numerical results of a neutrally buoyant particle in either Newtonian or Oldroyd-B fluids.

For the cases of two ball encounters under creeping flow conditions in a top-wall driven shear flow of Newtonian fluids, the trajectories of the two ball mass centers are consistent with the results obtained in [42] and also with those of the two balls in a two-wall driven shear flow. The swapping trajectories in a one-wall driven shear flow are actually like those of two balls coming toward each other and then later moving away in a two-wall driven shear flow due to the presence of the two walls. For the cases of a two-ball encounter under creeping flow conditions in a two-wall driven shear flow of Oldroyd-B fluids there are three different trajectory behaviors: pass, tumbling, and return trajectories; but the the trajectories of the two ball mass centers lose symmetry due to the effect of elastic force arising from viscoelastic fluids. Instead of returning back to the initial vertical displacement in Newtonian fluids, the balls migrate toward the moving wall and then rapidly migrate in higher viscoelasticity fluids. For two balls located close to each other initially in a top-wall driven shear flow of Oldroyd-B fluids, we have obtained that three binary encounters : pass, tumbling, and tumbling then kayaking. Since tumbling motion is not a stable motion, the two ball mass centers couldn't stay on shear plane all the time when two-ball chain tumbles.

4.2 Future work

The string of particles phenomenon in viscoelastic shear flow (see Fig. 4.1) has been observed experimentally in ,e.g., [25] and [39]. The numerical results of the three balls alignment in a viscoelastic fluid of Gieskus type has been obtained in [21]. However, their balls have been initially placed specially at certain position. Numerical simulation of particle strings in shear flow of viscoelastic fluids haven't been actually obtained to the best of our knowledge. It is believed that the property of the shear thinning is the key factor to have the string phenomenon of many particles. Therefore, the next step is to model the fluid-particle system by taking into account the shear thinning effect through the combination of the Carreau and Oldroyd-B models proposed in this dissertation and then simulate particle interactions in shear flow via such resulting model.

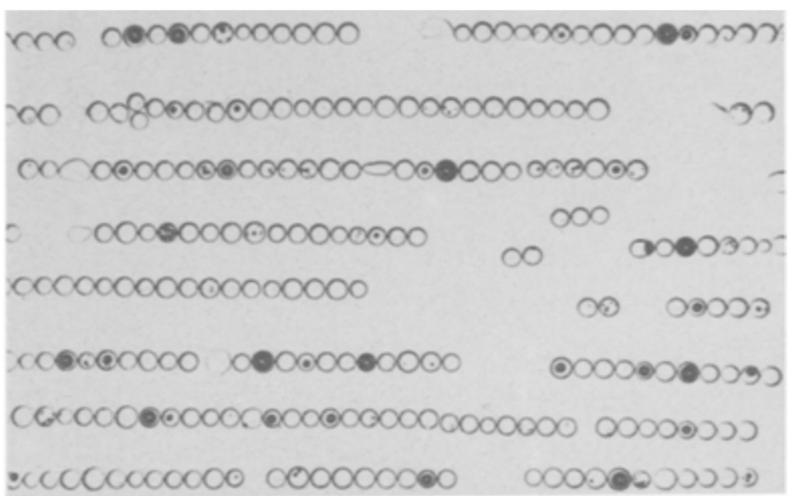

Figure 4.1: Particles alignment in polyisobutylene solution (J. Michele et al. Rheol. Acta 1977)

Another extension of the current dissertation work is to consider the finitely extensible nonlinear elastic (FENE) dumbbell model for viscoelastic fluid flow. In order to study the properties of dilute polymer fluid, the motion of polymer molecules in the fluid is modeled as a suspension of dumbbells or spring chains with finite extensibility (e.g., see [1] and [5]). It would be interesting to consider the fluid-particle and particle-particle interactions in non-Newtonian fluid flow of FENE type with particles and study the effect of the finite extensibility on the particle chains.

Acknowledgments

This work was supported by NSF (grant DMS-1418308).

Bibliography

[1] R. B. Bird, P. J. Dotson, and N. L. Johnson. Polymer solution rheology based on a finitely extensible beadspring chain model. *Journal of Non-Newtonian Fluid Mechanics*, 7:213–235, 1980.

[2] M. O. Bristeau, R. Glowinski, and J. Periaux. Numerical methods for the navier-stokes equations. applications to the simulation of compressible and incompressible viscous flows. *Computer Physics Reports*, 6:73–187, 1987.

[3] A. N. Brooks and T. J. R. Hughes. Streamline upwind/petrov-galerkin formulations for convection dominated flows with particular emphasis on the incompressible navier-stokes equations. *Computer Methods in Applied Mechanics and Engineering*, 32:199–259, 1982.

[4] P. J. Carreau. Rheological equations from molecular network theories. *Transactions of the Society of Rheology*, 16:99–127, 1972.

[5] M. D. Chilcott and J. M. Rallison. Creeping flow of dilute polymer solutions past cylinders and spheres. *Journal of Non-Newtonian Fluid Mechanics*, 29:381–432, 1988.

[6] Y. J. Choi, M. A. Hulsen, and H. E. H. Meijer. An extended finite element method for the simulation of particulate viscoelastic flows. *Journal of Non-Newtonian Fluid Mechanics*, 165:607–624, 2010.

[7] A. J. Chorin, T. J. R. Hughes, M. F. McCracken, and J. E. Marsden. Product formulas and numerical algorithms. *Communications on Pure and Applied Mathematics*, 31:205–256, 1978.

[8] G. D'Avino, G. Cicale, M. A. Hulsen, F. Greco, and P. L. Maffettone. Effects of confinement on the motion of a single sphere in a sheared viscoelastic liquid. *Journal of Non-Newtonian Fluid Mechanics*, 157:101–107, 2009.

[9] G. D'Avino and P.L. Maffettone. Particle dynamics in viscoelastic liquids. *Journal of Non-Newtonian Fluid Mechanics*, 215:80–104, 2015.

[10] E. J. Dean and R. Glowinski. A wave equation approach to the numerical solution of the navier-stokes equations for incompressible viscous flow. *Comptes Rendus de l'Académie des Sciences-Series I-Mathematics*, 325:783–791, 1997.

[11] G. D'Avino, P. L. Maffettone, F. Greco, and M. A. Hulsen. Viscoelasticity-induced migration of a rigid sphere in confined shear flow. *Journal of Non-Newtonian Fluid Mechanics*, 165:466–474, 2010.

[12] G. D'Avino, T. Tuccillo, P. L. Maffettone, F. Greco, and M. A. Hulsen. Numerical simulations of particle migration in a viscoelastic fluid subjected to shear flow. *Computers & fluids*, 39:709–721, 2010.

[13] R. Fattal and R. Kupferman. Constitutive laws for the matrix-logarithm of the conformation tensor. *Journal of Non-Newtonian Fluid Mechanics*, 123:281–285, 2004.

[14] R. Glowinski. Finite element methods for incompressible viscous flow. *Hand of Numerical Analysis*, 9:3–1176, 2003.

[15] R. Glowinski, T.-W. Pan, T. Hesla, and D. D. Joseph. A distributed lagrange multiplier/fictitious domain method for particulate flows. *International Journal of Multiphase Flow*, 25:755–794, 1999.

[16] R. Glowinski, T.-W. Pan, T. Hesla, D. D. Joseph, and J. Periaux. A fictitious domain approach to the direct numerical simulation of incompressible viscous flow past moving rigid bodies: application to particulate flow. *Journal of Computational Physics*, 169:363–426, 2001.

[17] J. Hao, T.-W. Pan, R. Glowinski, and D. D. Joseph. A fictitious domain/distributed lagrange multiplier method for the particulate flow of oldroyd-b fluids: A positive definiteness preserving approach. *Journal of Non-Newtonian Fluid Mechanics*, 156:95–111, 2009.

[18] H. H. Hu, N. A. Patankar, and M. Y. Zhu. Direct numerical simulations of fluid–solid systems using the arbitrary lagrangian–eulerian technique. *Journal of Computational Physics*, 169:427–462, 2001.

[19] M. A. Hulsen, R. Fattal, and R. Kupferman. Flow of viscoelastic fluids past a cylinder at high weissenberg number: stabilized simulations using matrix logarithms. *Journal of Non-Newtonian Fluid Mechanics*, 127:27–39, 2005.

[20] W. R. Hwang, M. A. Hulsen, and H. E. H. Meijer. Direct simulations of particle suspensions in a viscoelastic fluid in sliding bi-periodic frames. *Journal of Non-Newtonian Fluid Mechanics*, 121:15–33, 2004.

[21] N. O. Jaensson, M. A. Hulsen, and P. D. Anderson. Direct numerical simulation of particle alignment in viscoelastic fluids. *Journal of Non-Newtonian Fluid Mechanics*, 235:125–142, 2016.

[22] G. B. Jeffery. The motion of ellipsoidal particles immersed in a viscous fluid. *Proceedings of the Royal Society of London A: Mathematical, Physical and Engineering Sciences*, 102:161–179, 1922.

[23] D. D. Joseph. *Fluid dynamics of viscoelastic liquids*. Springer, New York, NY, 1990.

[24] A. Lozinski and R. G. Owens. An energy estimate for the oldroyd b model: theory and applications. *Journal of Non-Newtonian Fluid Mechanics*, 112:161–176, 2003.

[25] J. Micheleand, R. Pätzold, and R. Donis. Alignment and aggregation effects in suspensions of spheres in non-newtonian media. *Rheologica Acta*, 16:317–321, 1977.

[26] T.-W. Pan, C.-C. Chang, and R. Glowinski. On the motion of a neutrally buoyant ellipsoid in a three-dimensional poiseuille flow. *Computer Methods in Applied Mechanics and Engineering*, 197:2198–2209, 2008.

[27] T.-W. Pan and R. Glowinski. Direct simulation of the motion of neutrally buoyant circular cylinders in plane poiseuille flow. *Journal of Computational Physics*, 181:260–279, 2002.

[28] T.-W. Pan and R. Glowinski. Direct simulation of the motion of neutrally buoyant balls in a three-dimensional poiseuille flow. *Comptes Rendus Mécanique*, 333:884–895, 2005.

[29] T.-W. Pan, S.-L. Huang, S.-D. Chen, C.-C. Chu, and C.-C. Chang. A numerical study of the motion of a neutrally buoyant cylinder in two dimensional shear flow. *Computers & Fluids*, 87:57–66, 2013.

[30] T.-W. Pan, D. D. Joseph, and R. Glowinski. Simulating the dynamics of fluid–ellipsoid interactions. *Computers & structures*, 83:463–478, 2005.

[31] T.-W. Pan, S. Zhao, X. Niu, and R. Glowinski. A DLM/FD/IB method for simulating compound vesicle motion under creeping flow condition. *Journal of Computational Physics*, 300:241–253, 2015.

[32] R. Pasquino, N. Grizzuti F. Snijkers, and J. Vermant. Directed self-assembly of spheres into a two-dimensional colloidal crystal by viscoelastic stresses. *Langmuir*, 26:3016–3019, 2010.

[33] R. Pasquino, D. Panariello, and N. Grizzuti. Migration and alignment of spherical particles in sheared viscoelastic suspensions. a quantitative determination of the flow-induced self-assembly kinetics. *Journal of Colloid and Interface Science*, 394:49–54, 2013.

[34] C. S. Peskin. The immersed boundary method. *Acta numerica*, 11:479–517, 2002.

[35] D. Rajagopalan, R. C. Armstrong, and R. A. Brown. Finite element methdos for calculation of steady, viscoelastic flow using constitutive equations with a newtonian viscosity. *Journal of Non-Newtonian Fluid Mechanics*, 36:159–192, 1990.

[36] R. Scirocco, J. Vermant, and J. Mewis. Effect of the viscoelasticity of the suspending fluid on structure formation in suspensions. *Journal of Non-Newtonian Fluid Mechanics*, 117:183–192, 2004.

[37] F. Snijkers, G. D'Avino, P. L. Maffettone, F. Greco, M. A. Hulsen, and J. Vermant. Rotation of a sphere in a viscoelastic liquid subjected to shear flow. part ii. experimental results. *Journal of Rheology*, 53:459–480, 2009.

[38] F. Snijkers, R. Pasquino, and J. Vermant. Hydrodynamic interactions between two equally sized spheres in viscoelastic fluids in shear flow. *Langmuir*, 29:5701–5713, 2013.

[39] S. Van Loon, J. Fransaer, C. Clasen, and J. Vermant. String formation in sheared suspensions in rheologically complex media: The essential role of shear thinning. *Journal of Rheology*, 58:237–254, 2014.

[40] D. Won and C. Kim. Alignment and aggregation of spherical particles in viscoelastic fluid under shear flow. *Journal of Non-Newtonian Fluid Mechanics*, 117:141–146, 2004.

[41] S. Yoon, M. A. Walkley, and O.G. Harlen. Two particle interactions in a confined viscoelastic fluid under shear. *Journal of Non-Newtonian Fluid Mechanics*, 185:39–48, 2012.

[42] M. Zurita-Gotor, J. Bławzdziewicz, and E. Wajnryb. Swapping trajectories: A new wall-induced cross-streamline particle migration mechanism in a dilute suspension of spheres. *Journal of Fluid Mechanics*, 592:447–469, 2007.